

An Investigation into the Use of Low Volume - Fibre Reinforced Concrete for Controlling Plastic Shrinkage Cracking

by
Jaco-Louis Maritz

*Thesis presented in fulfillment of the requirements for the degree
Master of Science in Engineering at
Stellenbosch University*



Supervisor: Prof William Peter Boshoff
Faculty of Engineering
Department of Civil Engineering

March 2012

DECLARATION

By submitting this thesis electronically, I declare that the entirety of the work contained therein is my own, original work, that I am the authorship owner thereof (unless to the extent explicitly otherwise stated) and that I have not previously in its entirety or in part submitted it for obtaining any qualification.

March 2012

Signature:

.

SUMMARY

Plastic shrinkage cracking (PSC) in concrete is a well-known problem and usually occurs within the first few hours after the concrete has been cast. It is caused by a rapid loss of water from the concrete, either from the surface through evaporation or through absorption by dry subgrade or formwork in contact with the concrete and results in an overall reduction in concrete volume. If this volume reduction or shrinkage is restrained, plastic shrinkage cracks can occur.

Plastic shrinkage cracks create an unsightly appearance on the concrete surface which reduces the quality of the concrete structure. These cracks also develop weak points in the concrete which can be widened and deepened later on by drying shrinkage and thermal movement. As a result harmful substances may enter the cracks causing accelerated concrete deterioration. These cracks may also expose the steel reinforcement causing it to corrode more aggressively. Consequently, the aesthetic value, serviceability, durability and overall performance of the concrete will be reduced. Therefore it is important to consider methods of limiting PSC.

One of these methods is the addition of low volumes of polymeric fibres to concrete to reduce PSC. However, the application of this low volume fibre reinforced concrete (LV-FRC) is not clearly understood since there is a lack of knowledge and guidance available for the use of LV-FRC.

The objective of this study is to gain a full understanding of PSC behaviour in conventional concrete and LV-FRC by investigating the effects of evaporation and bleeding as well as the effect of various fibre properties on PSC. The following significant findings were attained:

- A basis for a crack prediction model in conventional concrete was developed using the average differences in cumulative evaporation and cumulative bleeding to create a crack prediction value (CPV). This preliminary model showed that there exists a certain CPV range (-0.2 to 0.4 kg/m² for this study) where a slight decrease in the CPV results in a significant PSC reduction. It also showed that if the CPV falls outside this range, varying the bleeding or evaporation conditions will have very little effect on the PSC.
- A study on the fibre properties in LV-FRC showed that there exist certain limits to the fibre volume, length and diameter where a further increase or decrease in value will have no or little effect on reducing PSC. It also showed that the effect of the fibres depend on the level of severity of PSC.

The knowledge gained from this investigation can serve as a basis for the design of a model that can predict the risk of PSC in conventional concrete and specify preventative measures needed to reduce this risk. It also provides information that can be used to develop guidelines for the effective use of LV-FRC.

OPSOMMING

Plastiese krimp krake (PKK) in beton is 'n bekende probleem en vorm gewoonlik binne die eerste paar uur nadat die beton gegiet is. Dit word veroorsaak deur die vinnige waterverlies vanuit die beton, óf deur verdamping vanaf die beton oppervalk óf deur absorpsie van 'n droeë grondlaag of bekisting wat in kontak is met die beton. Dit veroorsaak 'n algehele vermindering in beton volume. As hierdie krimp van die beton beperk word, kan plastiese krimp krake ontstaan.

PKK skep 'n onooglike voorkoms van die beton oppervlakte en verlaag die kwaliteit van die beton struktuur. Hierdie krake tree ook op as swak plekke in die beton wat later kan verbreed of verdiep deur droogkrimp en termiese beweging. Gevolglik kan skadelike stowwe vanuit die omgewing die krake binnedring wat lei tot versnelde agteruitgang van die beton. Hierdie krake kan ook die staalbewapening ontbloom wat veroorsaak dat dit vinniger roes. Gevolglik verminder die estetiese waarde, diensbaarheid, duursaamheid en algehele prestasie van die beton. Daarom is dit belangrik om metodes te ondersoek vir die beperking van PKK.

Een van hierdie metodes is die byvoeging van lae volumes polimeer vesels tot beton om PKK te verminder. Die toepassing van hierdie lae volume - vesel versterkte beton (LV-VVB) word egter nog nie volledig verstaan nie as gevolg van 'n algemene gebrek aan kennis en riglyne vir die gebruik van die LV-VVB.

Die doel van hierdie studie is om 'n volledige begrip van PKK gedrag in normale beton asook LV-VVB te kry. Dit word behaal deur die effek van verdamping en bloei op PKK sowel as die effek van verskillende vesel eienskappe op PKK te ondersoek. Die volgende noemenswaardige bevindinge is bekry.

- Die basis van 'n kraak voorspellingsmodel vir gewone beton is ontwikkel deur gebruik te maak van die gemiddelde verskil tussen die kumulatiewe verdamping en die kumulatiewe bloei om 'n kraak voorspellingswaarde (KVV) te vorm. Hierdie voorlopige model toon dat daar 'n sekere KVV interval ontstaan (-0,2 tot 0,4 kg/m² vir hierdie studie) waar slegs 'n effense vermindering in die KVV 'n geweldige vermindering in die PKK tot gevolg het. Dit dui ook aan dat, indien die KVV buite hierdie interval val, 'n verandering in die bloei of verdamping toestande 'n baie klein invloed op die PKK het.
- 'n Studie oor die vesel eienskappe in LV-VVB het gewys dat daar sekere grense is aan die vesel volume, lengte en deursnee waardes, waar 'n verdere toename of afname in waarde min of geen effek het op die vermindering van PKK nie. Dit wys ook dat die effek van die vesels grotendeels afhanklik is van die risiko vlak vir PKK.

Die kennis wat uit hierdie ondersoek opgedoen is, kan dien as 'n basis vir die ontwerp van 'n model wat die risiko van PKK in gewone beton kan voorspel en daarvolgens besluit op 'n voorkomingsmaatsreël om hierdie risiko te verminder. Dit bied ook inligting wat gebruik kan word om riglyne te ontwikkel vir die effektiewe gebruik van LV-VVB.

ACKNOWLEDGEMENTS

I would like to thank the following people for their assistance and support during this study:

- My supervisor, Prof Billy Boshoff for his patience, guidance and support throughout this study.
- Riaan Combrinck, for sharing his knowledge on Plastic Shrinkage Cracking.
- The staff at the workshop and laboratory at the Civil Engineering Department of the University of Stellenbosch, for their assistance during the experimental work.
- Finally, my Creator, for giving me the ability to complete this study.

CONTENTS

DECLARATION	i
SUMMARY	ii
OPSOMMING	iii
ACKNOWLEDGEMENTS	iv
LIST OF FIGURES	ix
LIST OF TABLES	xi
NOTATIONS AND ACRONYMS	xii
1. INTRODUCTION	1
2. BACKGROUND STUDY ON EARLY AGE CRACKING OF CONCRETE	3
2.1 Plastic shrinkage cracking (PSC)	4
2.1.1 Causes of PSC.....	5
2.1.2 Factors influencing PSC	6
2.1.3 Model for PSC behaviour.....	9
2.1.4 The consequences of PSC.....	10
2.1.5 Limiting PSC.....	11
2.2 Plastic settlement cracking.....	11
2.3 Concluding summary.....	12
3. LOW VOLUME – FIBRE REINFORCED CONCRETE (LV-FRC)	13
3.1 Advantages of LV-FRC.....	13
3.2 Typical fibre types and properties.....	14
3.2.1 Polypropylene fibres (PP fibres)	15
3.2.2 Fluorinated polypropylene fibres (FPP fibres).....	15
3.2.3 Polyester fibres (PE fibres)	15
3.3 Mechanisms resulting in crack control due to fibres	15
3.4 Mechanical properties of fibres influencing PSC.....	16
3.4.1 Interfacial shear bond stress	17

3.4.2	Fibre volume.....	19
3.4.3	Fibre aspect ratio.....	20
3.5	Effect of fibres on bleeding.....	20
3.5.1	Fibre type.....	21
3.5.2	Fibre volume.....	21
3.5.3	Fibre aspect ratio.....	21
3.6	Concluding summary.....	21
4.	EXPERIMENTAL FRAMEWORK.....	22
4.1	Test objectives.....	22
4.2	Climate chamber test setup.....	23
4.3	Test measurements.....	25
4.3.1	Evaporation.....	25
4.3.2	Bleeding.....	27
4.3.3	Capillary pressure.....	28
4.3.4	Setting time.....	28
4.3.5	Crack area.....	29
4.4	Test programme.....	30
4.4.1	PSC tests with conventional concrete.....	30
4.4.2	PSC tests with LV-FRC.....	31
4.4.3	Summary of all tests performed in the climate chamber.....	32
4.5	Materials.....	33
4.5.1	Fine aggregates.....	33
4.5.2	Coarse aggregates.....	36
4.5.3	Cement.....	36
4.5.4	Fibres.....	36
4.6	Mix proportions.....	37
4.6.1	Conventional concrete (Tests 1 to 9).....	37
4.6.2	LV-FRC (Tests 10 to 19).....	38

4.7	Test procedure	39
4.8	Concluding summary.....	40
5.	EXPERIMENTAL RESULTS	41
5.1	Test results for Objective 1: To investigate PSC behaviour and confirm the model for PSC behaviour	42
5.1.1	Typical results used to investigate PSC behaviour	42
5.1.2	Summaries of the cumulative Uno evaporation results.....	44
5.1.3	Summaries of the cumulative bleeding results	45
5.2	Test results for Objective 2: Investigation of PSC severity for different bleeding and evaporation conditions.....	46
5.3	Test results for Objective 3: Investigation on the effect of fibre properties on PSC and bleeding	50
5.4	Concluding summary.....	55
6.	DISCUSSION OF EXPERIMENTAL RESULTS.....	56
6.1	Discussion of test results for Objective 1: To investigate PSC behaviour and confirm the model for PSC behaviour	56
6.1.1	Cumulative evaporation	56
6.1.2	Cumulative bleeding.....	57
6.1.3	Drying time	57
6.1.4	Capillary pressure build-up and air entry	58
6.1.5	Setting times.....	59
6.1.6	Crack area.....	59
6.2	Discussion of test results for Objective 2: Investigation of PSC severity for different bleeding and evaporation conditions.....	60
6.2.1	The effect of bleeding and evaporation on PSC severity	60
6.2.2	Crack prediction model	61
6.3	Discussion of the test results for Objective 3: Investigation on the effect of fibre properties on PSC and bleeding	65
6.3.1	Fibre volume.....	65

6.3.2	Fibre aspect ratio.....	67
6.3.3	Fibre length.....	67
6.3.4	Fibre diameter	69
6.3.5	Fibre type.....	71
6.3.6	The effect of fibres on PSC and bleeding for different levels of PSC severity	72
6.4	Framework for guidelines for the use LV-FRC.....	74
6.4.1	When to use LV-FRC	74
6.4.2	How to apply LV-FRC	74
6.4.3	Recommendations for the LV-FRC application based on the results from this study ..	74
6.5	Concluding summary.....	75
7.	CONCLUSIONS AND FUTURE PROSPECTS	76
8.	REFERENCES.....	79

LIST OF FIGURES

Figure 2-1: Typical plastic shrinkage cracks (Illston <i>et al.</i> , 2001:138)	4
Figure 2-2: Bleeding water at concrete surface (Slowik <i>et al.</i> , 2008:557-559)	5
Figure 2-3: Menisci between top particles (Slowik <i>et al.</i> , 2008:557-559).....	5
Figure 2-4: Air penetrates system causing weak points (Slowik <i>et al.</i> , 2008:557-559)	6
Figure 2-5: Model for PSC behaviour (Combrinck, 2011:70)	9
Figure 2-6: Typical plastic settlement cracks (Illston <i>et al.</i> , 2001:138)	12
Figure 3-1: Fibre bridging a crack plane	16
Figure 3-2: Electron microscope images of pulled-out fibres (Combrinck, 2011:89)	18
Figure 3-3: Frictional shear caused by hydrated cement products and fine aggregates.....	19
Figure 3-4: Effect of increased fibre volume on the tensile load per fibre	19
Figure 4-1: Climate chamber layout (Combrinck, 2011:33)	24
Figure 4-2: PSC mould showing triangular inserts with added steel bars (Combrinck, 2011:33,117) .	24
Figure 4-3: Evaporation mould on electronic scale.....	25
Figure 4-4: Concrete temperature sensors	26
Figure 4-5: Anemometer for wind speed measurements.....	26
Figure 4-6: Bleeding moulds, syringe and shaped device used for bleeding measurements	27
Figure 4-7: Capillary pressure sensor	28
Figure 4-8: Vicat apparatus and setting time moulds	29
Figure 4-9: Typical image with measurements used to determine crack area	30
Figure 4-10: Grading of fine aggregates	34
Figure 4-11: SEM image of ultra-fine particles of the Malmesbury Sand	35
Figure 4-12: SEM image of ultra-fine particles of the Greywacke crusher dust	35
Figure 4-13: SEM image of cement particles.....	36
Figure 4-14: SEM images verifying fibre diameters	37
Figure 5-1: Results for Specimen 1 of Test 1 (high evaporation and low bleeding conditions).....	42
Figure 5-2: Results for Specimen 2 of Test 9 (low evaporation and high bleeding conditions).....	43
Figure 5-3: Results for Specimen 2 of Test 10b (addition of 0.1 % Polypropylene fibres)	43
Figure 5-4: Cumulative evaporation results for Tests 1 to 9	44
Figure 5-5: Cumulative evaporation results for Tests 10 to 19	44
Figure 5-6: Cumulative bleeding results for Tests 1 to 9.....	45
Figure 5-7: Cumulative bleeding results for Tests 10 to 19.....	45
Figure 5-8 a, b & c: Average results for a high evaporation climate (Tests 1 to 3)	47

Figure 5-9 a, b & c: Average results for a moderate evaporation climate (Tests 4 to 6)	48
Figure 5-10 a, b & c: Average results for a low evaporation climate (Tests 7 to 9)	49
Figure 5-11: Average crack area results: Effect of fibre volume	50
Figure 5-12: Bleeding results: Effect of fibre volume.....	50
Figure 5-13: Average crack area results: Effect of fibre length	51
Figure 5-14: Bleeding results: Effect of fibre length.....	51
Figure 5-15: Average crack area results: Effect of fibre diameter	52
Figure 5-16: Bleeding results: Effect of fibre diameter	52
Figure 5-17: Average crack area results: Effect of fibre type	53
Figure 5-18: Bleeding results: Effect of fibre type.....	53
Figure 5-19: Average crack area results: Effect of fibres at different levels of PSC severity	54
Figure 5-20: Bleeding results: Effect of fibres at different levels of PSC severity	54
Figure 6-1: Average final crack area at different bleeding and evaporation climate conditions.....	61
Figure 6-2: Illustration of the determination of the crack prediction value (CPV)	62
Figure 6-3: Crack prediction model	63
Figure 6-4: Crack prediction model with LV-FRC tests	65
Figure 6-5: Effect of fibre volume on the final crack area and total bleeding	66
Figure 6-6: Effect of fibre volume on bleeding.....	66
Figure 6-7: Effect of the fibre aspect ratio on the final crack area	67
Figure 6-8: Effect of fibre length on the final crack area and total bleeding	68
Figure 6-9: Effect of fibre length on bleeding	68
Figure 6-10: Effect of fibre diameter on the final crack area and total bleeding.....	69
Figure 6-11: Effect of fibre diameter on bleeding.....	70
Figure 6-12: Frictional shear on 20 and 35 μm fibre.....	71
Figure 6-13: Effect of fibre type on the final crack area.....	71
Figure 6-14: Effect of fibre type on bleeding	72
Figure 6-15: Effect of 0.1 % fibre addition on the final crack area for different PSC levels of severity	73
Figure 6-16: Effect of 0.1% fibre addition on bleeding for different levels of PSC severity	73

LIST OF TABLES

Table 3-1: Typical fibre mechanical properties (Daniel, 2001:40)	14
Table 4-1: Climate conditions	31
Table 4-2: Bleeding rate levels	31
Table 4-3: Alternating fibre properties used for tests with the reference value in bold	32
Table 4-4: Summary of experimental test programme	33
Table 4-5: Fine aggregate properties	34
Table 4-6: Range of fibre properties used in the experimental tests	36
Table 4-7: Mix proportions for low bleeding mix of conventional concrete tests	37
Table 4-8: Mix proportions for moderate bleeding mix of conventional concrete tests	38
Table 4-9: Mix proportions for high bleeding mix of conventional concrete tests	38
Table 4-10: Mix proportions for LV-FRC tests	39
Table 5-1: Summary of test details	41

NOTATIONS AND ACRONYMS

Notations:

cw = average crack width of all line segments at specific time interval [mm]

d = Fibre diameter

E = evaporation rate [$\text{kg}/\text{m}^2/\text{h}$]

L = Fibre length

nls = number of 10 mm line segments used to measure the crack length

RH = relative humidity [%]

S1 = Specimen 1

S2 = Specimen 2

T_a = air temperature [$^{\circ}\text{C}$]

T_c = concrete temperature [$^{\circ}\text{C}$]

V = wind velocity [km/h]

V_f = Volume fraction of fibres

τ = Interfacial shear bond stress

σ_{cu} = Ultimate bridging stress over unit crack area

Acronyms:

CA = crack area at specific time interval [mm^2]

CPV = Crack prediction value [kg/m^2]

FPP = Fluorinated Polypropylene

HB = High bleeding rate level

HE = High evaporation climate condition

LB = Low bleeding rate level

LE = Low evaporation climate condition

MB = Moderate bleeding rate level

ME = Moderate evaporation climate condition

PE = Polyester

PP = Polypropylene

PSC = Plastic Shrinkage Cracking

SANS = South African National Standards

1. INTRODUCTION

Concrete structures, especially structures with a large surface area compared to its volume (for example: slabs or floors), are generally vulnerable to plastic shrinkage cracking (PSC). PSC is a well-known problem occurring within the first few hours after the concrete has been cast and creates an unsightly appearance on the concrete surface. It can also form weak points in the concrete which could widen or deepen later on by further shrinkage or thermal movement (Holt, 2004:521). Aggressive substances may enter the cracks causing accelerated concrete deterioration. It can also lead to exposed reinforcement causing it to corrode more rapidly (Ismail *et al.* 2004:711). Consequently the aesthetic value, serviceability, durability and overall performance of the concrete will be reduced. Therefore it is important to further investigate the methods currently used to reduce the risk of PSC.

This study focuses on the method of adding a low volume of polymeric fibres to concrete at less than 0.3 % by volume of concrete creating low volume - fibre reinforced concrete (LV-FRC) in order to reduce the risk of PSC (Alhozaimy *et al.*, 1996:85 and Daniel *et al.*, 2001:55). Most low volume fibre applications make use of a 0.1 % per volume of concrete fibre addition (Bentur, 2002:2). Although this has proven to effectively reduce PSC (Wongtanakitcharoen, 2005:2 and Ma, 2002:165-169), further investigation is required to fully understand the effective application of LV-FRC.

This study provides a fundamental understanding of the behaviour of PSC in conventional concrete as well as LV-FRC for a number of varying factors and conditions. In terms of research significance, it serves as a basis for future research focusing on the development of guidelines for the use of LV-FRC. Since there is a considerable lack of guidance and knowledge available for LV-FRC, this research is of high importance. In fact, these guidelines will be the first of its kind in South Africa and to the author's knowledge, internationally. By applying these guidelines to the application of LV-FRC, it will be possible to predict the severity of PSC for a certain application and then decide on an appropriate countermeasure (of which the addition of a low volume of fibres is one example) to reduce the risk of PSC.

The primary objectives of this study are as follows:

- To fully understand the behaviour of PSC by investigating a model for PSC behaviour in conventional concrete as well as LV-FRC
- To investigate the severity of PSC for different bleeding and evaporation conditions
- To determine the effect of varying physical fibre properties on PSC and bleeding
- To ultimately serve as a basis from where guidelines for the use of LV-FRC can be developed and will form part of a larger research project on the effective use of LV-FRC

In order to gain the fundamental knowledge required to achieve these objectives a background study was performed on PSC as well as LV-FRC. Together with this, results obtained from experimental tests performed in a climate chamber provided information on the PSC behaviour for varying factors and conditions.

The report has the following basic layout of content:

- *Chapter 2* provides a background study on PSC. Primarily, the most important factors influencing PSC are identified and a model for the behaviour of PSC is also shown.
- *Chapter 3* provides a background study on LV-FRC. This chapter mainly identifies and discusses the fibre properties influencing PSC and bleeding.
- *Chapter 4* explains the experimental framework in terms of the test setup, measurements, materials and mix proportions used in this study.
- *Chapter 5* provides the results for the experimental tests.
- *Chapter 6* discusses the experimental results.
- *Chapter 7* includes the final conclusions and discusses future prospects.
- The Appendices provide additional information on the climate chamber performance as well as summaries of the results obtained from the climate chamber tests.

2. BACKGROUND STUDY ON EARLY AGE CRACKING OF CONCRETE

The early age cracking of concrete refers to cracking that occurs within the first few weeks after casting and can be divided into two types. The first type of early age cracking occurs while the concrete is still in its plastic state, roughly before the setting time (occurring within the first few hours after casting) of the fresh concrete. This is known as plastic cracking of concrete and is further divided into two forms: plastic settlement cracking and plastic shrinkage cracking.

The second type of early age cracking primarily occurs after the concrete has set. At this stage the hardening concrete will experience internal stresses if volume changes are restrained. If the tensile strength of the material is exceeded, cracking will occur. Volumetric change has been reported to be the main cause of early age cracking and is a result of the following: (Bentur, 2002:19)

Thermal deformations:

Thermal deformation can occur due to temperature fluctuations from external influences or from heat of hydration within the concrete.

Shrinkage:

Shrinkage can be divided into two types: autogenous and drying. Autogenous shrinkage occurs because there is a reduction in material volume as water is consumed by hydration. Drying shrinkage, on the other hand, occurs as water is lost to the atmosphere through evaporation.

Creep:

Creep is defined as the time dependant strain in a material when placed under a sustained load. (Bentur, 2002:20)

Although all of these factors have an impact on early age cracking, the focus of this study is on the effects of plastic cracking. This chapter includes sections on both forms of plastic cracking; however, the emphasis of this study will be on plastic shrinkage cracking.

2.1 Plastic shrinkage cracking (PSC)

Plastic shrinkage cracking (PSC) usually occurs within the first few hours after casting. It can easily be identified by its roughly straight but discontinuous and parallel formation (Figure 2-1) spaced between 0.3 m to 2 m apart on the concrete surface (Kellerman *et al.*, 2009:92). This can especially be observed in concrete structures with a large surface area compared to its volume such as slabs or floors. Although plastic shrinkage cracks are generally relative thin cracks and can sometimes be mistaken as harmless, they may reach a width of up to 2 mm and often penetrate the entire depth of the concrete component (Slowik *et al.*, 2008:557). Harmful substances may enter these cracks resulting in corrosion of steel reinforcement and overall concrete deterioration. This could lead to failure of the concrete structure.

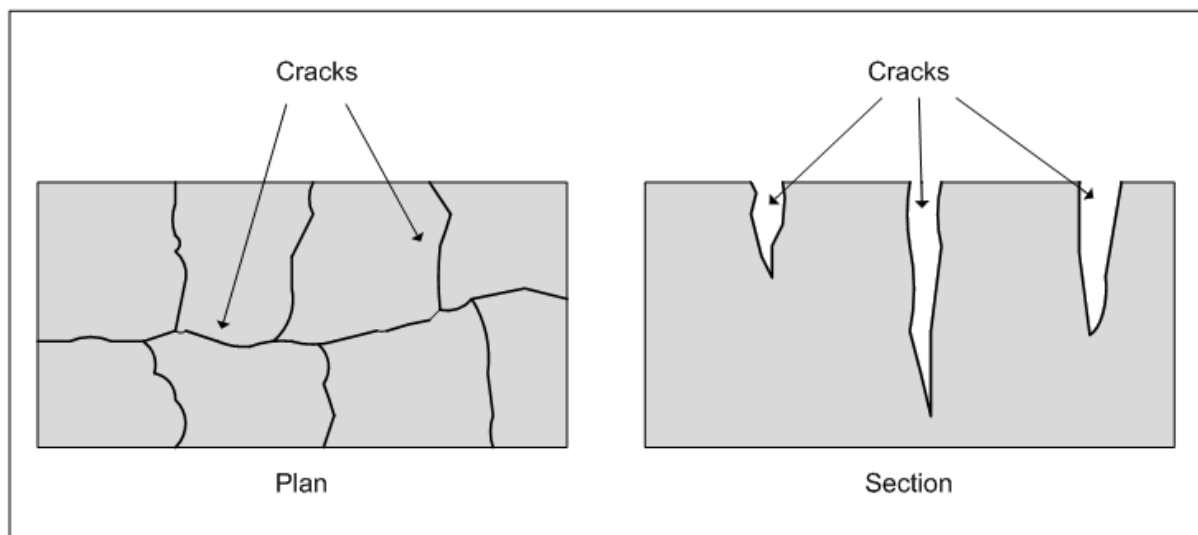


Figure 2-1: Typical plastic shrinkage cracks (Illston *et al.*, 2001:138)

Plastic shrinkage is caused by the rapid loss of water from the concrete, either from the surface by evaporation or absorbed by dry subgrade or absorbent formwork in contact with the concrete. The loss of water causes a reduction in concrete volume leading to shrinkage of the concrete. Although plastic shrinkage on its own is harmless, there generally exists a form of restraint in the concrete which causes shrinking concrete to crack. This is known as plastic shrinkage cracking.

As the focus of this study is on plastic shrinkage cracking, this section further reports on the causes of PSC as well as factors that have an influence on the severity of PSC. A model is also introduced for PSC behaviour. Finally, it is explained why PSC in concrete is a problem and a method to reduce PSC is presented.

2.1.1 Causes of PSC

Physical processes rather than chemical reactions are the predominant reason for cracking of concrete in the plastic state (Slowik *et al.*, 2008:557). The physical process and main mechanism responsible for PSC is capillary pressure build-up.

After casting of concrete the solid particles settle causing the concrete to bleed (Figure 2-2). When the bleeding water at the concrete surface starts to evaporate, menisci form between the top particles of the concrete (Figure 2-3). The menisci are formed as a result of adhesive forces and surface tension.

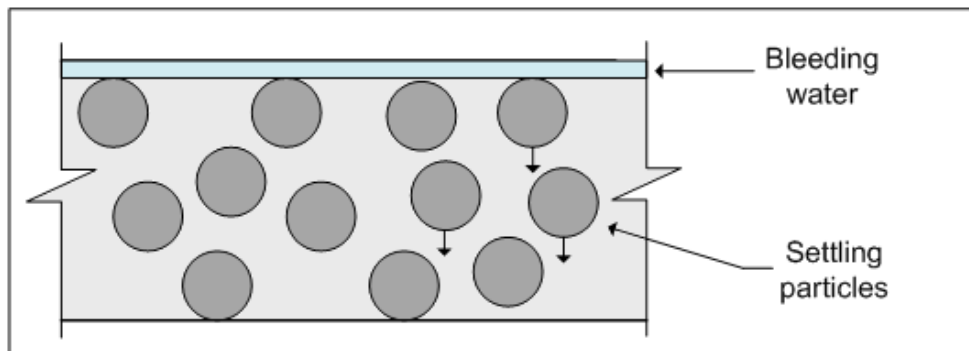


Figure 2-2: Bleeding water at concrete surface (Slowik *et al.*, 2008:557-559)

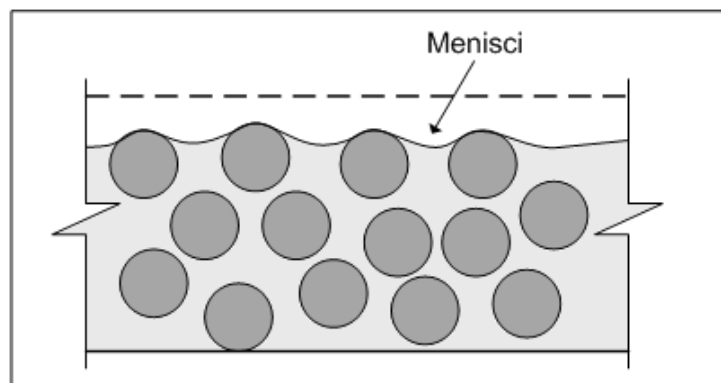


Figure 2-3: Menisci between top particles (Slowik *et al.*, 2008:557-559)

A system of interconnected pores filled with capillary water exists between the concrete particles. The curvature of the water menisci causes negative capillary pressure in the capillary water which results in a contraction of the plastic material. Ongoing evaporation causes further reduction of menisci radii (increased menisci curvature) increasing capillary pressure resulting in a further volume reduction. After a certain pressure value has been reached, the radii of the menisci are too small (curvature too great) to bridge the gaps between the particles (Figure 2-4) and air will penetrate the system locally.

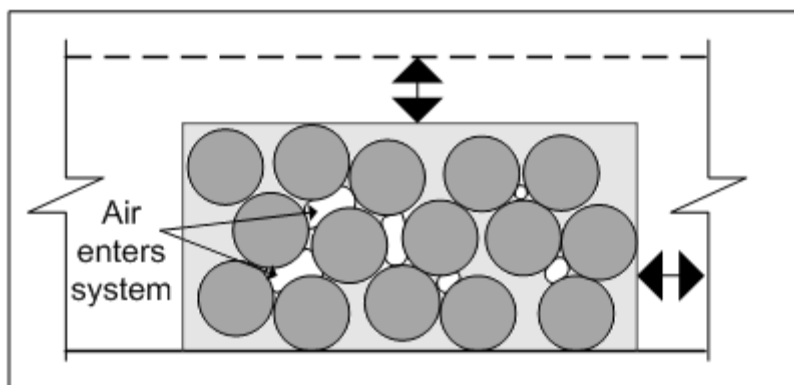


Figure 2-4: Air penetrates system causing weak points (Slowik *et al.*, 2008:557-559)

Contracting forces between the particles in the air penetrated regions are much smaller than contracting forces of particles in the water filled regions resulting in weak points in the system. If shrinkage is restrained and the cohesive forces are overcome (most likely in the weaker air filled regions) cracks are formed. These cracks are defined as plastic shrinkage cracks. (Slowik *et al.*, 2008:557-559)

2.1.2 Factors influencing PSC

PSC can be influenced by many interdependent factors. The effect of these factors also changes continuously over time which increases the complexity of PSC even further. The following factors have been identified as the most significant and play a key role throughout this study.

2.1.2.1 Evaporation rate

As previously mentioned, capillary pressure build-up causing PSC is influenced by the evaporation of water from the concrete surface. Plastic shrinkage occurs after the cumulative amount of evaporated water exceeds the cumulative amount of water supplied to the surface from within the concrete via bleeding. Factors influencing the evaporation rate include air temperature, concrete temperature, wind speed and relative humidity (Uno, 1998:368).

The air temperature has an effect on the evaporation rate by influencing the relative humidity as well as the concrete temperature. The higher the air temperature, the higher is the rate of water loss through evaporation.

The effect of concrete temperature actually refers to the concrete water temperature which is influenced by the temperature of the concrete materials. A higher surface water temperature (moved to concrete surface via bleeding) leads to a higher rate of evaporation. The concrete water temperature can also increase over time due to the heat of hydration process within the concrete.

Wind can dramatically influence the evaporation rate and controlling the wind speed is considered to be one of the most effective ways to control PSC (Uno, 1998:368). Wind continuously removes evaporated water molecules into the atmosphere allowing more molecules to evaporate. An increase in wind speed can increase the evaporation rate considerably.

A model was developed by Uno (1998:368) to calculate the evaporation rate from the concrete surface by using measured values of the current air temperature, concrete temperature, wind speed and relative humidity. This model from Uno (Equation 2.1) is used throughout this study to determine the concrete water evaporation. However, it should be mentioned that Uno's equation was developed for open water evaporation. The implication of this is discussed in Section 2.1.3.1.

$$E = 5([T_c + 18]^{2.5} - r[T_a + 18]^{2.5})(V + 4) \times 10^{-6} \dots\dots\dots(\text{Equation 2.1})$$

with:

E = evaporation rate [kg/m²/h]

T_c = concrete temperature [°C]

r = RH/100 (with RH = relative humidity) [%]

T_a = air temperature [°C]

V = wind velocity [km/h]

2.1.2.2 Bleeding

Bleeding in concrete can be identified by the formation of a layer of water on the concrete surface shortly after it has been placed. In extreme cases this can amount to two percent or more of the concrete depth (Illston *et al.*, 2001:136). There are two types of bleeding: normal bleeding and channel bleeding.

Normal bleeding occurs due to the settlement of the solid particles (for normal concrete: cement, fine and coarse aggregates) while the concrete is in the fresh state. The solid particles are denser than the mixing water and therefore settle downward due to gravitational force displacing the water up towards the concrete surface. The water which then accumulates on the concrete surface is known as bleeding water. Bleeding stops when there is no more downward movement of solid particles due to concrete setting or formation of hydration products (Powers, 1968:535).

Channel bleeding can occur in addition to normal bleeding and has a much higher bleeding rate than normal bleeding. It occurs when channels form within the concrete where in water can move up

towards the concrete surface. Channel bleeding can be identified by the formation of small craters at the mouth of the channel on the concrete surface (Powers, 1968:534).

There are a number of factors that can influence the rate and capacity (total amount) of normal bleeding. These factors include: concrete permeability, initial water content, concrete depth, water absorption from within the concrete or its surroundings, aggregate content and fineness, vibration time and intensity, capillary pressure and hydration (Combrinck, 2011:11-14). Of these factors permeability and aggregate fineness are of highest interest for this study as it is used to achieve different bleeding rates.

The permeability of the concrete influences the rate at which water can flow upwards through the porous concrete material towards the surface (Combrinck, 2011:12). The more permeable the concrete material, the higher is the rate of bleeding.

The bleeding of the concrete also depends on the fines content which, for this study, includes cement particles and dust (particles passing the 75 μm sieve) from the fine aggregate. The greater this fraction is the lower the bleeding. Bleeding is especially controlled by the amount of ultra-fine material smaller than 5 μm (Addis, 1998:88). The bleeding rate and capacity also decreases with an increase in specific surface area (Powers, 1968:553-580). The specific surface area mainly depends on the amount and size of fines and the particle shape.

2.1.2.3 Concrete composition

The composition of the concrete mainly refers to the size and the composition of the particles used in the concrete material. Particle size and distribution not only influences the bleeding of the concrete but has an effect on the capillary pressure which causes PSC. Smaller particles distributed close to each other near the concrete surface have smaller meniscus radii between them increasing the capillary pressure (as explained in Section 2.1.1) leaving the material more vulnerable to cracking (Slowik *et al.*, 2009:467).

2.1.2.4 Restraint

As previously mentioned, PSC can only occur if the shrinkage is restrained. These restraints can be internal (the concrete itself) or external (external components).

Internal restraint is the result of a differential volume reduction within the concrete. This is caused by the top part of a slab shrinking more due to evaporation from the surface. The underlying concrete then acts as an internal restraint to the shrinking concrete above and results in PSC (Addis, 1998:15).

External restraint includes rough formwork or sub-grade which restrains the shrinkage of the concrete. Steel reinforcement used in structural concrete can also act as restraints.

2.1.3 Model for PSC behaviour

Combrinck (2011:70) proposed a model (Figure 2-5) indicating the typical behaviour of plastic shrinkage cracks as well as the important events taking place around the time that PSC occurs. These events are discussed in this section.

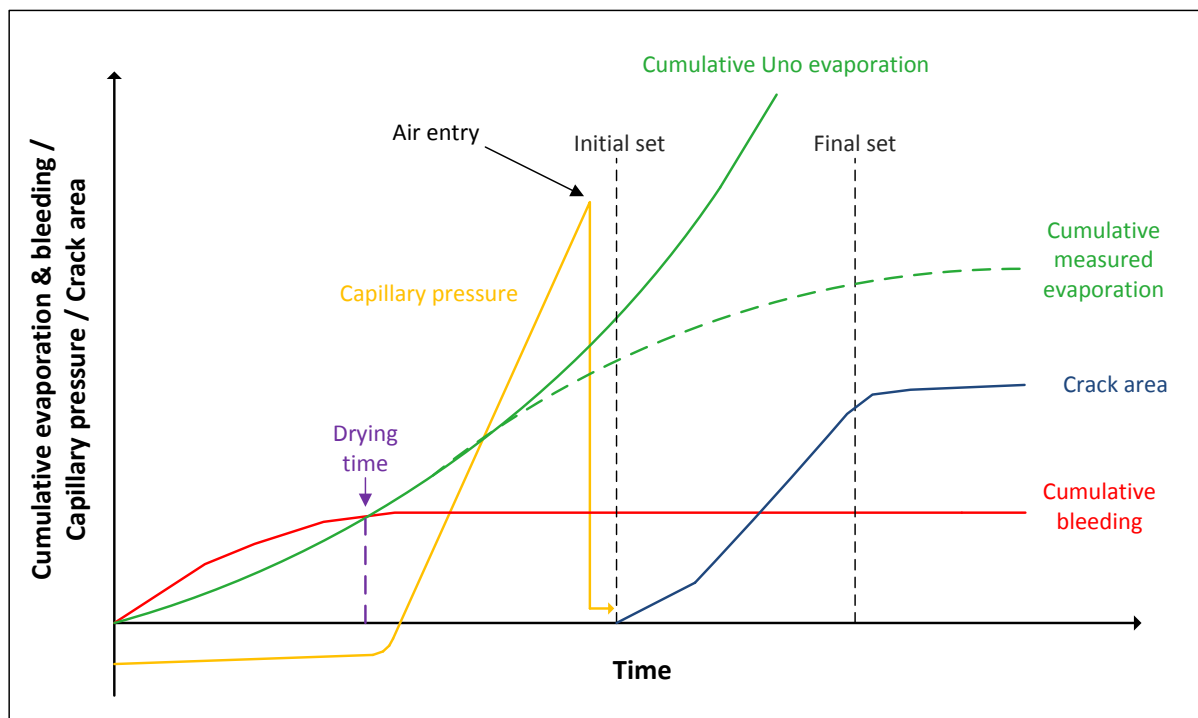


Figure 2-5: Model for PSC behaviour (Combrinck, 2011:70)

2.1.3.1 Cumulative evaporation

The Uno evaporation rate slightly increases over time due to the increasing concrete temperature resulting in a continuous increase in the cumulative value. On the other hand the measured evaporation rate decreases after time. The reason for the different behaviour is that the Uno evaporation considers open water evaporation while the scale evaporation measures the true amount of water lost from the concrete. Therefore the scale evaporation rate decreases as the concrete sets and less water is transferred to the concrete surface via bleeding. However, the results for both the Uno and scale evaporation will be identical at least until the drying time is reached since the evaporation of the bleeding water on the concrete surface before the drying time is considered as open water evaporation.

2.1.3.2 Cumulative bleeding

The bleeding rate is high initially and then decreases with time until bleeding stops. This is the point at which the cumulative bleeding becomes constant.

2.1.3.3 Drying time

The drying time is defined as the time at which the cumulative amount of evaporation equals the cumulative amount of bleeding. This is also the time at which capillary pressure starts to build up in the concrete. (Combrinck, 2011:71)

2.1.3.4 Capillary pressure

The capillary pressure is fairly stable until the drying time is reached. At this time the model indicates a steep incline as capillary pressure starts to build up until it instantly drops once air entry occurs.

2.1.3.5 Air entry

The time of air entry usually occurs just before the first crack is observed close to the initial setting time. It is believed that no plastic shrinkage cracks will occur before air entry has taken place (Slowik *et al.*, 2008:559).

2.1.3.6 Initial set

The initial setting time is the time at which the concrete paste can be easily moulded by hand without damaging the paste structure. This is defined and determined using the test procedure outlined in SANS 50196-3 (2006).

2.1.3.7 Final set

The final setting time is the time at which moulding of the concrete will result in visible damage to the paste structure. This is defined and determined using the test procedure outlined in SANS 50196-3 (2006).

2.1.3.8 Crack area

The most likely period for PSC to occur is between the initial and final setting times. Crack growth starts out rapidly but generally the crack area stabilises before the final setting time.

2.1.4 The consequences of PSC

Plastic shrinkage cracks create an unsightly appearance on the concrete surface which reduces the quality of the concrete structure and often leaves the client dissatisfied. These cracks also develop weak points in the concrete which can be widened and deepened later on by drying shrinkage and thermal movement. As a result external harmful substances may enter the cracks causing

accelerated concrete deterioration. These cracks may also expose the steel reinforcement causing it to corrode more rapidly. Consequently, the aesthetic value, serviceability, durability and overall performance of the concrete will be reduced (Wongtanakitcharoen, 2005:1).

2.1.5 Limiting PSC

It is clear that bleeding and evaporation play a major role in PSC. By controlling these two factors it is therefore possible to control PSC to a great extent. A number of methods are currently used to reduce the amount of concrete water evaporating from the concrete surface. Wind breaks, sun shades, moisture retaining coverings and fog sprays are just a few of these methods and is referred as external methods for limiting PSC. However, it is not always possible to implement some of these methods as it depends on the casting conditions and require additional labour after concrete placement. If these methods are not implemented correctly, it could reduce their effectiveness and result in a decreased concrete quality. An example of this is the overuse of fog sprays. If an excess of water is sprayed onto the concrete, it will lead to an accumulation of water on the surface. This will create a weaker concrete surface also known as surface laitance. However, these methods can be effective if implemented correctly.

Another effective method currently used in the concrete industry to limit PSC is the addition of a low volume of synthetic fibres to concrete at the mixing stage. The effectiveness of this method depends on the implementation of these fibres and is also the focus of this study. Fibres and their application are discussed in Chapter 3.

2.2 Plastic settlement cracking

Plastic settlement cracking usually occurs when concrete bleeding and settlement are high and some restraint is present (Mehta *et al.*, 2006:380). Restraints can include reinforcement in a beam or slab or a change in section depth, e.g. at the junction of web and flange in a T-beam or coffer slab. In the case of a concrete member where horizontal reinforcement is present, the settlement above the steel bars is less than the settlement around the bar causing plastic settlement cracks along the line of the bars (Figure 2-6) (Kellerman *et al.*, 2009:92). The same effect occurs at the junction of the flange and the web of a concrete T-beam where the change in section depth causes the concrete in the web to settle more than in the flange. This results in plastic settlement cracks as shown in Figure 2-6.

Plastic settlement cracking most likely occurs in conjunction with PSC and therefore is of relevance to this study. However, the aim of this study is to investigate PSC, therefore plastic settlement is not

included. The moulds (Figure 4-2) were designed in such a way that the effect of plastic settlement is insignificant.

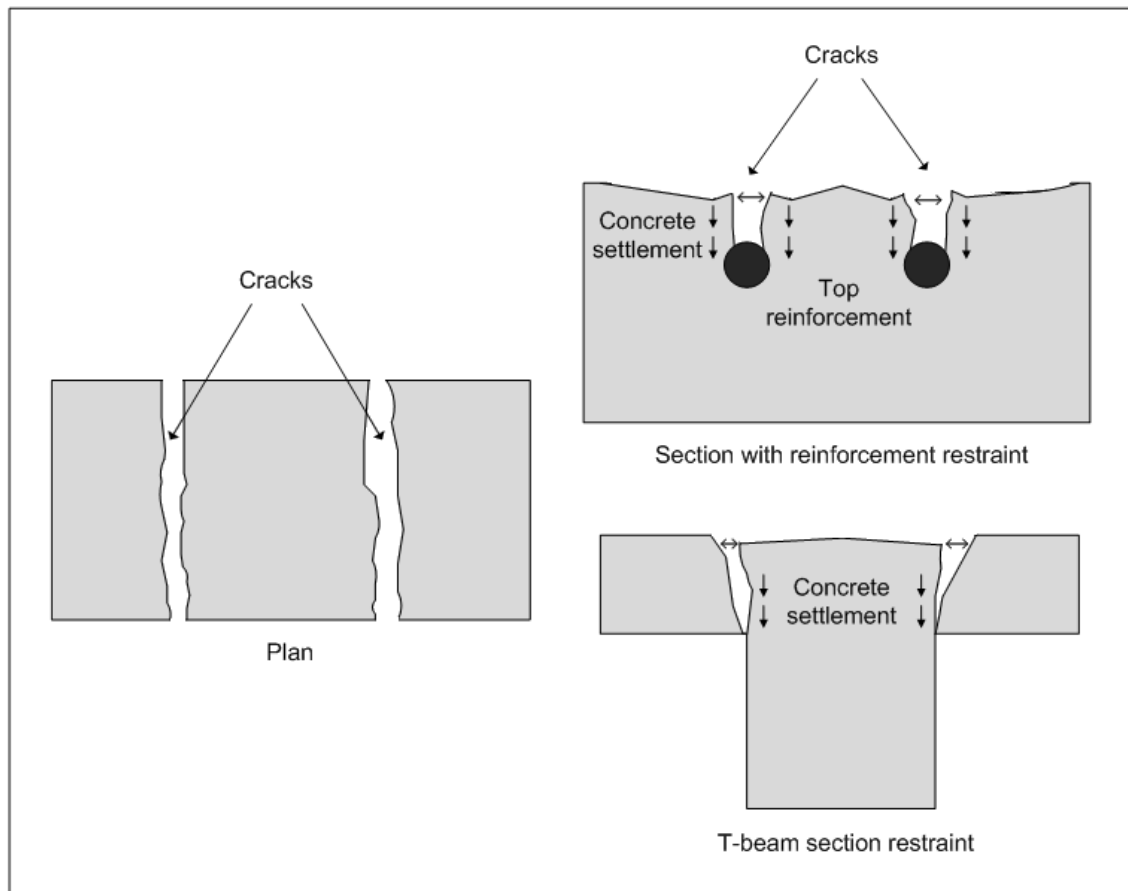


Figure 2-6: Typical plastic settlement cracks (Illston *et al.*, 2001:138)

2.3 Concluding summary

This chapter explains how capillary pressure results in PSC and identifies the main factors influencing PSC as the evaporation rate, bleeding, concrete composition and restraint. It also presents a model indicating the typical behaviour of PSC and the events leading up to it. Finally, PSC as a threatening problem in the concrete industry is discussed followed by a few methods to limit the occurrence of PSC. One of these methods used to limit PSC is the addition of a low-volume of fibres to the concrete is the focus of the next chapter.

3. LOW VOLUME – FIBRE REINFORCED CONCRETE (LV-FRC)

One of the main concerns when working with a cement-based matrix is its brittle type of failure under a tensile or impact load. To increase the toughness and tensile properties of concrete fibres can be added to the concrete matrix (Hannant, 1978:1). One of these fibre applications in concrete is the addition of synthetic fibres to carry the tensile stresses created by restrained shrinkage of concrete in its plastic state, thus controlling plastic shrinkage cracking (PSC).

The two synthetic fibre volume applications commonly used is a low-volume percentage (less than 0.3 % by volume) and a high-volume percentage (0.3 to 0.8 % by volume of concrete) (Alhozaimy *et al.*, 1996:85 and Daniel *et al.*, 2001:55). The addition of low-volume percentage fibres to concrete will hence be referred to as low volume – fibre reinforced concrete or LV-FRC.

The majority of low volume - fibre applications are currently at the 0.1 % by volume level. This is probably due to the fact that properties such as concrete strength are unaffected with the addition of fibres at this volume level while a reduction in PSC is still eminent (Banthia, 2005:44 and Pelisser, 2010:2174-2176). There is, however, a lack of knowledge on the effective application of LV-FRC.

This chapter will focus on the fundamental knowledge required to understand the use of a low volume of fibres for controlling PSC.

3.1 Advantages of LV-FRC

The first and probably most important advantage of adding a low volume of fibres to conventional concrete is the reduction of PSC of concrete in the fresh state when the concrete matrix has low tensile strength. However, once the concrete has hardened the magnitude of tensile strength of the concrete far exceeds the tensile strength provided by the fibres making its contribution to the overall tensile strength of the structure ommissible. Nevertheless, these fibres can improve other mechanical properties of the concrete matrix in the hardened state including increased ductility, impact

resistance and resistance to crack widening all contributing to an increase in durability (Illston *et al.*, 2001: 419-420).

Another advantage of synthetic fibres is the additional increase of fire resistance provided to the concrete structure. A fire could heat the moisture within the concrete to a point where it turns to steam. If the steam is unable to escape it causes a pressure build-up within the concrete. This creates spalling of the concrete and exposes the steel reinforcement to the heat of the fire. The heat reduces the structural value of the steel and can cause the structure to fail. The advantage of LV-FRC is that fibres combust when exposed to extreme heat, creating channels for the steam (pressure) to be released. This prevents spalling and ultimately prevents structural failure (Hannant, 1978:95).

External PSC limiting methods like sun shades, wind breaks moisture retaining coverings and fog sprays have to first be erected and monitored requiring additional labour. In certain situations it might even be impossible to use these methods due to site limitations or positional difficulty in which case the addition of fibres can be advantageous. In most cases however, a low volume of fibres can be combined with external methods for limiting PSC.

3.2 Typical fibre types and properties

Synthetic fibres are available in fibrillated as well as monofilament forms where the latter is normally circular in cross-section and also the form used in this study (Hannant, 1978:81). Numerous fibre types are currently available for use in LV-FRC but only the two most common types are used in this study namely polypropylene (with and without surface treatment) and polyester fibres. A summary of typical fibre properties are shown in Table 3-1 and each fibre type is discussed in the following sections.

Table 3-1: Typical fibre mechanical properties (Daniel, 2001:40)

Fibre type	Polypropylene	Fluorinated Polypropylene	Polyester
Typical diameter [μm]	20 - 40	20 - 40	20
Relative density	0.90 - 0.91	0.90 - 0.91	1.34 - 1.39
Tensile strength [MPa]	140 - 700	140 - 700	230 - 1100
Elastic modulus [GPa]	3.5 - 4.8	3.5 - 4.8	17
Ultimate elongation [%]	15	15	12 - 150
Ignition temperature [$^{\circ}\text{C}$]	600	600	600
Melt, oxidation or decomposition temperature [$^{\circ}\text{C}$]	165	165	260
Water absorption per ASTM D 570 [% by mass]	0	0	0.4
Surface treatment	none	fluorination	none

3.2.1 Polypropylene fibres (PP fibres)

Monofilament PP fibres are produced in an extrusion process in which the material is hot drawn through a die of circular cross-section. PP fibres are hydrophobic and therefore are not expected to bond chemically in a concrete matrix. Bonding has been shown to occur through mechanical interaction (Ma *et al.*, 2002:167).

3.2.2 Fluorinated polypropylene fibres (FPP fibres)

FPP fibre properties are similar to that of normal PP fibres except for the added surface treatment. FPP fibres are treated with fluorine gas (F_2) in a process known as fluorination. This changes the polarity of the fibre surface increasing the water absorption on the surface. Effectively this could increase the bond strength due to the hydration from the absorbed water with cement particles (Forrester, 2004:8-9).

3.2.3 Polyester fibres (PE fibres)

PE fibres are hydrophilic (does absorb water) and generally do not affect hydration of portland cement concrete (Golding, 1959:288-289). They are also temperature sensitive and temperatures above normal can alter their properties. High alkaline environments can also result in decomposition of the fibre. This is believed to be caused by hydrolysis of the $-CO-O-$ group in an ester (Halse, 1987:280). However, this is not a problem since PE fibres are used primarily for PSC reduction while possible decomposition of PE fibres takes place long after this.

3.3 Mechanisms resulting in crack control due to fibres

Fresh concrete has a low tensile strength which is often exceeded by the tensile stresses created from restrained shrinkage leading to PSC. After crack initiation the concrete matrix no longer provides any tensile resistance in that region and the fibres are the only additional resistance to crack widening. It is important to realize however, that the fibres only provide additional resistance once cracking has occurred. The fibres crossing the crack plane bond with the concrete matrix on either side keeping it together (Figure 3-1). Thus, the theoretical performance of the composite material depends on the mechanical properties of the fibres and the matrix as well as on the strength of the bond between the two. More details on the physical properties of the fibres including bond strength are provided in the next section.

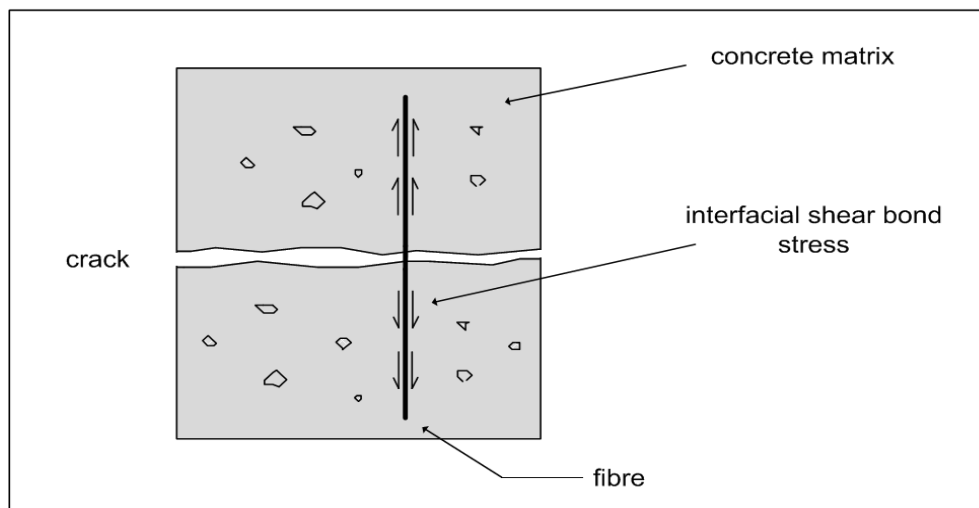


Figure 3-1: Fibre bridging a crack plane

3.4 Mechanical properties of fibres influencing PSC

Hannant (1978:24) proposed a model (Equation 3.1), to calculate the ultimate stress sustained across a crack plane of a composite after cracking.

$$\sigma_{cu} = \frac{1}{2} \tau V_f \left(\frac{L}{d} \right) \dots\dots\dots(\text{Equation 3.1})$$

with:

σ_{cu} = ultimate bridging stress over a crack plane

τ = interfacial shear bond stress

V_f = volume fraction of fibres

L = fibre length

d = fibre diameter

L/d = fibre aspect ratio

The following assumptions apply to this model for short, randomly distributed, 3-D orientated fibres:

- all the fibres pull-out rather than break;
- all the fibres are straight without hooks all; and
- the fibres remain straight.

Although this model was derived for hardened concrete, it is believed to also be applicable to concrete in the fresh state. The mechanical properties that influence the crack bridging stress include:

- interfacial shear bond stress between the fibre and the concrete matrix;
- fibre volume;
- fibre length; and
- fibre diameter.

This model gives a theoretical indication of the impact that each of these factors has on the ultimate bridging stress. Since these factors have a significant impact on PSC they form an important part of this study and are discussed in detail in the following sections.

3.4.1 Interfacial shear bond stress

An interfacial shear bond stress between the fibres and the concrete matrix is necessary to transfer tensile stress from the concrete matrix to the fibres. It should be obvious that if an adhesive interfacial shear bond does not exist, no tensile stress can develop in the fibres in which case the strength of the composite is the same as the strength of the matrix (Johnston, 2001:28).

Initially, this interfacial shear bond stress is relatively low while the composite is still in its fresh state and PSC is likely to occur. Combrinck (2011:89) performed experiments where single fibres were pulled out of a concrete mix at different times to investigate the development of interfacial shear bond stress over time. These tests showed interfacial shear bond stress values of 0.22 kPa for polypropylene fibres pulled out of a concrete mix after one hour while values for the same test after 5 hours reached stresses of more than 21 kPa (Combrinck, 2011: 123). Therefore it is assumed that the fibres will pull-out rather than rupture. However, the interfacial shear bond stress is time dependant and increases significantly over time as hydration takes place. Figure 3-2 shows electron microscope images of these pulled out fibres clearly indicating the increase in frictional skid marks on the fibre surface as time progresses. This is an indication of the increased frictional bond between the fibres and concrete paste.

The mechanisms responsible for interfacial shear bond stress include adhesion, friction and mechanical interlocking and depend on the fibre type. Most synthetic fibres in monofilament form (as the ones used for this study) are smooth, straight and have a circular cross-section and therefore mechanical interlocking is unlikely to occur. Mechanical interlocking normally occurs with fibrillated fibres or monofilament fibres with hooked ends. However, adhesion and friction does occur and

depend mainly on the surface texture/deformation and surface coatings of the fibres as well as the particles surrounding the fibres (Johnston, 2001:40-47).

Surface texturing during the manufacturing process can significantly improve the resistance of a fibre against pull-out due to increased friction and adhesive bond resulting from the roughened fibre surface. Fibre surface deformities also increases interfacial shear bond stress due to the same roughening effect. Another example is the embedment of tiny particles such as condensed silica fume on the surface of otherwise smooth poorly adhesive fibres creating a rough surface for improved shear resistance. This frictional shear resistance is especially important for fibres without hooks or other special end anchorage (Johnston, 2001:40-47).

Surface coatings of fibres can have different effects on the interfacial bond strength depending on the purpose of the coating. Surface coatings are primarily applied to improve adhesiveness, for example FPP fibres. Other coatings can be used to protect fibres against harmful substances but may also affect the bond between the fibre and the concrete paste. Applying a surface coating can also smoothen out an otherwise rough surface fibre and thus reduce bonding potential.

The particles surrounding the fibres cause a frictional shear which increases the frictional bond stress of the fibres. These particles include fine aggregates and hydrated cement products. Figure 3-3 shows how the fine aggregates and hydrated cement products causes friction on the fibre surface.

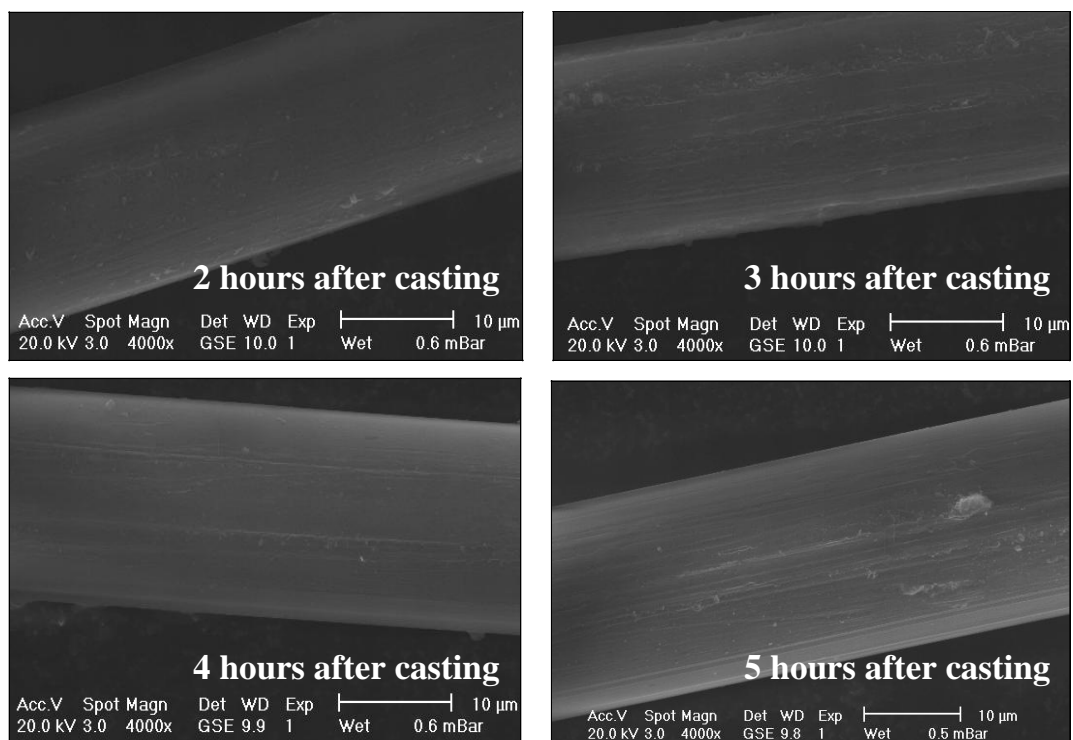


Figure 3-2: Electron microscope images of pulled-out fibres (Combrinck, 2011:89)

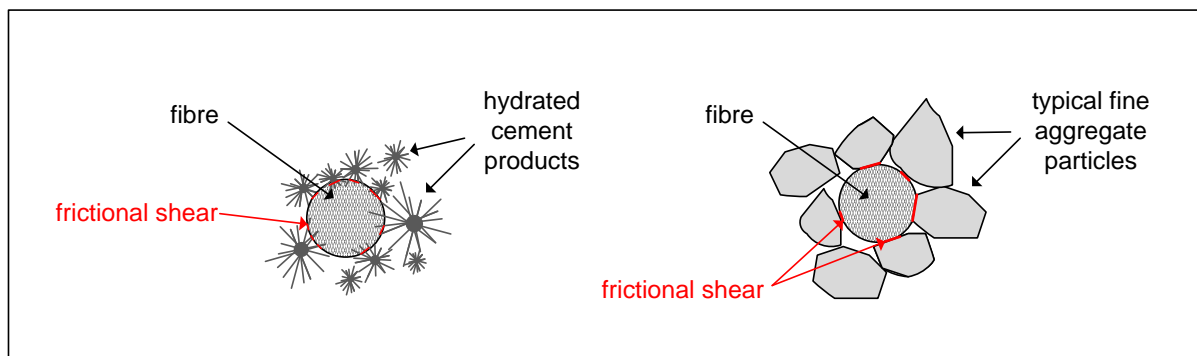


Figure 3-3: Frictional shear caused by hydrated cement products and fine aggregates

3.4.2 Fibre volume

Fibre quantities are generally expressed as a percentage of the total volume of the concrete mix. The reason for this is to simplify the comparison of different fibre types used in LV-FRC since each type has different relative densities. Thus, two different fibre types of the same size and the same volume percentage will have the same number of fibres per unit volume even though they have a different total mass.

Most synthetic fibre applications use 0.1 % by volume of fibres. The reason for this is that there is a noticeable effect on controlling PSC at this dosage level without having a significant impact on other concrete properties such as concrete strength (Banthia, 2005:44 and Pelisser, 2010:2174-2176). However, it is of interest to this study to investigate the effect of different fibre volumes.

Theoretically, an increase in fibre volume will increase the number of fibres crossing the crack plane which means that the area of stress transfer from the matrix to each individual fibre is less. This results in a lower tensile load per fibre and therefore fibre debonding is less likely to occur, ultimately leading to a higher tensile load capacity resulting in a reduction in PSC.

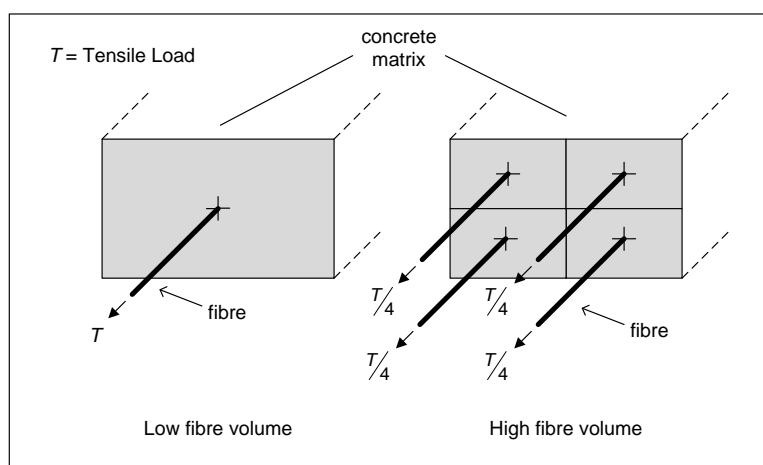


Figure 3-4: Effect of increased fibre volume on the tensile load per fibre

3.4.3 Fibre aspect ratio

The fibre aspect ratio (L/d ratio) is defined as the ratio of the length (L) to the diameter (d) of a single fibre. Thus, a longer fibre with a small diameter would have a large aspect ratio compared to a shorter fibre with a large diameter. The significance of the diameter and length of fibres with regards to PSC will be discussed separately in this section.

At a specific fibre length and volume fraction the use of smaller diameter fibres can be more effective than fibres with a larger diameter. The reason for this is the larger overall surface area of the smaller diameter fibres compared to the same volume of larger diameter fibres (Bagherzadeh, 2011:7-9). This results in an increased interfacial shear bond stress area between the fibres and the concrete matrix resulting in a better stress transfer to the fibre. The smaller diameter fibres will also have a higher number of individual fibres per volume. This means that there are more fibres crossing a crack plane per section. As a result the space between unsupported parts in the concrete matrix (space between fibres) will become smaller reducing the concentration of stresses thus improving crack growth resistance (Banthia, 2006:1266). However, if the fibre diameter becomes too small for the surrounding particles to grip or cause friction, an interfacial shear bond stress cannot develop.

On the other hand, for a constant fibre volume and diameter, the fibre length can influence PSC in one of the following ways. A shorter fibre means there are more fibres available to cross the crack plane and limit PSC while a longer fibre will mean fewer fibres per volume fraction but might have a significantly higher interfacial shear bond stress that could result in less PSC.

It is therefore apparent that one cannot simply increase the aspect ratio in order to increase PSC resistance. Deciding on the ideal fibre length and diameter is of great interest in order to effectively apply LV-FRC.

3.5 Effect of fibres on bleeding

As previously discussed bleeding plays an important role in PSC. Therefore it is important to consider the effect of fibre addition on the bleeding of concrete. Fibres can influence bleeding as follows (Qi *et al.*, 2003:390):

- bleeding water can be reduced due to the hydrophilic (water absorbing) nature of some fibres such as polyester fibres;
- bleeding can also be reduced due to the fibres decreasing the settlement of particles which is the main mechanism causing bleeding; and

- bleeding rate can be increased due to fibres acting as channels along which the bleeding water can move to the surface more easily.

The same physical fibre properties discussed in Section 3.4 affects the concrete bleeding which in turn influences PSC. This section further discusses how the fibre type, fibre volume and fibre aspect ratio indirectly affects PSC by means of bleeding influence.

3.5.1 Fibre type

Some fibres like polyester fibres are less hydrophobic than others which mean that some water is absorbed by the fibres. This could decrease the amount of water available for bleeding.

3.5.2 Fibre volume

An increased fibre volume increases the number of fibres obstructing particle settlement. Therefore the bleeding rate and amount will decrease. On the other hand, an increased fibre volume can also mean more channels are formed for bleeding water to move to the surface which then increases the bleeding rate again. Thus, the influence of the fibre volume on bleeding depends on which of these mechanisms has the dominant effect (Abdulrahman, 1995:183).

3.5.3 Fibre aspect ratio

Generally, an increase in fibre length will decrease particle settlement resulting in reduced bleeding. The fibre diameter can influence bleeding in two ways. For a specific fibre length and volume, the smaller diameter fibres will be more than the larger diameter fibres leading to a higher number of fibres causing obstruction of particle settlement and consequently reducing the bleeding. On the other hand, this increase in number of fibres creates more channels along which the water can move to the surface increasing the bleeding rate.

3.6 Concluding summary

In this chapter it is apparent that the addition of a low volume of fibres to concrete is usually effective in reducing PSC. There are some cases however, where the addition of fibres can prove ineffective. This could either be a result of fibres decreasing bleeding or some physical fibre properties not contributing to the resistance of PSC. The experimental framework for the PSC tests as well as the LV-FRC tests are discussed in the following chapter.

4. EXPERIMENTAL FRAMEWORK

This chapter firstly provides an overview of the objectives of the experimental tests performed in this study. It also discusses the setup, measurements, programme, materials and mix proportions of the tests performed. Finally, it describes the typical procedure of a test.

These experimental tests can be divided into two groups. The first group of tests are performed on conventional concrete to investigate the fundamentals of plastic shrinkage cracking (PSC) focussing on PSC behaviour for different evaporation and bleeding conditions. The second groups of tests are performed on low volume-fibre reinforced concrete (LV-FRC) to determine the effect of physical fibre properties on PSC.

4.1 Test objectives

These experimental tests were performed to achieve the following three objectives:

Objective 1

All the experimental tests will be used to fully understand the behaviour of PSC. It will also be used to confirm the model of PSC behaviour (as described in Section 2.1.3) and determine whether it is acceptable for both conventional concrete as well as LV-FRC.

Objective 2

The first group of experimental tests will be used to investigate the severity of PSC for different evaporation and bleeding conditions.

Objective 3

The second group of experimental tests will primarily be used to determine the effects of different physical fibre properties on PSC. These results could be used to create a framework for a PSC design model.

4.2 Climate chamber test setup

The experimental tests were performed in a state of the art climate chamber. The chamber was mainly designed to simulate ideal conditions for the formation of plastic shrinkage cracks. This was achieved by controlling the temperature, wind speed and relative humidity within the chamber by using a heating element, axial fans and a dehumidifier respectively. The axial fans can be set to a certain speed using a variable speed drive to achieve a desired wind speed within the chamber while temperature and relative humidity can be controlled electronically and values can be preset to create a stable environmental condition. The climate chamber can create conditions with a maximum temperature of 50 °C, minimum relative humidity of 10 % and a maximum wind speed of 70 km/h.

The system (refer to Figure 4-1) starts with the fans creating airflow while a dehumidifier sucks moist air out and blows dry air in. The dry air is heated by a heating element while flowing through the system until it reaches screens positioned to increase flow uniformity. The end result is dry hot air blowing uniformly over the exposed surface of the concrete specimens.

The inside of the chamber compartment is lined with PVC and the wind tunnel is made of galvanized steel sheeting. The test compartment is covered with clear perspex covers. This creates a frictionless surface all around the flowing air and, together with the aerodynamic design of the wind tunnel (Figure 4-1), ensures a smooth uniform air flow within the system. The chamber frame is also covered with waterproofed plywood for insulation. All this contributes to producing a stable environmental condition.

The moulds used for measuring PSC of the concrete specimens are made of PVC. They are based on the design proposed for fresh concrete testing by ASTM C 1579 (2006). The PSC moulds are 600 x 200 x 100 mm (length x width x height) in size with three triangular inserts at the bottom (Figure 4-2). The small triangles act as restraints while the large middle triangle creates a weak point in the specimen forcing PSC to occur directly above it. This simplifies the measuring of the plastic shrinkage cracks. The only alteration to the proposed ASTM C 1579 design is the addition of two steel bars with the purpose of increasing the restraint to plastic shrinkage. Two PSC moulds were used per test to obtain an average result, therefore two tests can be performed simultaneously if they both are to be performed under the same climate conditions.

In addition to the four PSC moulds, the climate chamber also contains two 200 x 200 x 100 mm (length x width x height) moulds used to determine the evaporation (Figure 4-3). These moulds are placed on electronic scales measuring the loss in mass of the concrete specimen. The weight loss represents the weight of evaporated water.

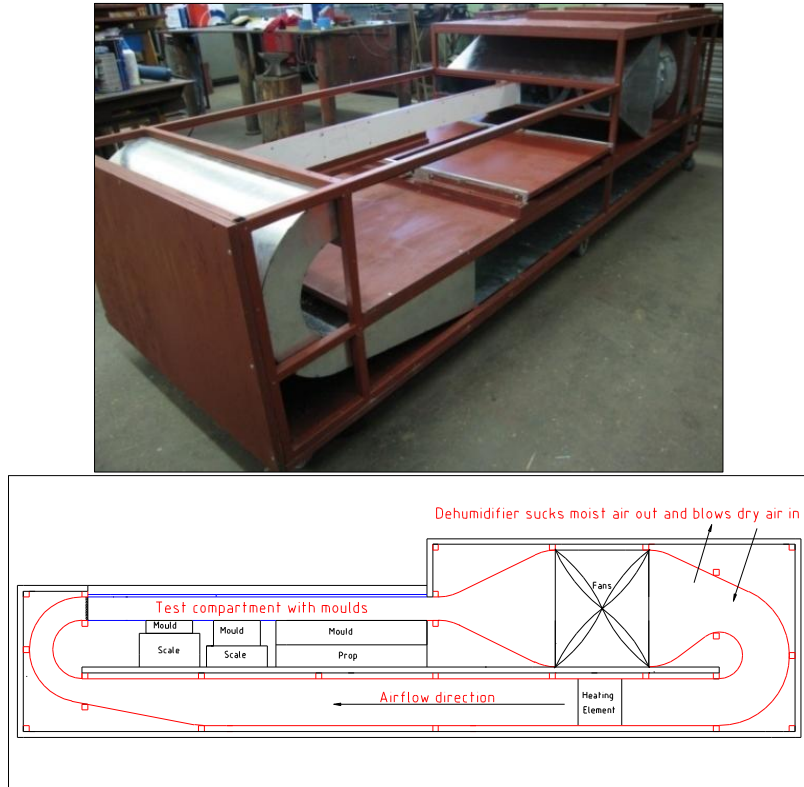


Figure 4-1: Climate chamber layout (Combrinck, 2011:33)



Figure 4-2: PSC mould showing triangular inserts with added steel bars (Combrinck, 2011:33,117)



Figure 4-3: Evaporation mould on electronic scale

4.3 Test measurements

To investigate PSC behaviour the evaporation, bleeding, capillary pressure, setting times and the crack area were measured. All these tests were performed in the climate chamber except for the bleeding tests which were performed in a climate controlled room (with a constant temperature of 23°C and a relative humidity of 60 %). The method for each test is discussed in the following sections as well as a description of the relevant apparatus.

4.3.1 Evaporation

The evaporation from the concrete can be determined by two methods. One method is to place the concrete specimen on an electronic scale which measures the mass reduction of the specimen as evaporation takes place (Figure 4-3). The loss in mass is equal to the mass of moisture evaporated from the concrete. Although this is the most effective method of measuring the true evaporation, another method was used. The reason for this is that the scales were found to be sensitive to small temperature changes. This phenomenon is elaborated in Appendix A.

The alternative method of measuring evaporation is by using Uno's model (Equation 2.1) to determine the evaporation rate from the relative humidity, air temperature, concrete temperature and wind speed measurements. It is explained in Appendix A why the use of Uno's equation instead of the scale evaporation is acceptable for this study.

The relative humidity, air temperature, concrete temperature and wind speed measurements were performed as follows:

4.3.1.1 Relative humidity

The humidity within the climate chamber is controlled by a dehumidifier. The readings were taken at one second intervals and logged onto a computer.

4.3.1.2 Air temperature

The air within the climate chamber can be heated to a specified temperature by means of a heating element. The air temperature was measured with a temperature sensor that logs data points on a computer. Readings were also taken at one second intervals.

4.3.1.3 Concrete temperature

The temperature within the concrete specimen was measured with a temperature sensor that logs data points on a computer. Readings were also taken at one second intervals. The sensors were inserted into copper (effective heat conductors) sleeves placed into the concrete through the side of the mould (Figure 4-4). The sleeves prevent damage to the sensors by the hardening concrete.

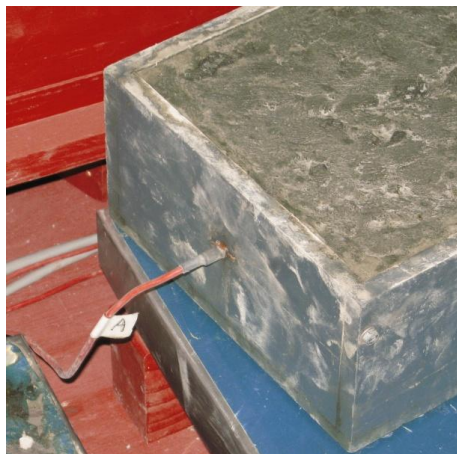


Figure 4-4: Concrete temperature sensors

4.3.1.4 Wind speed

Specified constant wind speeds can be achieved by changing the speed of the two axial fans using a variable speed drive. A small anemometer with a rotary fan (Figure 4-5) was used to verify the wind speed measurements in km/h. It has an accuracy of $\pm 3\%$ for winds of up to 150 km/h.



Figure 4-5: Anemometer for wind speed measurements

4.3.2 Bleeding

The bleeding was measured using a method developed by Josserand *et al.* (2004). A cylindrical PVC mould (bleeding mould) with a height and diameter of 120 mm was used as shown in Figure 4-6. However, the bleeding mould was only filled with concrete to a height of 100 mm. This is to ensure an identical concrete depth in the bleeding moulds and the moulds used in the climate chamber. Therefore the bleeding, evaporation and crack area for each concrete mix can be compared since the influence of concrete depth is eliminated.



Figure 4-6: Bleeding moulds, syringe and shaped device used for bleeding measurements

A track was made on the surface of the concrete in the bleeding mould using a shaped device as shown in Figure 4-6. The moulds were then covered to prevent evaporation from taking place. Bleeding water accumulates in the tracks and was extracted at 20 minute intervals for measuring purposes using a 10 ml syringe. Using a scale with 0.1 gram sensitivity the mass of the extracted water was measured. As the water in the syringe usually also contains tiny particles of cement and fine aggregate, the extracted water was measured twice, once with the particles and then again once only the water has been transferred to another container. Between intervals the entire bleeding mould with concrete specimen was also weighed to determine the small amount of bleeding water that has been lost due to evaporation.

The bleeding measurements were performed in a climate controlled room with a humidity of 60 % and a temperature of 23°C. Ideally the bleeding specimens should be placed in the climate chamber together with the other concrete specimens. However, it was not possible to perform the bleeding measurements while the bleeding specimens were in the chamber. Also, since particle settlement

plays such a significant role in bleeding, it was decided not to place the bleeding specimens in the chamber and remove them every 20 minutes since these disturbances could easily influence the particle settlement. Therefore it was decided to place the bleeding specimens in the climate controlled room where measurements could easily be taken while conditions remained constant for all tests and movement of the specimens could be kept to a minimum. Unfortunately this means that the bleeding measurements were performed at a lower temperature than the other measurements (in the climate chamber) which could influence the setting times slightly and in turn influences the bleeding. Therefore the results from the bleeding measurements may slightly differ to the actual bleeding taking place in the concrete specimens within the climate chamber. It is believed that the delayed setting time due to lower temperatures could mean that the results indicate a slightly higher bleeding rate and capacity. However, since this small margin of error is the same for all tests, it is considered as acceptable for this study.

4.3.3 Capillary pressure

The capillary pressure was measured using a method based on experiments performed by Slowik *et al.* (2008). Small electronic pressure sensors were extended with metal tubes with a diameter of 3 mm. The tubes were filled with distilled water and plugged with a sponge at the end to prevent solid particles from entering. The tubes were inserted into the concrete specimen (PSC mould) 35 mm from the concrete surface. Their main purpose was to extend the sensor to just above the middle triangle of the PSC mould (see Figure 4-2) as this is where PSC is likely to occur. Figure 4-7 shows the pressure sensor used to measure capillary pressure.



Figure 4-7: Capillary pressure sensor

4.3.4 Setting time

A Vicat apparatus was used to perform a normal penetration test to determine the initial and final setting times of the concrete. This was done in accordance with SANS 50196-3 (2006:9-14). The initial setting time is reached when the standard 1.1 mm diameter initial setting time needle

with:

CA = crack area at specific time interval [mm^2]

cw = average crack width of all line segments at specific time interval [mm]

nls = number of 10 mm line segments used to measure the crack length

It is believed that this method results in accurate and precise crack measurements as all measurements are performed by the same consistent procedure. Figure 4-9 shows an example of how these measurements were performed.

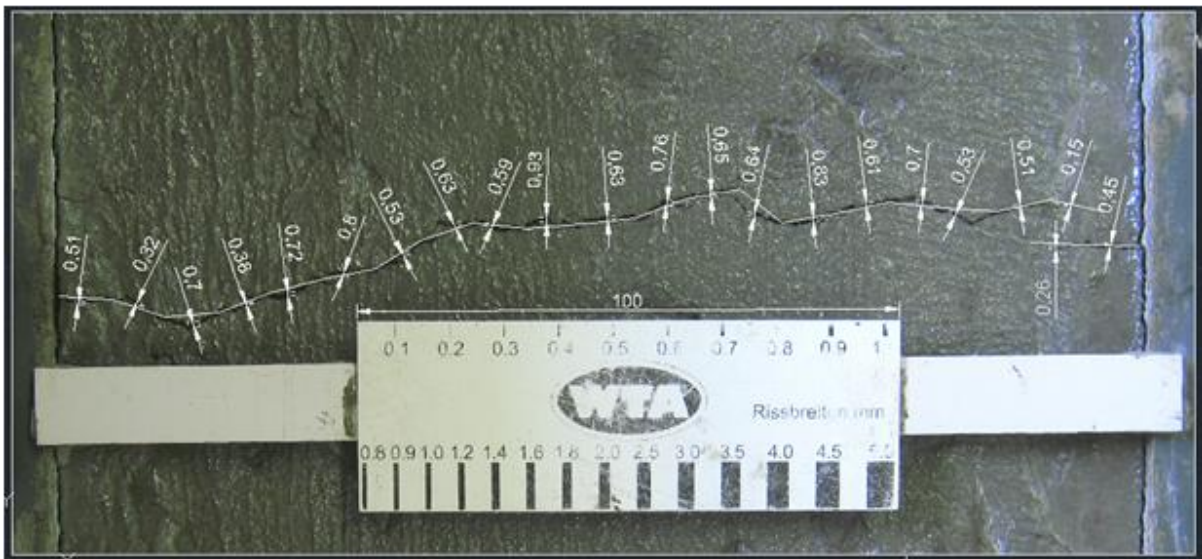


Figure 4-9: Typical image with measurements used to determine crack area

4.4 Test programme

The experimental tests performed can be divided into two groups. The first group includes the PSC tests with conventional concrete used for Objectives 1 and 2 (see Section 4.1). The second group includes the PSC tests with LV-FRC and is used for Objectives 1 and 3. This section discusses each group of tests and provides a summary of all tests performed.

4.4.1 PSC tests with conventional concrete

This group of tests is primarily used to determine PSC behaviour for concrete with different bleeding levels in different climate conditions. The following three different climate conditions and bleeding levels were combined to create nine different PSC situations altogether.

4.4.1.1 Climate conditions

Uno (1998:372) as well as Pelisser (2010:2172) considered an evaporation rate of 1.0 kg/m²/h to be an extreme condition. Based on this the three different climate conditions used resulted in evaporation rates of ± 1.0, 0.6 and 0.2 kg/m²/h. These are considered to be a high, moderate and low evaporation rates, respectively, and are defined as the HE, ME and LE climate conditions respectively. The climate conditions are selected by using Uno's equation (Equation 2.1) to calculate the evaporation rate. The required evaporation rate can be obtained by changing the wind speed, humidity and/or air temperature in the climate chamber. A concrete temperature of 23°C was used, as this was the initial temperature of the concrete specimens. For this study only the wind speed and relative humidity was varied, while the temperature was kept constant to achieve the different evaporation rates. Table 4-1 shows the climate conditions used in this study.

Table 4-1: Climate conditions

	Low evaporation climate condition (LE)	Moderate evaporation climate condition (ME)	High evaporation climate condition (HE)
Concrete temperature [°C]	23	23	23
Air temperature [°C]	40	40	40
Humidity [%]	15	15	10
Wind speed [km/h]	3	13	21
Evaporation rate [kg/m ² /h]	0.24	0.59	1.03

4.4.1.2 Bleeding levels

The three bleeding levels were chosen by the same criteria as the evaporation rates. Therefore the high, moderate and low bleeding rate levels are also ± 1.0, 0.6 and 0.2 kg/m²/h respectively (Table 4-2). These conditions are defined as the HB, MB and LB bleeding levels respectively. To achieve these bleeding rates the composition of the concrete specimens had to be varied. To ensure comparability only the grading of fine aggregates of each mix were changed to achieve the different bleeding levels. A detailed discussion of this is included in Sections 4.5 and 4.6.

Table 4-2: Bleeding rate levels

	Low bleeding rate level (LB)	Moderate bleeding rate level (MB)	High bleeding rate level (HB)
Bleeding rate [kg/m ² /h]	0.2	0.6	1.0

4.4.2 PSC tests with LV-FRC

The tests performed with LV-FRC are mainly used to determine the effect of the physical fibre properties on PSC. This was achieved by changing a single physical fibre property at a time, keeping

all other factors influencing PSC constant for all tests. Therefore the concrete evaporation rate, bleeding, concrete composition and restraints are identical for each test, except for the change in fibre property and the resulting influence this has on the bleeding rate.

All tests were performed using the HE climate condition and using a LB concrete specimen (as described in Sections 4.4.1.1 and 4.4.1.2) with the exception of one test with a high bleeding rate level. This combination of high evaporation and low bleeding is considered to be a severe PSC risk. The reason for the use of this combination is so that the influence of the fibres can be more pronounced and thus easier to observe.

The fibre properties under investigation include the fibre volume, length, diameter and type. A standard value for each property was chosen while one value was varied to investigate its influence. These properties are presented in Table 4-3 with the standard value printed in bold.

Table 4-3: Alternating fibre properties used for tests with the reference value in bold

Fibre volumes (%)	0.05, 0.075, 0.1 & 0.15
Fibre lengths (mm)	6, 12 & 24
Fibre diameters (μm)	20 & 35
Fibre types	polypropylene , fluorinate polypropylene & polyester

In addition, one test is performed with a high bleeding rate specimen to investigate the effect of fibres when the PSC risk is lower.

4.4.3 Summary of all tests performed in the climate chamber

Table 4-4 includes a summary of the experimental tests performed showing the evaporation climate condition, bleeding rate level, fibre properties and the relevance of each test to this study.

Although the standard fibre type used for this study is Polypropylene, the fibre length tests (Tests 14 to 16) were performed with Polyester as the standard fibre type, 20 μm as the standard fibre diameter and 0.065 % as the standard fibre volume. The 0.065 % volume resulted in the same dosage (in mass) as for the 0.1 % polypropylene tests because of the different relative densities. The reason for the use of polyester is that these were the only fibres available at the time of testing that had different lengths while all other properties remained identical. However, this is still acceptable since Tests 14 to 16 were only compared to each other and only have one varying fibre property, namely the fibre length.

Table 4-4: Summary of experimental test programme

Test Details		Evaporation Climate Conditions	Bleeding Rate Level	Fibre Properties				Investigation Relevance / Effect of:
Group	Number			Type	Volume [%]	Length [mm]	Diameter [μ m]	
PSC tests with conventional concrete	1	High	Low	-	-	-	-	PSC behaviour for different evaporation and bleeding conditions
	2	High	Moderate	-	-	-	-	
	3	High	High	-	-	-	-	
	4	Moderate	Low	-	-	-	-	
	5	Moderate	Moderate	-	-	-	-	
	6	Moderate	High	-	-	-	-	
	7	Low	Low	-	-	-	-	
	8	Low	Moderate	-	-	-	-	
	9	Low	High	-	-	-	-	
PSC tests with LV-FRC	10a	High	Low	Polypropylene	0.1	12	35	Standard / Control
	10b	High	Low	Polypropylene	0.1	12	35	
	11	High	Low	Polypropylene	0.05	12	35	Fibre volume
	12	High	Low	Polypropylene	0.075	12	35	Fibre volume
	13	High	Low	Polypropylene	0.15	12	35	Fibre volume
	14	High	Low	Polyester	0.065	6	20	Fibre length
	15	High	Low	Polyester	0.065	12	20	Fibre length
	16	High	Low	Polyester	0.065	24	20	Fibre length
	17	High	Low	Polypropylene	0.1	12	20	Fibre diameter
	18	High	Low	Fluorinated Polypropylene	0.1	12	35	Fibre type
19	High	High	Polypropylene	0.1	12	35	Fibres at lower PSC risk	

4.5 Materials

This section describes the materials used for the experimental tests. These materials include aggregates, cement and fibres.

4.5.1 Fine aggregates

The fine aggregates play a significant role in this study as it was the only mix component that was varied in order to achieve different bleeding rates. The fine aggregates used were Greywacke crusher dust sieved through a 2 mm sieve and a coarse, natural sand known locally as Malmesbury Sand. The crusher dust was sieved to increase the fineness which will decrease the bleeding. Figure 4-10 shows the grading of these two sand types in accordance with SANS 1083 (2002).

Figure 4-10 indicates that these two sands have a similar grading except for the high dust content (material passing the 75 μ m sieve) found in the crusher dust.

The natural sand (Malmesbury Sand) serves as the base material of the fine aggregates in this study. This is blended with increasing fractions of crusher dust to reduce the amount of bleeding. The reason for a reduction of bleeding is made clear when considering the properties of these two sands. The fine aggregate properties are given in Table 4-5. The fineness modulus was determined according to SANS 1083 (2002:2-4). The two sands are further discussed in the following two sections.

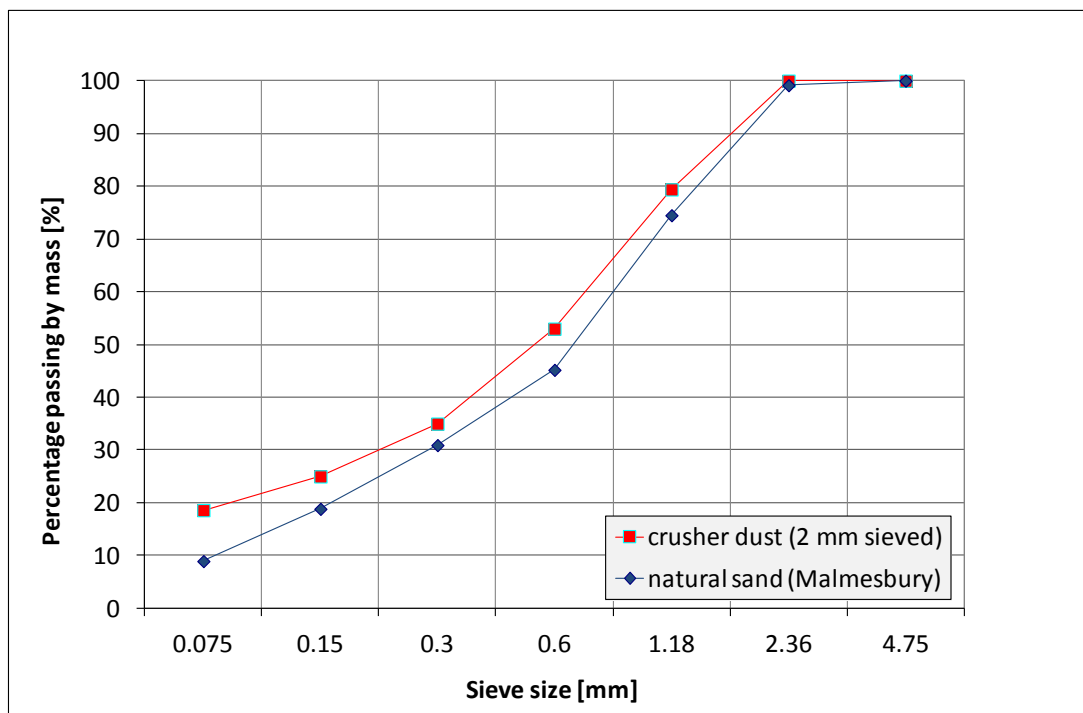


Figure 4-10: Grading of fine aggregates

Table 4-5: Fine aggregate properties

Fine aggregate	Fineness modulus	Relative density	Particle shape
Natural sand (Malmesbury)	2.3	2.69	rounded
Greywacke crusher dust (2mm sieved)	2.1	2.6	angular

4.5.1.1 Natural sand (Malmesbury Sand)

Natural sand is formed by natural disintegration of rock and therefore has a rounded particle shape. The concrete specimens containing only the Malmesbury Sand have a high bleeding rate and capacity. The reason for this is the lack of ultra fine dust particles ($< 5 \mu\text{m}$) as well as the lower surface area of the rounded particles (as explained in Section 2.1.2.2). Figure 4-11 shows a scanning electron microscope (SEM) image of the particles passing the $75 \mu\text{m}$ sieve. This image indicates the rounded particle shape and also shows that the smallest particle sizes vary between 20 and $40 \mu\text{m}$.

The images in Figures 4-11 to 4-13 were taken at the same magnification and therefore the particle sizes can be easily compared.

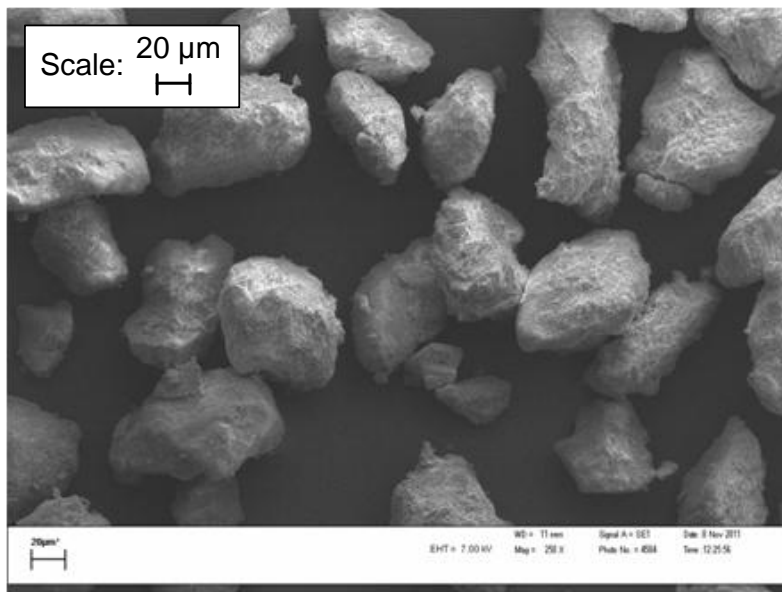


Figure 4-11: SEM image of ultra-fine particles of the Malmesbury Sand

4.5.1.2 Greywacke crusher dust

Crusher dust is formed by the mechanical crushing of rock and therefore typically has an angular particle shape. Increasing the fraction of crusher dust decreases the bleeding rate and capacity significantly. This can be explained by the high amount of fine particles smaller than $5\ \mu\text{m}$ as well as the angular shape of the particles (as explained in Section 2.1.2.2). Figure 4-12 shows a SEM image of the crusher dust particles passing the $75\ \mu\text{m}$ sieve. This image clearly indicates the angular particle shape as well as the high amount of fine particles smaller than $5\ \mu\text{m}$.

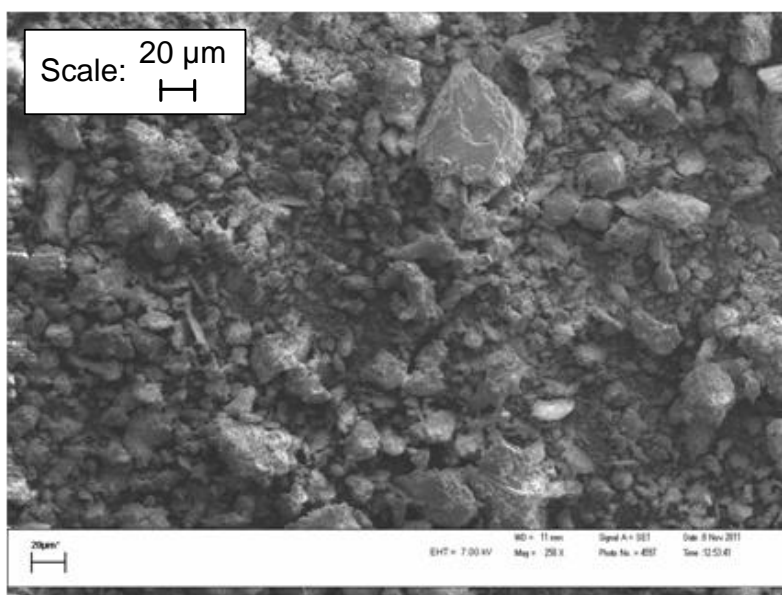


Figure 4-12: SEM image of ultra-fine particles of the Greywacke crusher dust

4.5.2 Coarse aggregates

Greywacke stone with a nominal size of 19 mm and relative density of 2.71 was used for all experimental tests. The stone was graded in accordance with SANS 1083 (2002).

4.5.3 Cement

A CEM II 32.5 cement with a relative density of 3.0 was used for all experimental tests as supplied by PPC (Pretoria Portland Cement Co. Ltd.). A SEM image of the cement particles is provided (Figure 4-13) to give an idea of how the particle size of the fine aggregates compare to the cement. The influence of the cement particles on bleeding is discussed in Section 2.1.2.2.

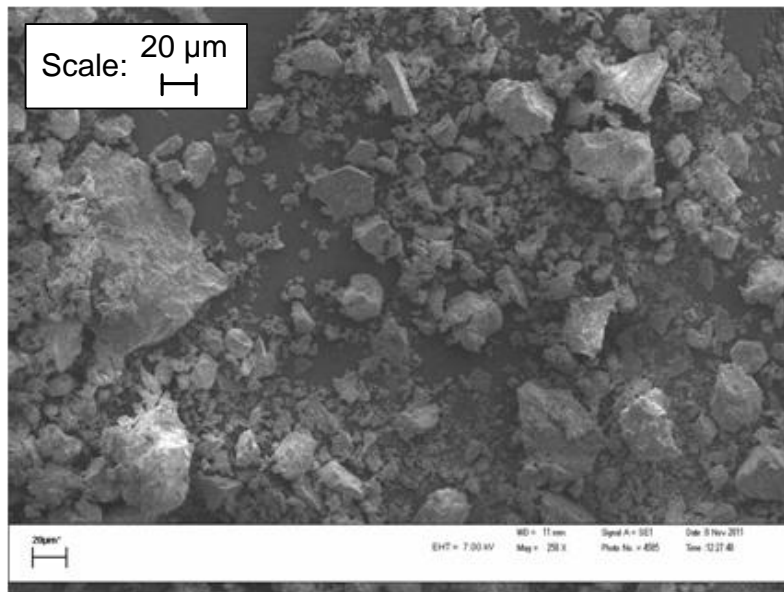


Figure 4-13: SEM image of cement particles

4.5.4 Fibres

As previously mentioned the fibres used in this study are polypropylene, fluorinated polypropylene and polyester fibres. These fibres were supplied by Sapy (South African Polypropylene Yarns) (Pty) Ltd., Chryso SA (Pty) Ltd. and Hosaf Fibres (Pty) Ltd, respectively. A summary of the important properties of the fibres used in this study is shown in Table 4-6.

Table 4-6: Range of fibre properties used in the experimental tests

Fibre type	Relative density	Volume fractions [%]	Dosages [kg/m ³]	Lengths [mm]	Diameters [μm]
Polypropylene	0.9	0.05 - 0.15	0.45 - 1.35	12	20 - 35
Fluorinated polypropylene	0.9	0.1	0.9	12	35
Polyester	1.38	0.065	0.9	6 - 24	20

To verify the diameters of the fibres used in the experimental tests, SEM images were taken for all the diameters of each fibre type used. They are shown in Figure 4-14.

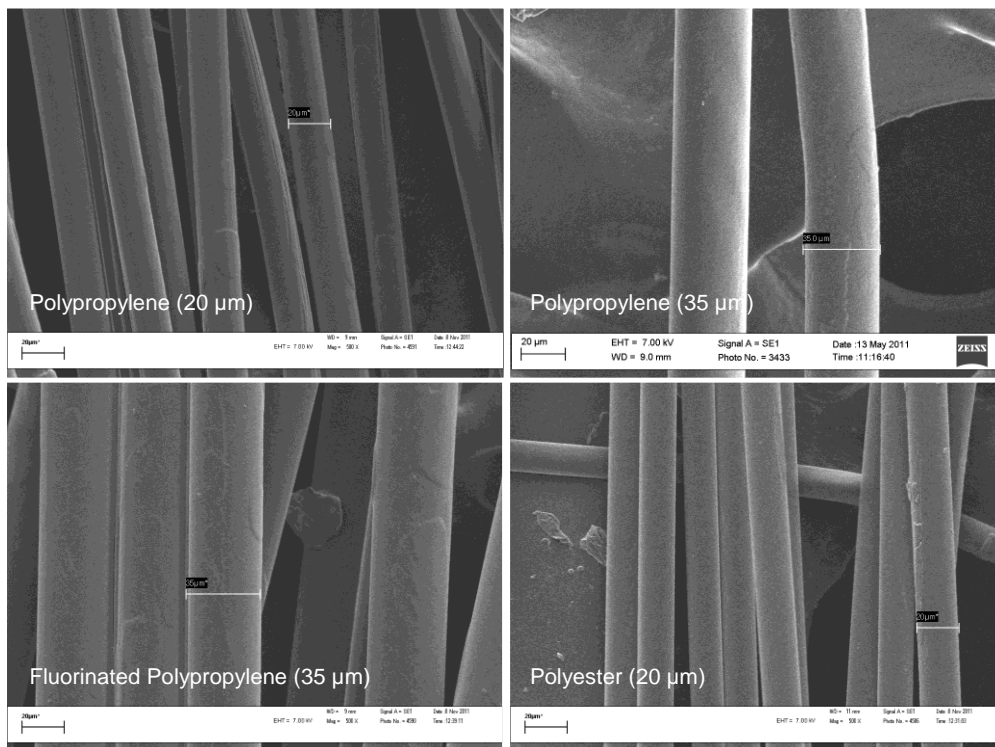


Figure 4-14: SEM images verifying fibre diameters

4.6 Mix proportions

The mix proportions for the conventional concrete tests as well as the LV-FRC tests are discussed in the following sections.

4.6.1 Conventional concrete (Tests 1 to 9)

Three different mixes (high, moderate and low bleeding mixes) were designed for the conventional concrete tests. These mixes all have the same water, cement (thus the same w/c ratio of 0.4) and coarse aggregate content. Only the fineness of the fine aggregate differed for each mix. Tables 4-7 to 4-9 indicate the mix proportions for each mix.

Table 4-7: Mix proportions for low bleeding mix of conventional concrete tests

Content	[kg/m ³]
Water	226
Cement (CEM II 32.5)	564
19 mm Greywacke stone	876
Natural sand (Malmesbury)	238
Greywacke crusher dust (2 mm sieved)	461

The low bleeding mix had poor workability but showed good cohesion and no segregation. The slump test readings varied between 20 and 40 mm. The fine aggregates consisted of 65 % crusher dust and 35 % natural sand.

Table 4-8: Mix proportions for moderate bleeding mix of conventional concrete tests

Content	[kg/m ³]
Water	226
Cement (CEM II 32.5)	564
19 mm Greywacke stone	876
Natural sand (Malmesbury)	511
Greywacke crusher dust (2 mm sieved)	177

The moderate bleeding mix had an average workability and good cohesion as well as no segregation. The slump test readings varied between 60 and 80 mm. The fine aggregates consisted of 25 % crusher dust and 75 % natural sand.

Table 4-9: Mix proportions for high bleeding mix of conventional concrete tests

Content	[kg/m ³]
Water	226
Cement (CEM II 32.5)	564
19 mm Greywacke stone	876
Natural sand (Malmesbury)	681
Greywacke crusher dust (2 mm sieved)	0

The high bleeding mix was extremely workable but was at the verge of segregation. However, the mix was still acceptable as a high bleeding concrete mix. The slump test readings varied between 140 and 160 mm. Only natural sand was used as fine aggregate.

It should be kept in mind that the main purpose of these mixes was to create different levels of bleeding and therefore their workability and cohesion are of minor importance.

4.6.2 LV-FRC (Tests 10 to 19)

All the LV-FRC tests were performed with the low bleeding mix with the exception of one high bleeding LV-FRC test. Table 4-10 shows the mix proportions for each LV-FRC test with the fibre additions as the main variation.

All the low bleeding mixes with added fibres showed very little workability with slump tests of between 5 and 10 mm. Once again it should be kept in mind that the workability is of minor importance for this study.

Table 4-10: Mix proportions for LV-FRC tests

Components	Test number									
	10	11	12	13	14	15	16	17	18	19
	Content [kg/m ³]									
Water	226	226	226	226	226	226	226	226	226	226
Cement (CEM II 32.5)	564	564	564	564	564	564	564	564	564	564
19 mm Greywacke stone	876	876	876	876	876	876	876	876	876	876
Malmesbury sand	238	238	238	238	238	238	238	238	238	681
Greywacke crusher dust (2 mm sieved)	461	461	461	461	461	461	461	461	461	0
Polypropylene fibres (12 mm, 20 µm)	-	-	-	-	-	-	-	0.9	-	-
Polypropylene fibres (12 mm, 35 µm)	0.9	0.45	0.675	1.35			-	-	-	0.9
Fluorinated Polypropylene fibres (12 mm, 35 µm)	-	-	-	-	-	-	-	-	0.9	-
Polyester fibres (6 mm, 20 µm)	-	-	-	-	0.9	-	-	-	-	-
Polyester fibres (12 mm, 20 µm)	-	-	-	-	-	0.9	-	-	-	-
Polyester fibres (24 mm, 20 µm)	-	-	-	-	-	-	0.9	-	-	-

4.7 Test procedure

Firstly, the heating element and fans were switched on the day before testing in order for the climate chamber to stabilise at the required temperature and wind speed. It was only necessary to switch on the dehumidifier two hours before the test for the relative humidity to stabilise. The mix components were placed in a climate controlled room with a temperature of 23°C the previous day to ensure a constant initial concrete temperature of 23°C at the time of mixing. The mixing water was also placed in the climate room the previous day and therefore had to be measured again just before mixing to ensure that evaporated water could be replaced.

Before mixing, each mould received a thin layer of oil to ensure a frictionless surface and to simplify the demoulding process. The capillary pressure sensors and tubes were then prepared and placed in the moulds.

The dry components were mixed for 30 seconds before the water was added. The concrete was then mixed for another 150 seconds. At this time the fibres (if included) were added while the mixing continued for another 150 seconds.

When mixing was completed, a slump test was performed before filling the PSC and evaporation moulds and vibrating them until the majority of entrapped air has escaped. The setting moulds were filled with the concrete paste obtained from the concrete vibrated through a 4.75 mm sieve. All the moulds were placed in the climate chamber except for the bleeding moulds which were placed in a climate controlled room. The setting times, bleeding and crack area measurements (items not measured by the computer) were conducted at 20 minute intervals. The crack area was measured until one hour after the final setting time of the concrete.

4.8 Concluding summary

This chapter discussed the experimental framework for the PSC tests performed with conventional concrete as well as with LV-FRC. Both groups of tests were performed in the state of the art climate chamber designed to simulate conditions resulting in a specific evaporation rate. Bleeding, setting times, capillary pressure and crack growth measurements were performed and used to investigate PSC behaviour as well as the influence of fibres on PSC. The results of the experimental tests are presented in the next chapter.

5. EXPERIMENTAL RESULTS

This chapter presents the experimental results obtained from tests performed with conventional concrete as well as LV-FRC. Table 5-1 provides a summary of the test details as well as a test code used to easily identify the varying factors of each test.

Table 5-1: Summary of test details

Test Details		Investigation Relevance / Effect of:	Test Code*
Group	Number		
PSC tests with conventional concrete	1	PSC behaviour for different evaporation and bleeding conditions	T1_HE_LB
	2		T2_HE_MB
	3		T3_HE_HB
	4		T4_ME_LB
	5		T5_ME_MB
	6		T6_ME_HB
	7		T7_LE_LB
	8		T8_LE_MB
	9		T9_LE_HB
PSC tests with LV-FRC	10a	Standard / Control	T10a_HE_LB_PP_0.1%_12mm_35µm
	10b		T10b_HE_LB_PP_0.1%_12mm_35µm
	11	Fibre volume	T11_HE_LB_PP_0.05%_12mm_35µm
	12		T12_HE_LB_PP_0.075%_12mm_35µm
	13		T13_HE_LB_PP_0.15%_12mm_35µm
	14	Fibre length	T14_HE_LB_PE_0.065%_6mm_20µm
	15		T15_HE_LB_PE_0.065%_12mm_20µm
	16		T16_HE_LB_PE_0.065%_24mm_20µm
	17	Fibre diameter	T17_HE_LB_PP_0.1%_12mm_20µm
	18	Fibre type	T18_HE_LB_FPP_0.1%_12mm_35µm
19	Fibres at lower PSC risk	T19_HE_HB_PP_0.10%_12mm_35µm	
<p>*Test Code = Test number_Evaporation climate condition_Bleeding level_Fibre type_Fibre volume_Fibre length_Fibre diameter</p> <p>with:</p> <p>HE = High Evaporation climate condition</p> <p>ME = Moderate Evaporation climate condition</p> <p>LE = Low Evaporation climate condition</p> <p>HB = High Bleeding rate level</p> <p>MB = Moderate Bleeding rate level</p> <p>LB = Low Bleeding rate level</p> <p>PP = Polypropylene fibres</p> <p>FPP = Fluorinated Polypropylene fibres</p> <p>PE = Polyester fibres</p>			

The individual test results are divided into sections according to the test objectives as described in Section 4.1. Appendix B provides all the plastic shrinkage cracking results used for these objectives as well as summarising graphs of the concrete temperature and air temperature results for both the conventional concrete as well as the LV-FRC tests.

5.1 Test results for Objective 1: To investigate PSC behaviour and confirm the model for PSC behaviour

In this section typical PSC test results used to investigate the model for PSC behaviour are shown. All of the results can be found in Appendix B. Also included in this section are summaries of the evaporation and bleeding results obtained for each test.

5.1.1 Typical results used to investigate PSC behaviour

Figure 5-1 shows typical results complying with the model for PSC behaviour while Figure 5-2 shows results that slightly disagrees with the model behaviour. Figure 5-3 shows typical results of the PSC behaviour for a LV-FRC test. The results are further discussed in Chapter 6.

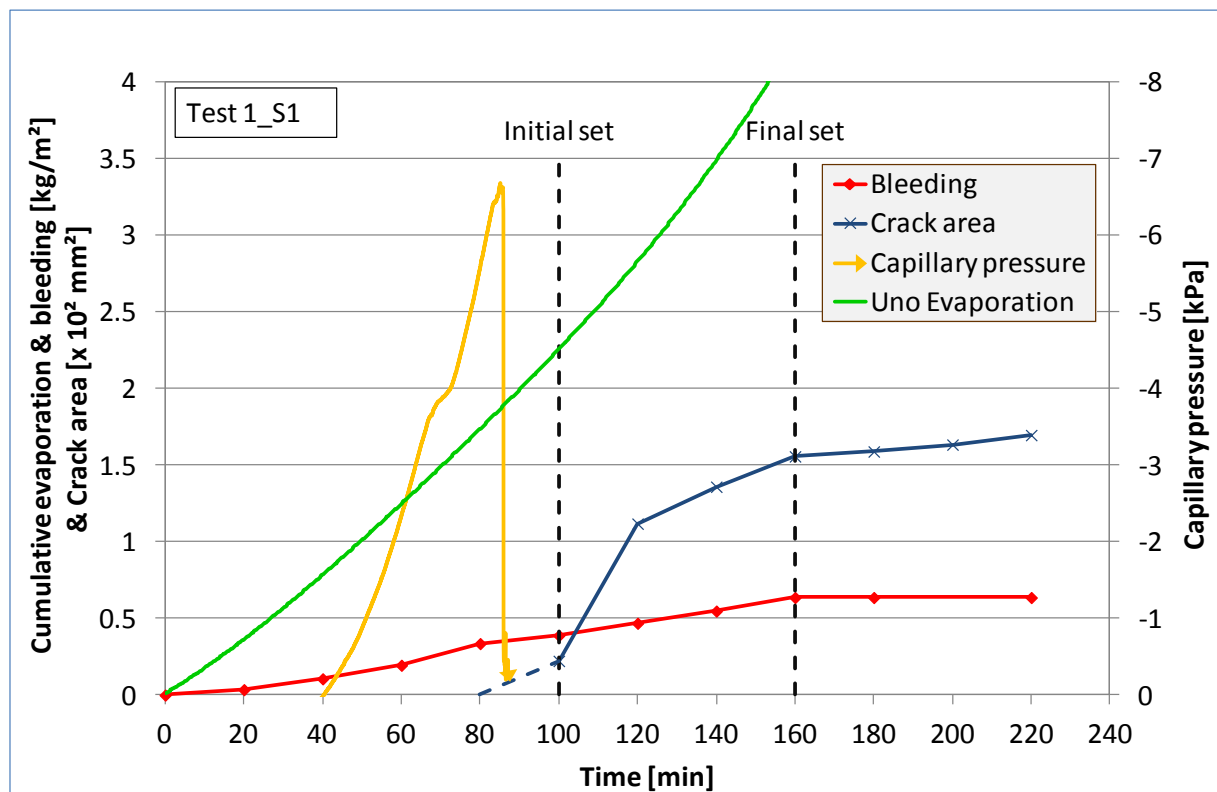


Figure 5-1: Results for Specimen 1 of Test 1 (high evaporation and low bleeding conditions)

Chapter 5: Experimental results

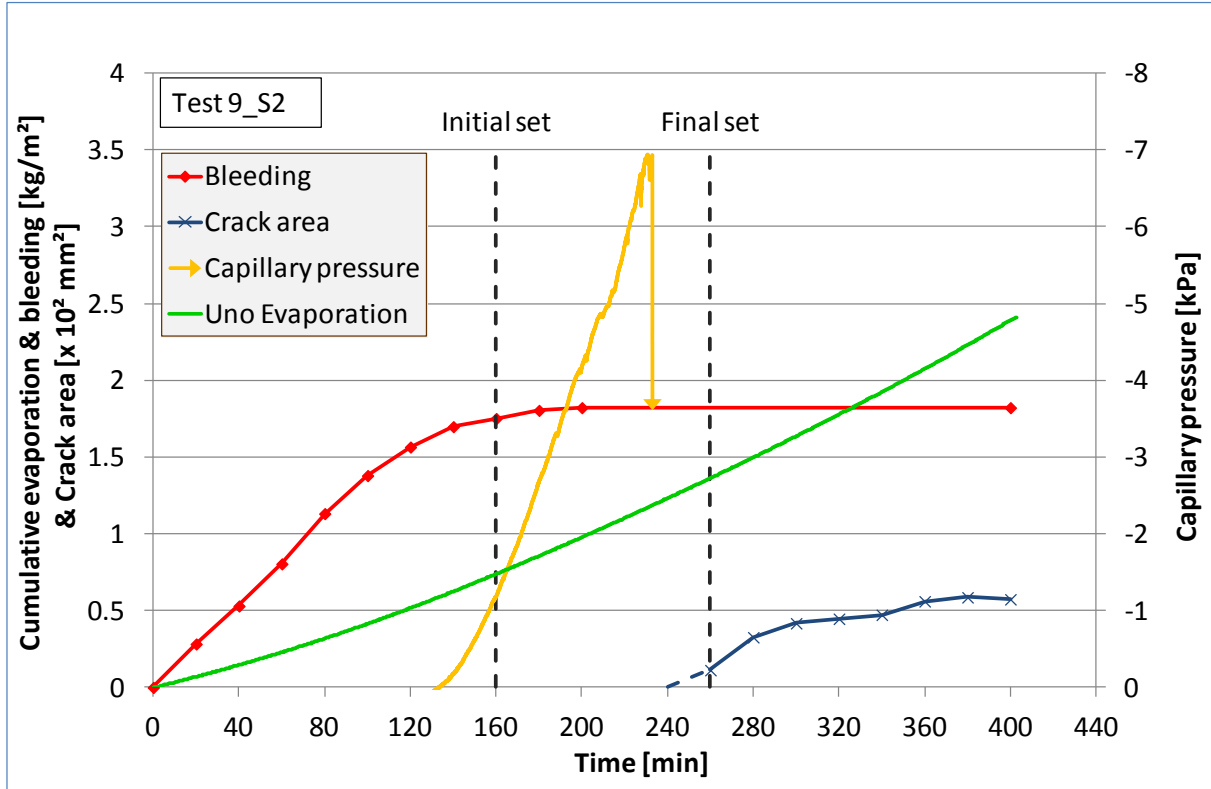


Figure 5-2: Results for Specimen 2 of Test 9 (low evaporation and high bleeding conditions)

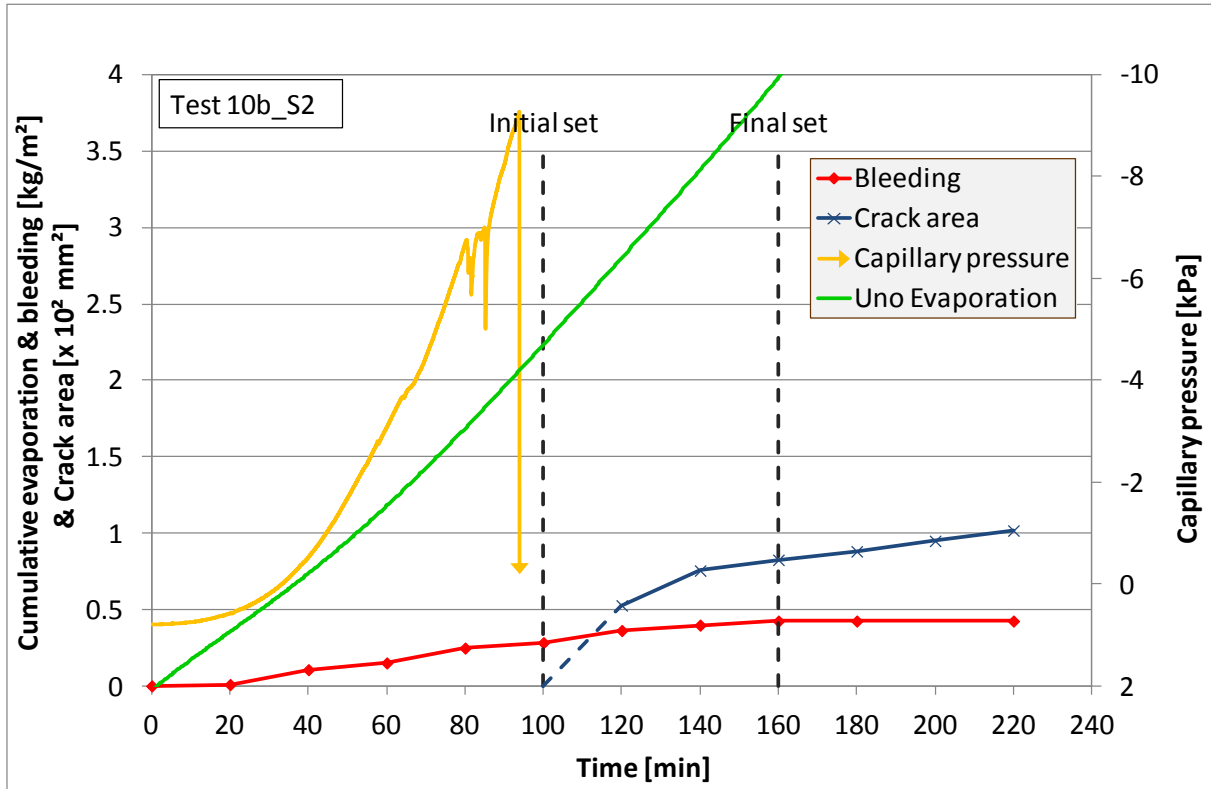


Figure 5-3: Results for Specimen 2 of Test 10b (addition of 0.1 % Polypropylene fibres)

5.1.2 Summaries of the cumulative Uno evaporation results

Figures 5-4 and 5-5 show the results of the Uno evaporations for all conventional concrete as well as LV-FRC tests. The results indicate that the requirements for the evaporation climate conditions as prescribed in Section 4.4 were achieved.

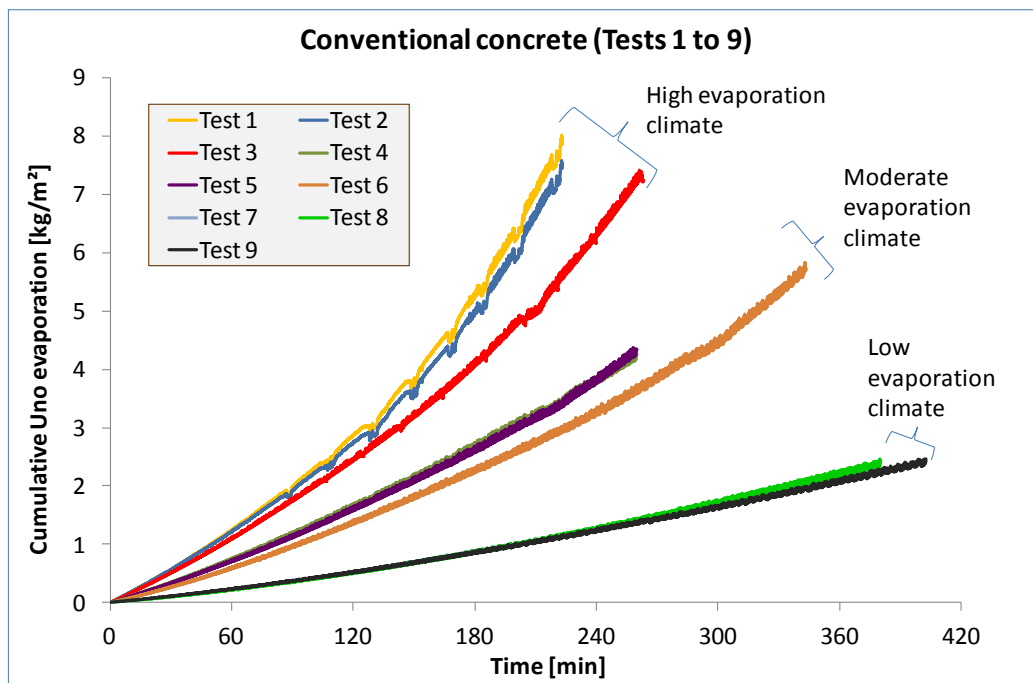


Figure 5-4: Cumulative evaporation results for Tests 1 to 9

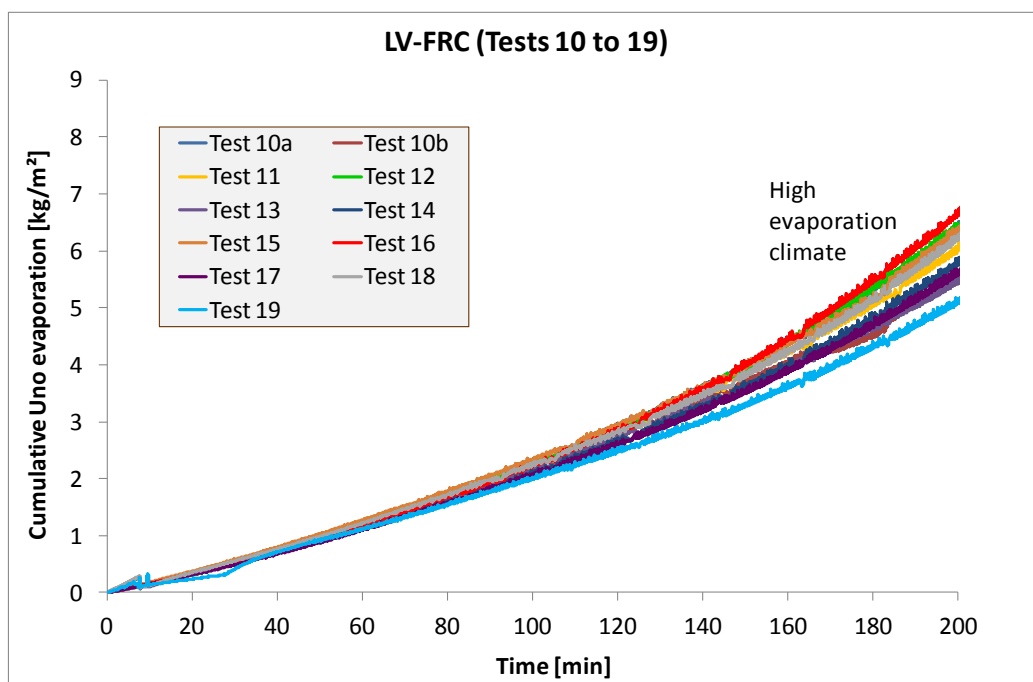


Figure 5-5: Cumulative evaporation results for Tests 10 to 19

5.1.3 Summaries of the cumulative bleeding results

Figures 5-6 and 5-7 show the bleeding results of all conventional concrete as well as LV-FRC tests. The results indicate that the requirements for the bleeding levels as prescribed in Section 4.4 were achieved. Although the bleeding results for Test 9 is slightly lower than required, it is still higher than the moderate bleeding level of the same climate condition (Test 8) and therefore still considered as acceptable.

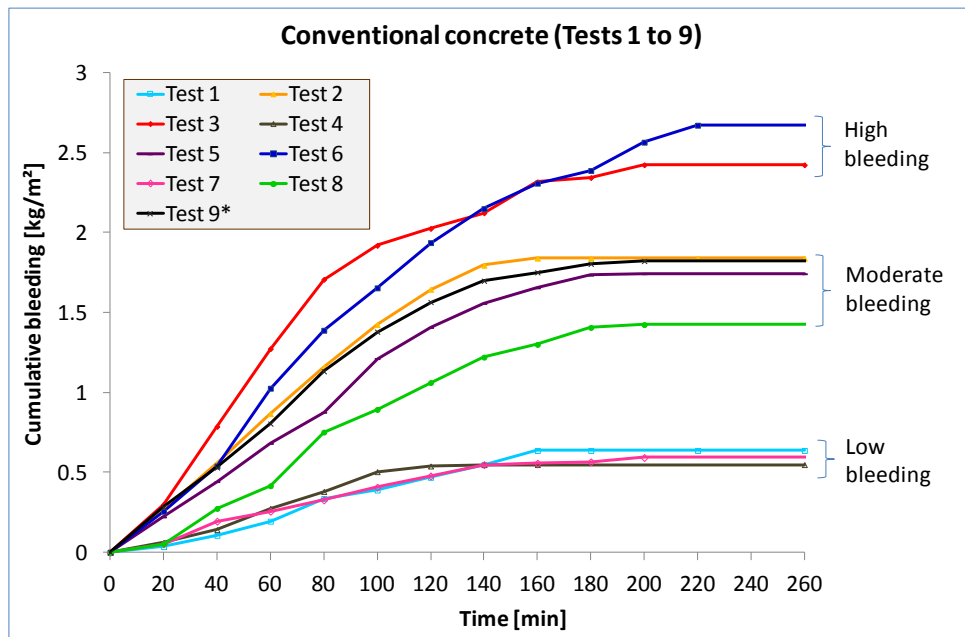


Figure 5-6: Cumulative bleeding results for Tests 1 to 9

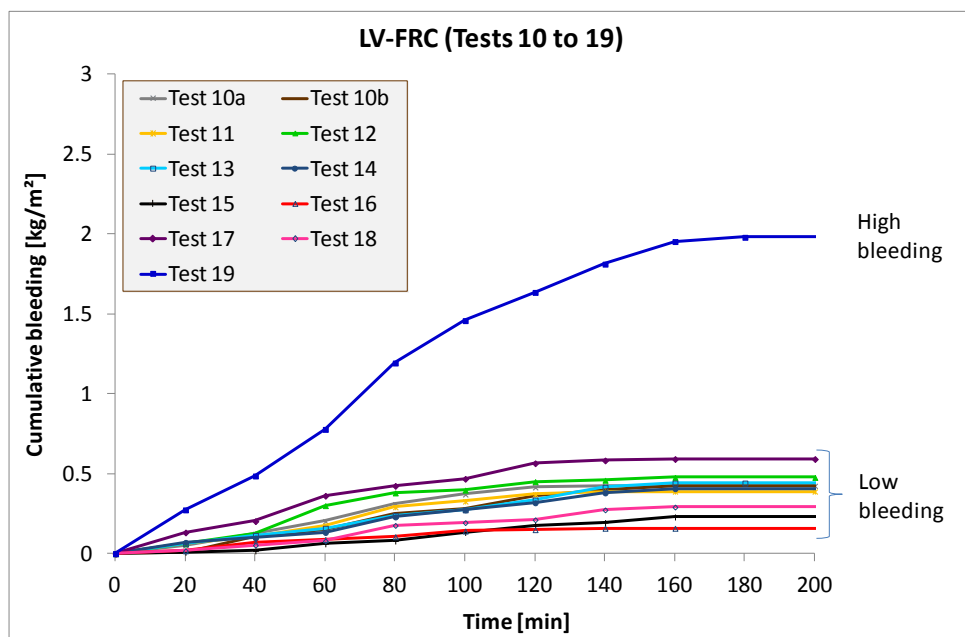


Figure 5-7: Cumulative bleeding results for Tests 10 to 19

5.2 Test results for Objective 2: Investigation of PSC severity for different bleeding and evaporation conditions

This section shows the results used for the investigation of the PSC severity under different bleeding and evaporation conditions. These results include the Uno evaporation, bleeding measurements, setting times and average crack area measurements (average of the two specimens per test) for the tests performed with conventional concrete (Tests 1 to 9). For each evaporation climate condition, Figures 5-8 to 5-10 show the results for the three different bleeding conditions:

- a) low bleeding;
- b) moderate bleeding; and
- c) high bleeding

The results shown hereafter are discussed in Chapter 6.

Chapter 5: Experimental results

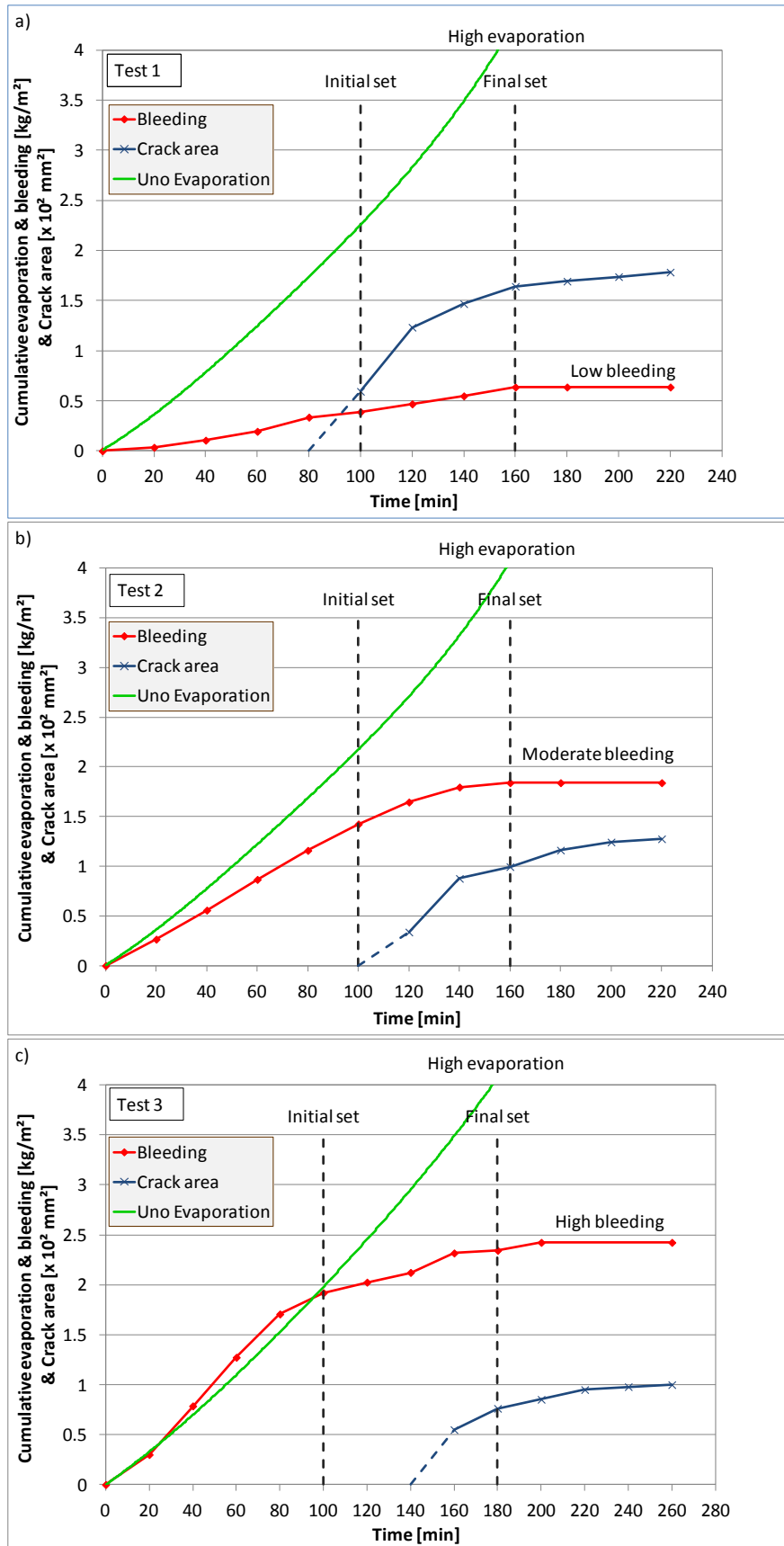


Figure 5-8 a, b & c: Average results for a high evaporation climate (Tests 1 to 3)

Chapter 5: Experimental results

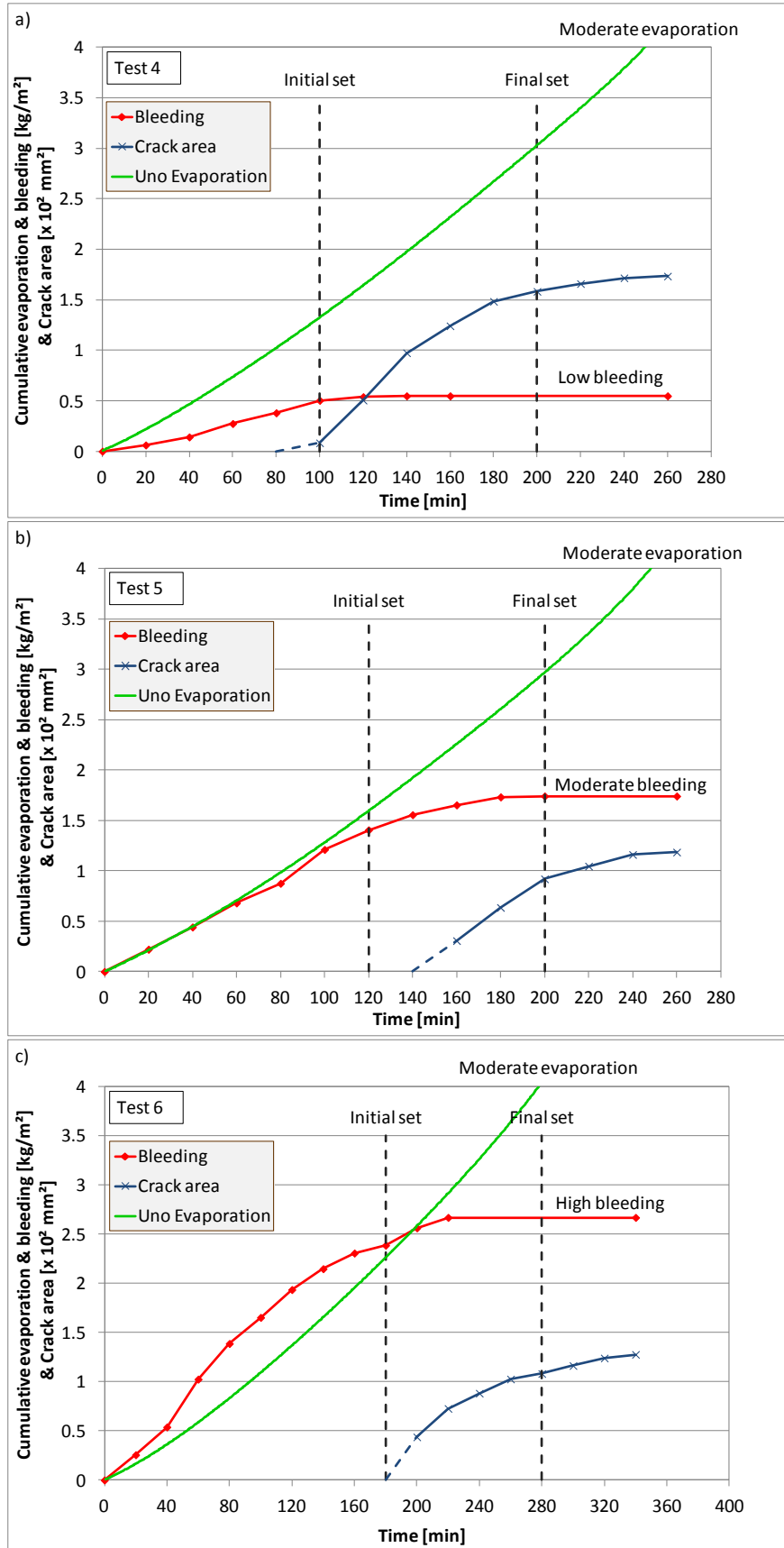


Figure 5-9 a, b & c: Average results for a moderate evaporation climate (Tests 4 to 6)

Chapter 5: Experimental results

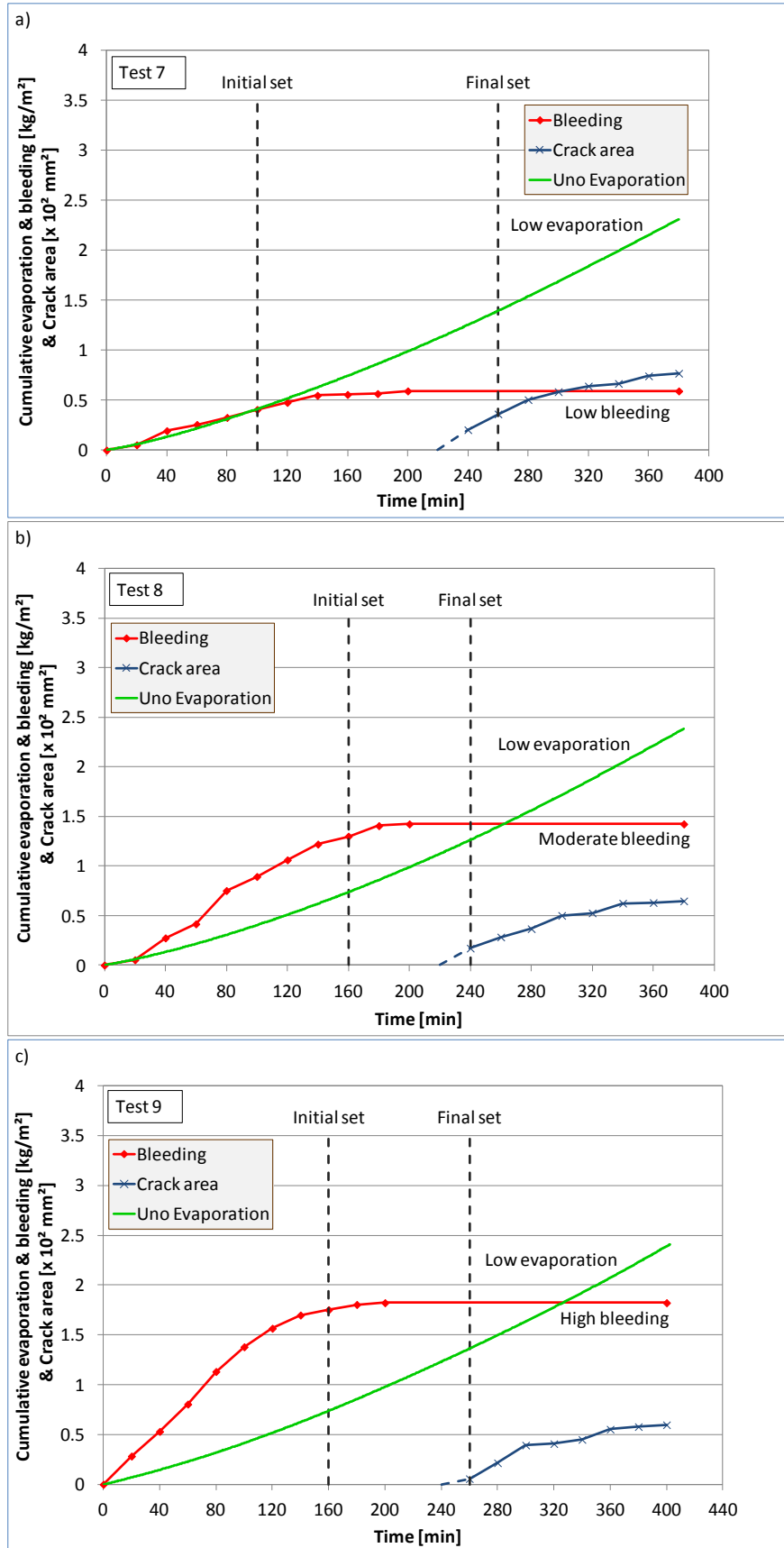


Figure 5-10 a, b & c: Average results for a low evaporation climate (Tests 7 to 9)

5.3 Test results for Objective 3: Investigation on the effect of fibre properties on PSC and bleeding

This section provides the results used to investigate the effect of different fibre properties on PSC. These tests were performed with LV-FRC (Tests 10 to 19). Each graph includes the average crack area measurements (taken from the two specimens per test) of the tests involved to investigate the concerned fibre property. The bleeding results are also shown to determine the effect of the varying fibre properties on bleeding. For specific test details refer to Table 5-1.

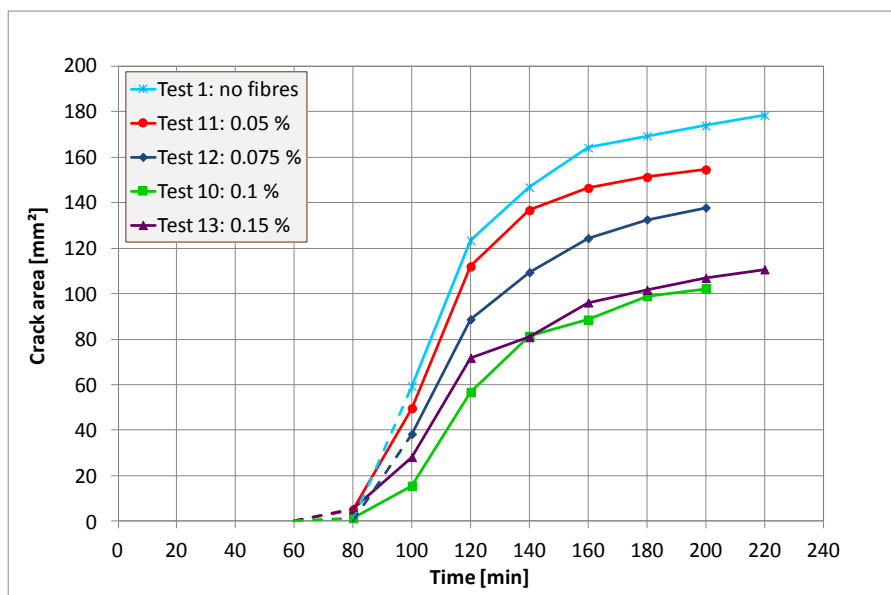


Figure 5-11: Average crack area results: Effect of fibre volume

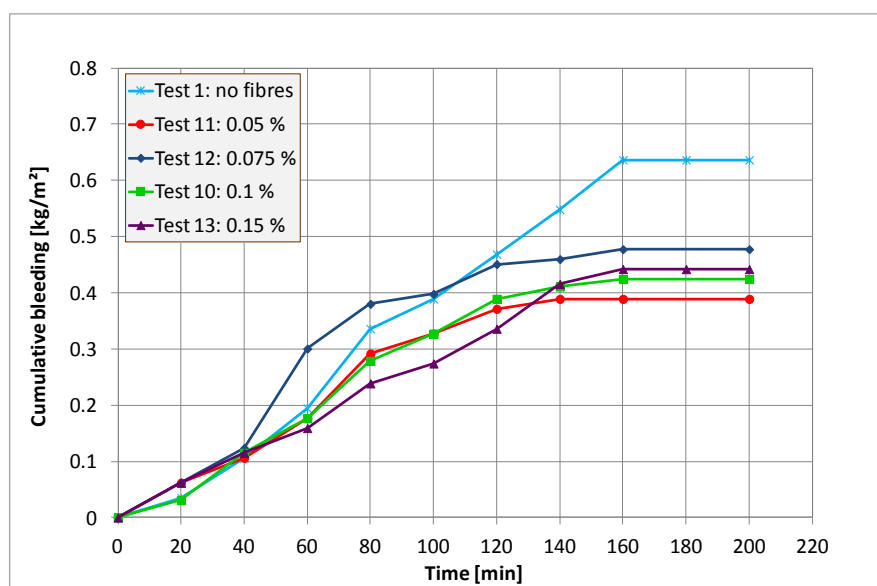


Figure 5-12: Bleeding results: Effect of fibre volume

Chapter 5: Experimental results

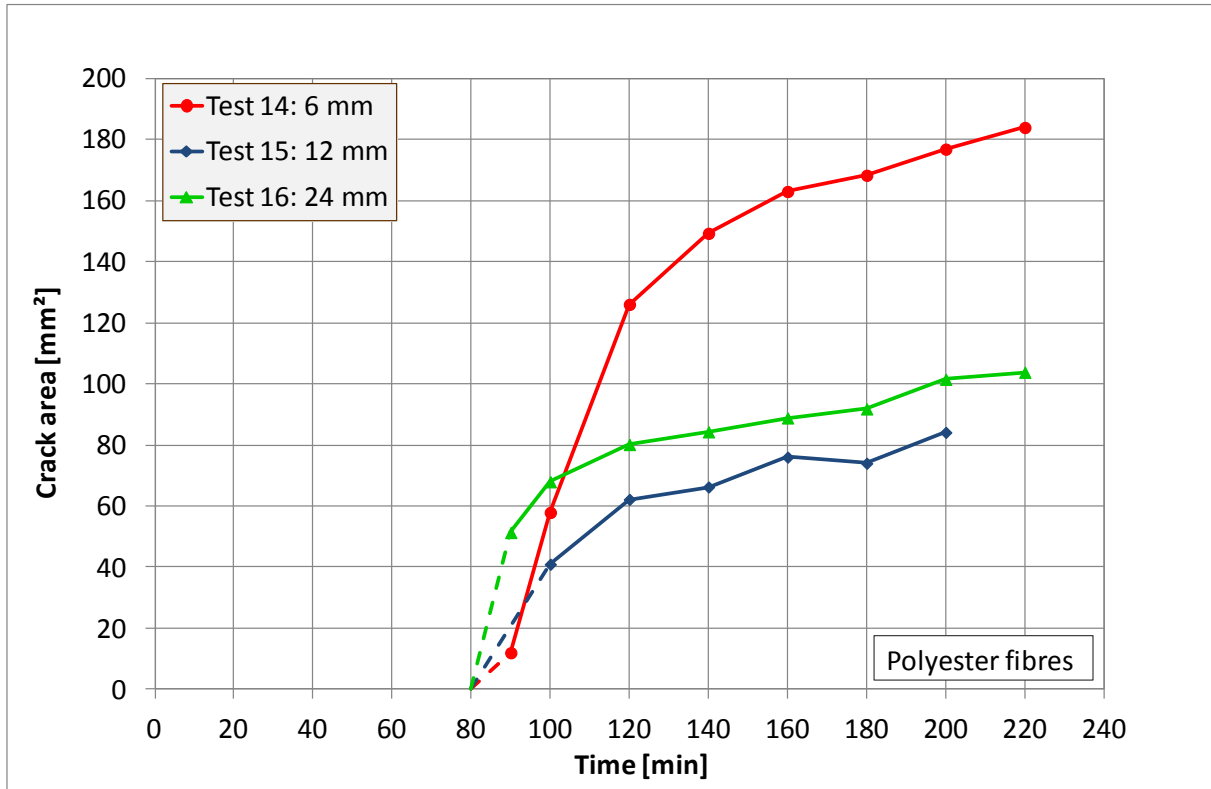


Figure 5-13: Average crack area results: Effect of fibre length

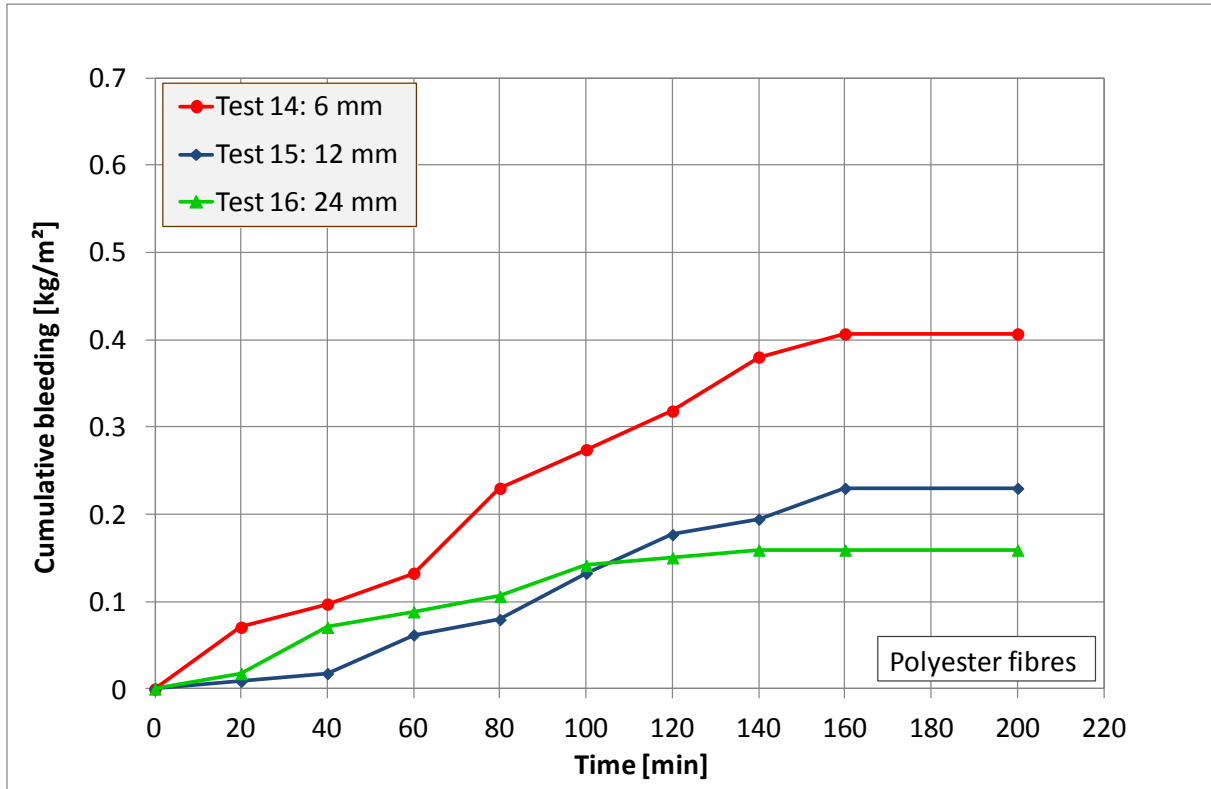


Figure 5-14: Bleeding results: Effect of fibre length

Chapter 5: Experimental results

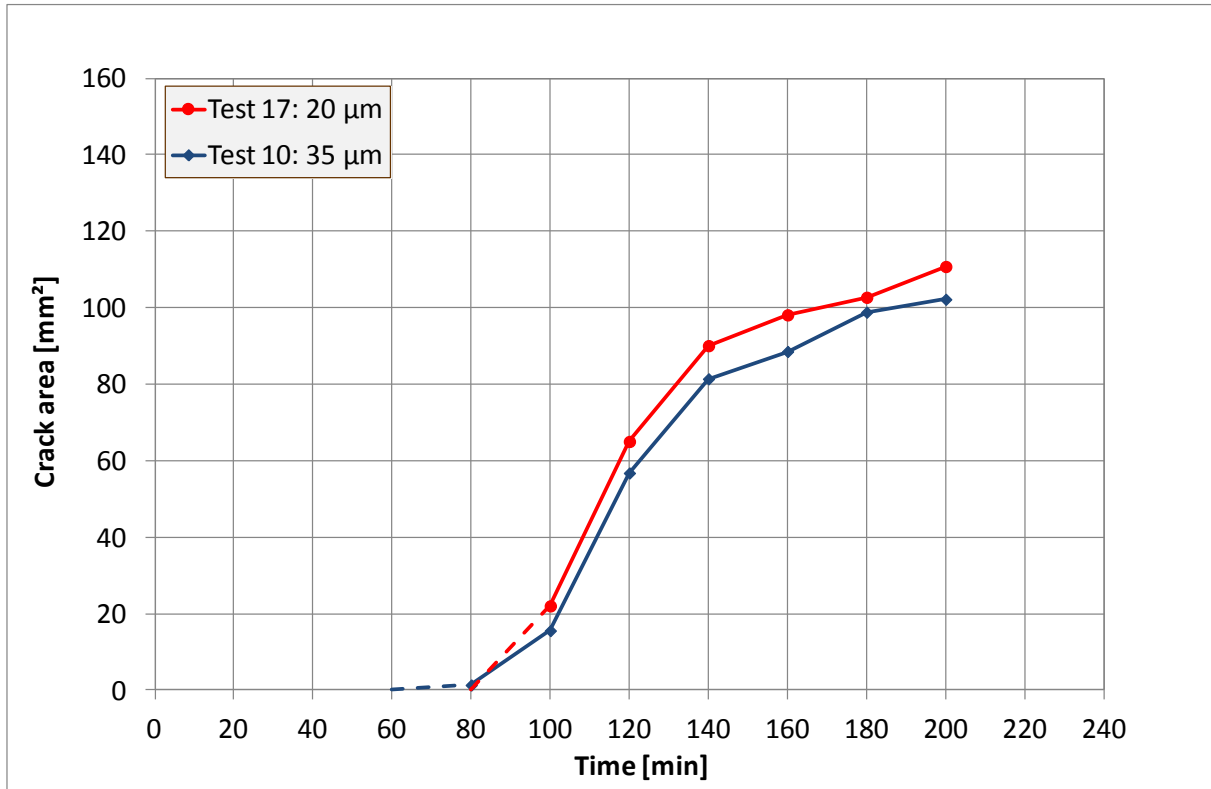


Figure 5-15: Average crack area results: Effect of fibre diameter

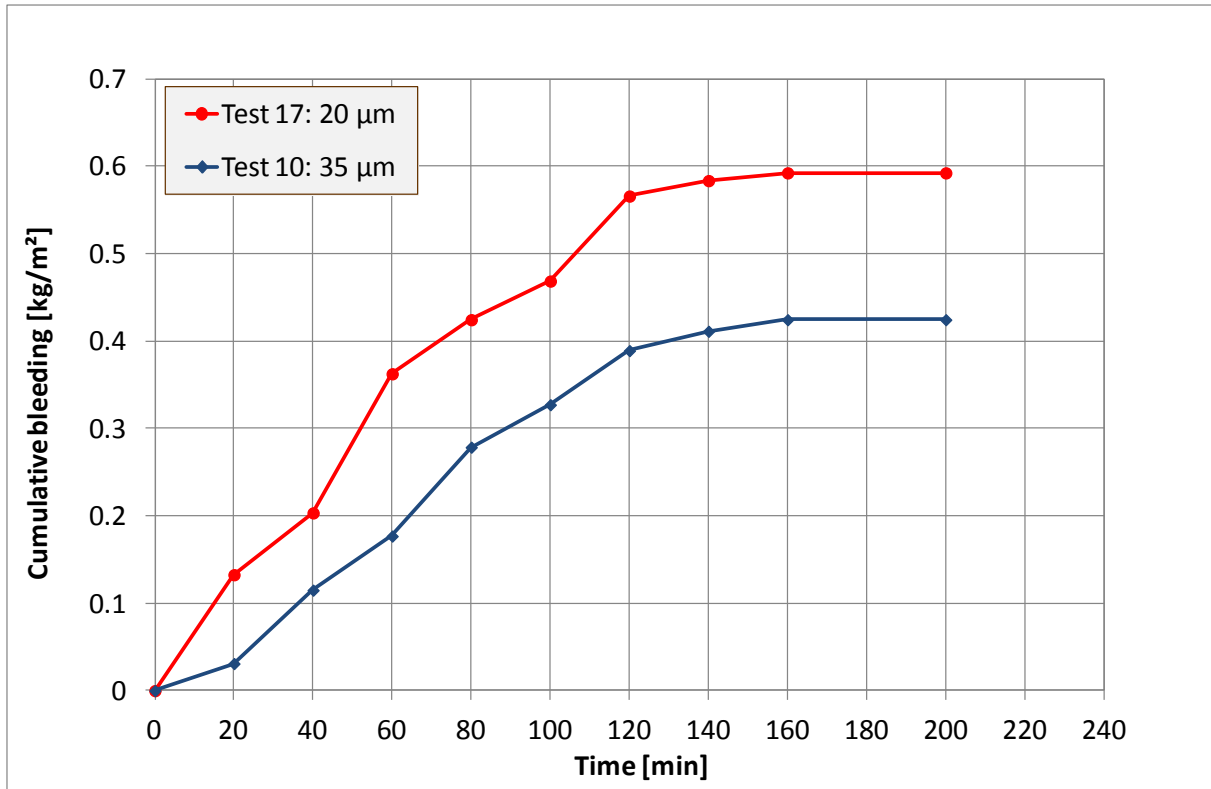


Figure 5-16: Bleeding results: Effect of fibre diameter

Chapter 5: Experimental results

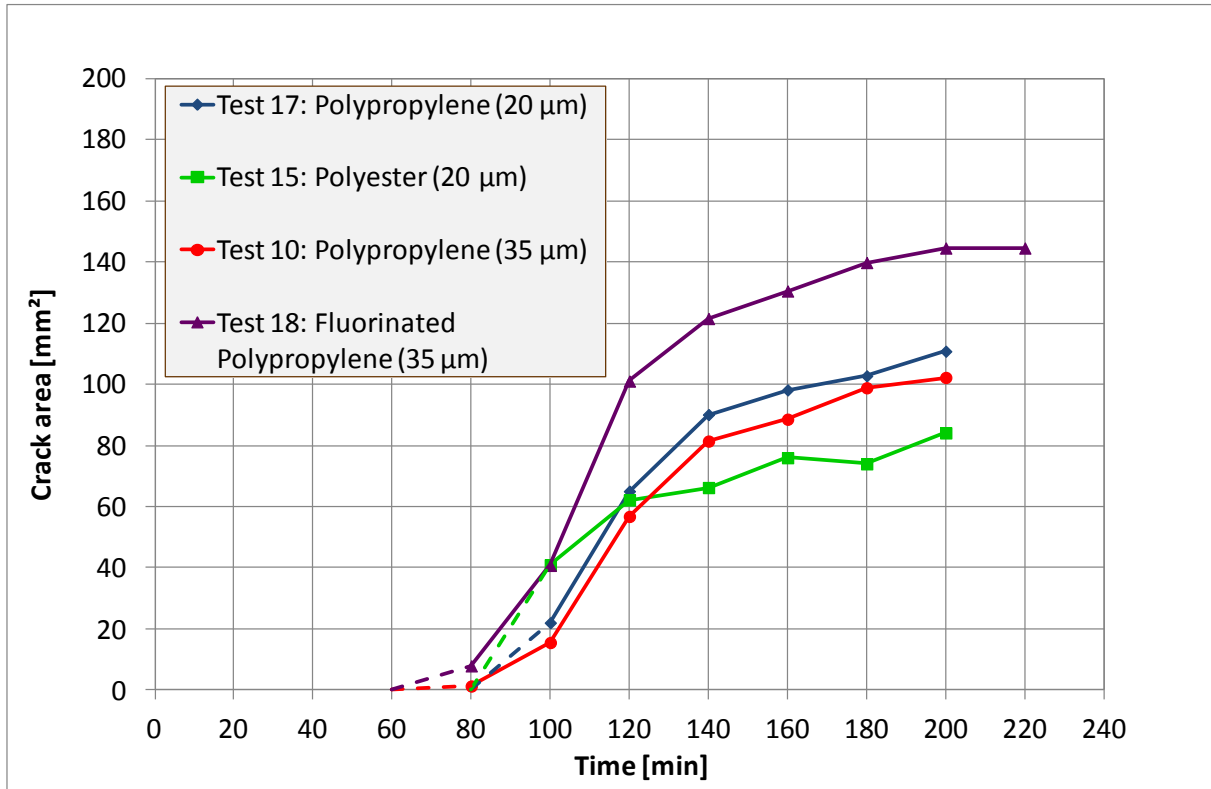


Figure 5-17: Average crack area results: Effect of fibre type

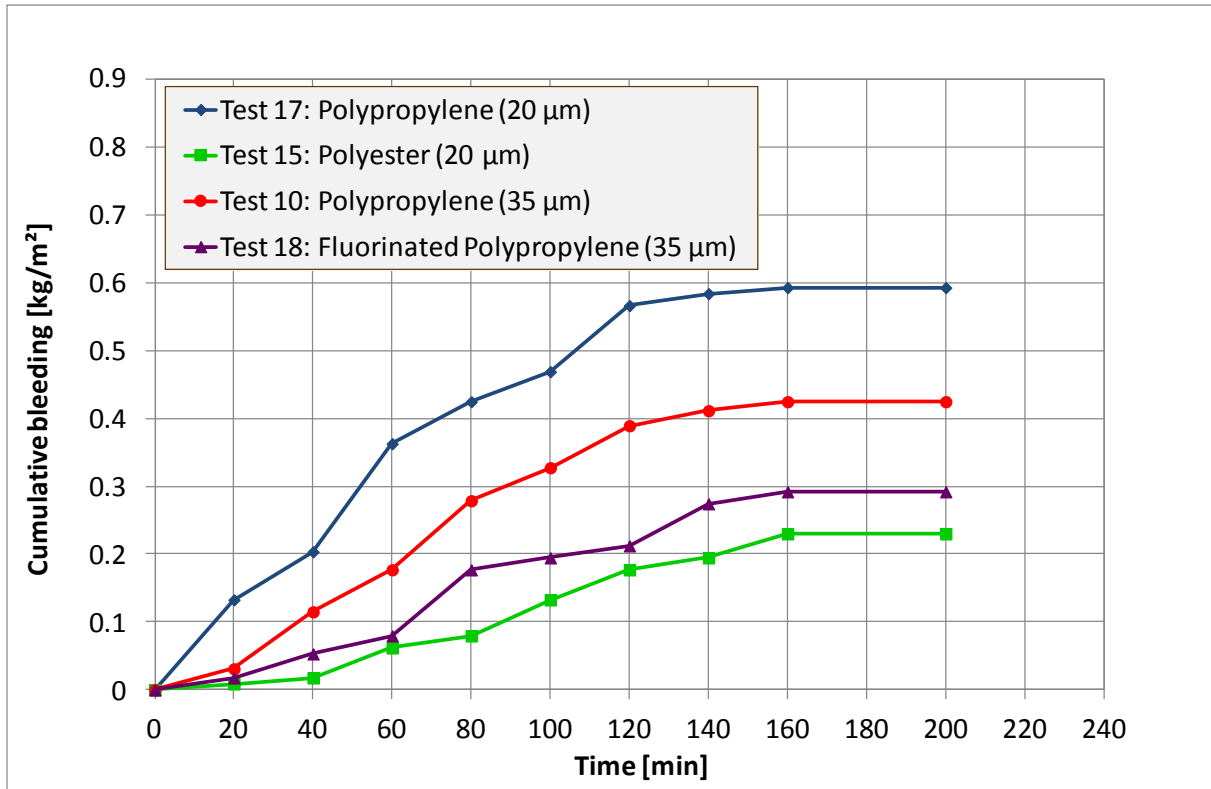


Figure 5-18: Bleeding results: Effect of fibre type

Chapter 5: Experimental results

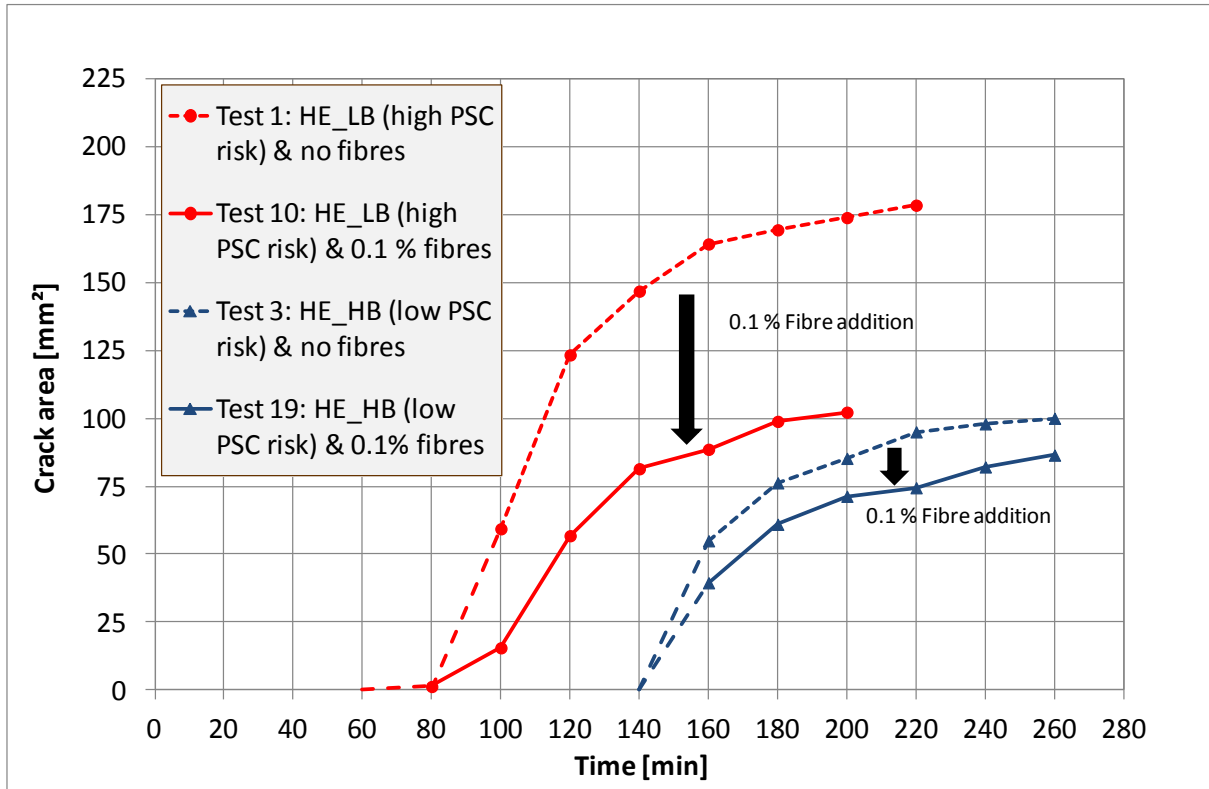


Figure 5-19: Average crack area results: Effect of fibres at different levels of PSC severity

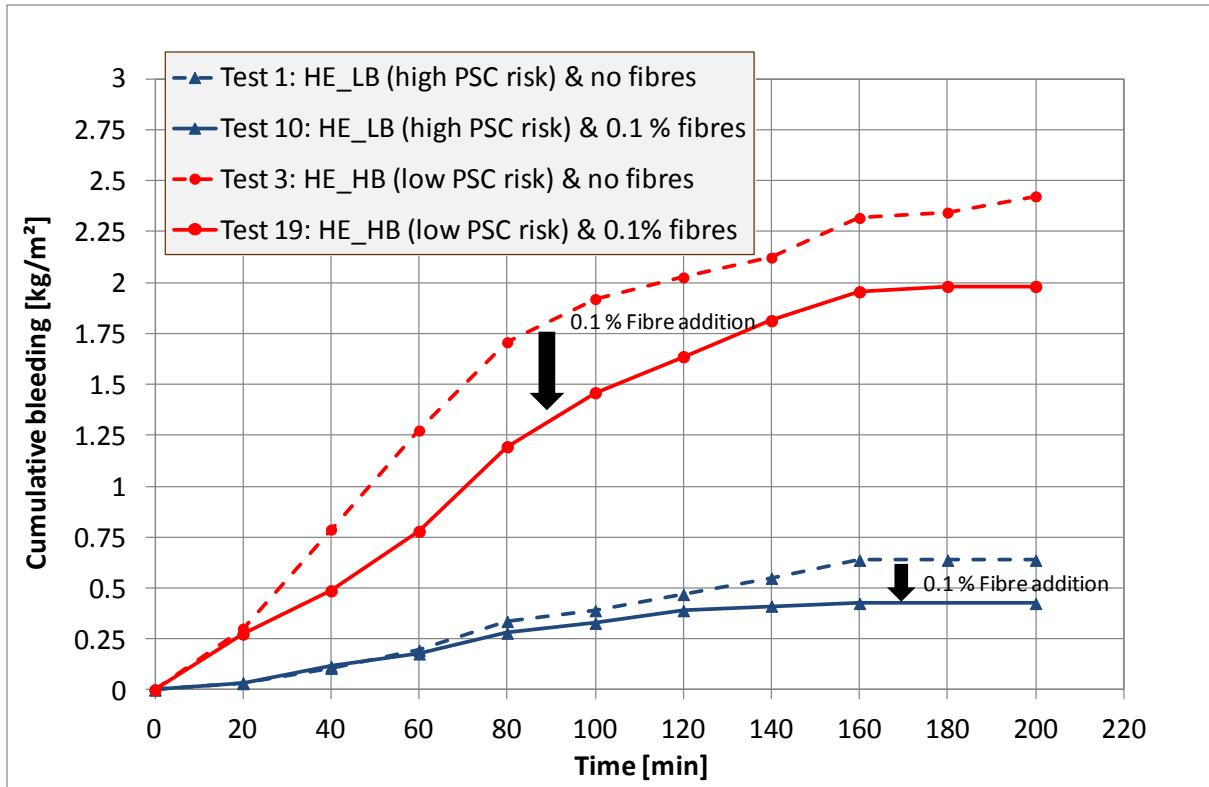


Figure 5-20: Bleeding results: Effect of fibres at different levels of PSC severity

5.4 Concluding summary

In this chapter the results of each experimental test were given. It was divided into sections in terms of test objective relevance. For the first test objective, Figures 5-1 to 5-3 showed typical PSC behaviour results while Figures 5-4 to 5-7 summarised the evaporation and bleeding results obtained from all tests. Figures 5-8 to 5-10 showed the crack area for different bleeding and evaporation conditions. The third objective requires information on the effect of fibre properties on PSC and bleeding and was presented in Figures 5-11 to 5-20.

These results are discussed in detail in the following chapter.

6. DISCUSSION OF EXPERIMENTAL RESULTS

This chapter provides detailed discussions of all the results presented in Chapter 5. These discussions are once again divided into sections according to the test objectives described in Section 4.1.

6.1 Discussion of test results for Objective 1: To investigate PSC behaviour and confirm the model for PSC behaviour

This section discusses the behaviour of PSC by referring to the results from the tests performed with conventional concrete as well as LV-FRC (Tests 1 to 19). The main objective is to determine whether the behaviour of PSC in conventional concrete as well as LV-FRC agrees with that of the model described in Section 2.1.3. The events taking place in the model of PSC behaviour can be summarised as follows:

When the cumulative amount of evaporation equals the cumulative amount of bleeding the drying time commences. At this point in time capillary pressure starts to build up until the point of air entry at which the capillary pressure instantly drops. From here on cracks can start to initiate, with the majority of crack growth taking place between the initial and final setting times. Crack stabilization usually occurs at the final setting time (refer to Figure 2-5).

The results for Objective 1 are discussed in terms of these main events occurring during the time of PSC.

6.1.1 Cumulative evaporation

The cumulative evaporation determined by Uno's equation resulted in the desired evaporation conditions (Section 4.4.1.1) for each test. The increase in evaporation rate over time is a result of the influence of the air temperature which is much higher than the temperature of the concrete. Therefore the warmer air surrounding the concrete increases the concrete temperature which in turn has an effect on the evaporation rate. A summary of the cumulative evaporations is provided in Section 5.1.2.

It is also important to remember that Uno's equation was developed for open water evaporation and therefore will produce results that are increasingly higher than the actual evaporation from the concrete specimen as time increases (as shown in Figure 2-5: Model for PSC behaviour). However, the evaporation from Uno's equation and the actual evaporation from the concrete specimen will be identical at least until the drying time is reached. The reason for this is that, until the drying time is reached, bleeding water will be present on the concrete surface which can be considered as open water evaporation.

The relevance hereof for this study is that the evaporation from Uno's equation might show a slightly higher evaporation at the initial setting time. The initial setting time is regarded as the latest point of interest of the evaporation results as will be explained in Section 6.2.2. Since the drying time and initial setting time is typically not far apart, there is only a slight difference in evaporation obtained from Uno's equation and the actual evaporation from the concrete specimen. Therefore the use of Uno's equation to determine the evaporation is regarded as acceptable for this study. In Appendix A the Uno evaporation and the measured evaporation (actual evaporation) are compared and the use of Uno's equation is explained.

6.1.2 Cumulative bleeding

The cumulative bleeding measurements agrees with the desired bleeding (Section 4.4.1.2) for each test. The bleeding behaviour of all the tests generally agreed with that of the model which illustrates an initial bleeding rate period that decreases over time until the rate is zero. At this time the cumulative bleeding amount has reached its limit. A summary of the cumulative bleeding for each test is provided in Section 5.1.3.

6.1.3 Drying time

The drying time commences as the cumulative amount of evaporation equals the cumulative amount of bleeding. The model suggests that the drying time signifies the start of capillary pressure build-up and therefore no PSC can occur before the drying time has been reached (Combrinck, 2011:71).

Most of the results agreed with the model. It is especially clear in the tests with an early drying time where the drying time is followed by capillary pressure build-up. In a few cases the initial evaporation rate is higher than the bleeding rate resulting in an immediate (after zero minutes) drying time (for example Figure 5-1). Here the drying time is also followed by capillary pressure build-up.

However, this does not seem to be the case with the tests performed under conditions of a low evaporation climate and a high bleeding level (for instance Tests 8 and 9) resulting in a much later drying time. Here it seems that the capillary pressure build-up, air entry and crack onset occurred before the drying time has been reached contradicting the model behaviour (see Figure 5-2). Two possible explanations for this can be provided. One possible explanation can be that the bleeding was measured at another climate condition (as explained in Section 4.3.2) and therefore the bleeding results for a test sample that has a later setting time (for example tests performed under the low evaporation climate condition) could show more extended bleeding than the actual bleeding in the climate chamber. This extended bleeding will then result in a later drying time and therefore could be the reason why the capillary pressure build-up, air entry and crack onset occurred before the drying time. Another possible explanation could be that Uno's equation (Equation 2.1) might underestimate the evaporation at low evaporation conditions. This will also result in a drying time which commences later than it should and could explain the reason for the deviation from the model behaviour.

6.1.4 Capillary pressure build-up and air entry

The capillary pressure results generally agreed with the model behaviour. Capillary pressure build-up started more or less at the drying time (with the exception of the few cases explained in Section 6.1.3) and continued to build up until the point of air entry. All tests gave a clear indication of when air entry took place as shown by the instant drop in capillary pressure.

It is important to take into account that the capillary pressure measurements occurred locally and therefore only gave an indication of the capillary pressure at a specific point in the specimen. Although the pressure sensors are positioned at the most likely point of air entry there may be some cases where air entry has already occurred at another position and therefore was not detected by the sensor. One example of this can be seen in Figure B-4 where it seems that capillary pressure continues to build up for almost an hour after PSC has already been observed. In this case air entry has most likely occurred much earlier, but not yet at the exact position of the sensor.

Some of the capillary pressure measurements are not available due to malfunction of the sensors as explained in Appendix C. There are also a few results that showed irregularities in the capillary pressure curve but still gives an indication of the time of air entry (for example Figure B-2). These irregularities are also explained in Appendix C.

6.1.5 Setting times

The initial setting time typically indicates the time at which cracks start to occur while the final setting time typically indicates the time at which the crack area stabilises. It is important to take into account that the indicated setting time may have occurred at any moment within the preceding 20 minute time period. For example, if the initial setting time is measured and indicated at the 100 minute mark it means that initial set could have taken place any time between the 80 and 100 minute marks.

6.1.6 Crack area

The first 20 minutes of crack area is indicated with a dashed line to indicate that the cracks could have started any time within that 20 minute time segment and is further explained in Appendix D. The crack area was measured until a time of one hour after the final set has occurred to show how crack growth has stabilised.

Most of the results showed a rapid initial crack growth that stabilised at the final setting time. The majority of crack growth occurred between the initial and final setting times with crack onset mostly occurring just after air entry. An average of 83 % of the finally measured crack areas occurred before the final setting time (as illustrated in Appendix D). This agrees with the model of PSC behaviour. A comparison of the crack results for the two specimens of each test showed that the results are relatively close to one another. These results are also provided in Appendix D.

There are however a few tests that did not show this behaviour. These were once again mainly the tests performed under low evaporation climate conditions (Tests 7 to 9). For these tests it can be seen that crack onset (time at which crack is first visible) only just occurred before or more or less at the final setting time. Therefore, the measurement duration of these three tests were extended by an additional hour after the final set to ensure that the cracks have stabilised by the time the final crack area was measured. Nevertheless, the results disagree with the model behaviour and show that crack growth and stabilization can occur after the final setting time. This shows that the proposed model of PSC behaviour is not valid under conditions of low evaporation rates. However, it could also be argued that the majority of these cracks could have been present before the final setting time but were not clearly visible due to the presence of water in the cracks. Another explanation could be that although the rate of capillary pressure build-up is lower than for the high evaporation climate conditions, the end pressure at the time of air entry was normally significantly higher than the air entry pressures reached for the high evaporation conditions. This indicates that there was a considerable capillary pressure present near the final setting time that could be high

enough to cause cracks even in a concrete paste that is near its final setting time and therefore has a relative higher strength and stiffness than at the initial setting time.

In conclusion, it is proposed that the model should also account for possible crack growth and stabilisation for at least an hour after the final setting time for conditions with low evaporation rates. However, in general the results showed that the proposed model for the behaviour of PSC is acceptable and gives an adequate representation or prediction basis for PSC behaviour.

6.2 Discussion of test results for Objective 2: Investigation of PSC severity for different bleeding and evaporation conditions

In this section the effect of different bleeding and evaporation conditions on the severity of PSC using the results obtained from the conventional concrete tests (Tests 1 – 9) are discussed. Figures 5-22 to 5-30 shows the cumulative bleeding, cumulative evaporation and average crack area (average of the two specimens per tests) results for each of these tests. By using these results a crack prediction model was created giving further understanding of PSC behaviour for different bleeding and evaporation conditions.

6.2.1 The effect of bleeding and evaporation on PSC severity

Figure 6-1 summarises the results by showing the average final crack area against the bleeding and evaporation conditions for each conventional concrete test conducted.

The following conclusions could be drawn from these results:

- Low bleeding and high evaporation climates resulted in the most severe PSC
- The lower the bleeding rate, the more pronounced the influence of the high evaporation rate
- The high and moderate climate conditions have a significantly higher influence than the low evaporation climate condition regardless of the bleeding level

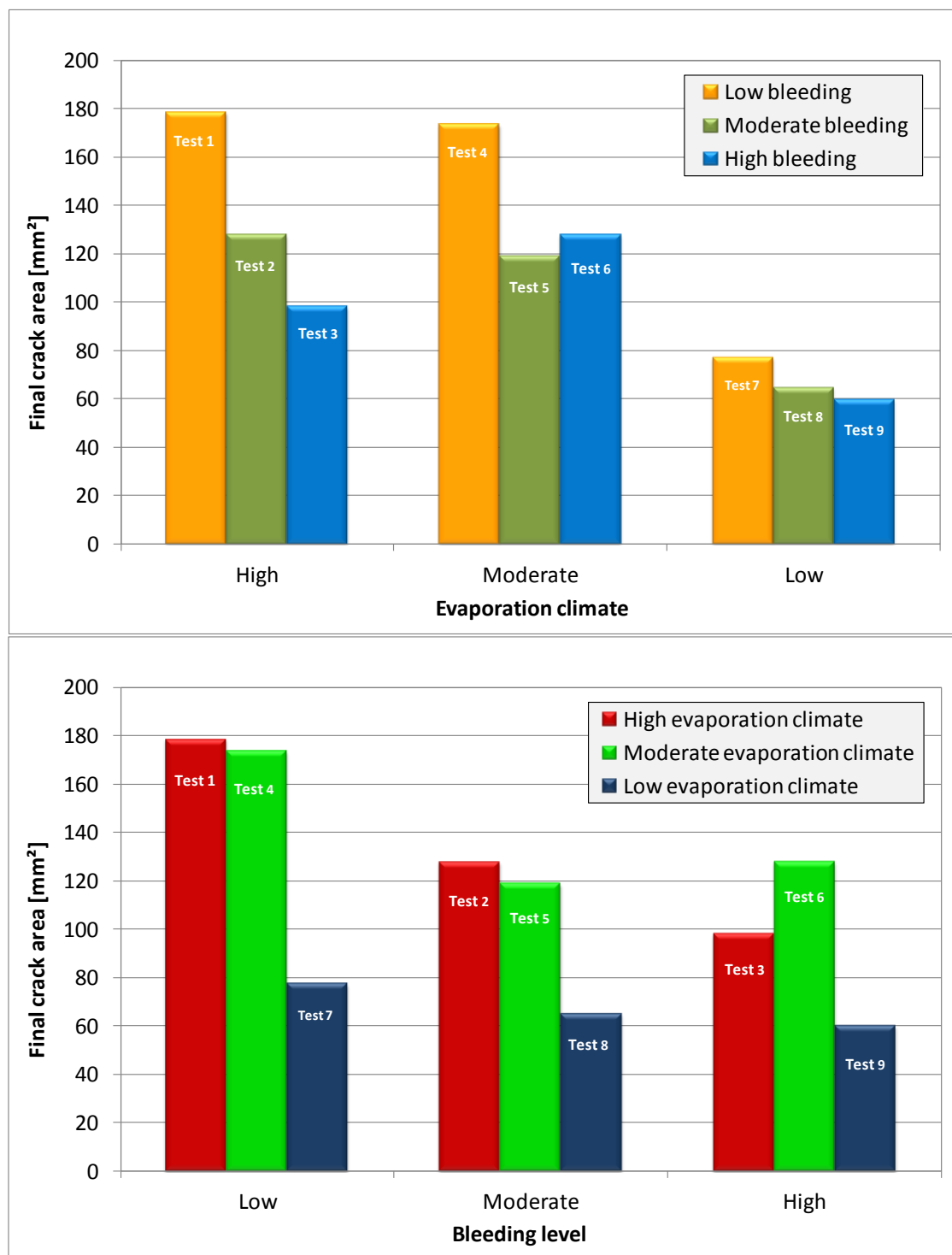


Figure 6-1: Average final crack area at different bleeding and evaporation climate conditions

6.2.2 Crack prediction model

The purpose of this crack prediction model is to create a better understanding of the level of severity of plastic shrinkage cracks that can be expected for certain bleeding and evaporation conditions. This model is still in the early stages of development and serves only as a basis for future prospects

Chapter 6: Discussion of experimental results

as described in Chapter 7. The final aim is to produce a detailed model that will predict the level of PSC that can be expected for conventional concrete at certain conditions and then also prescribe the appropriate countermeasure (for example addition of fibres) to reduce the PSC risk.

The model uses the final measured crack area against the netto amount of water lost from the concrete for each of the conventional concrete tests (Tests 1 to 9). This netto amount of water refers to the amount of water lost from the concrete that will result in capillary pressure build-up. I.e., it is the difference between the cumulative amount of evaporation and the cumulative amount of bleeding up to the initial setting time. This amount is referred to as the crack prediction value or CPV. The reason for using the initial setting time is that it can easily be determined in the industry (more easily than for example the air entry time) and still serves as a comparable time at which cracking potential can be measured.

Results from Test 1 are used to illustrate how the CPV can easily be determined as shown in Figure 6-2. When considering the evaporation and bleeding curves in Figure 6-2, five different time segments (of 20 minutes each) can be distinguished before the initial setting time. The average cumulative amount of evaporation and bleeding (kg/m^2) for each segment is then determined from the measured data. Finally, the average values for each bleeding segment is subtracted from the average values of each evaporation segment. This results in a netto amount of water lost for each segment. Finally an average of the netto values from the five segments is determined to obtain a crack prediction value (CPV) (kg/m^2).

The model can be divided into three distinct zones. Each zone is discussed separately and shown in Figure 6-3. This shows the results of the CPV against the final crack areas for the tests performed with conventional concrete. These results create the basis for the crack prediction model.

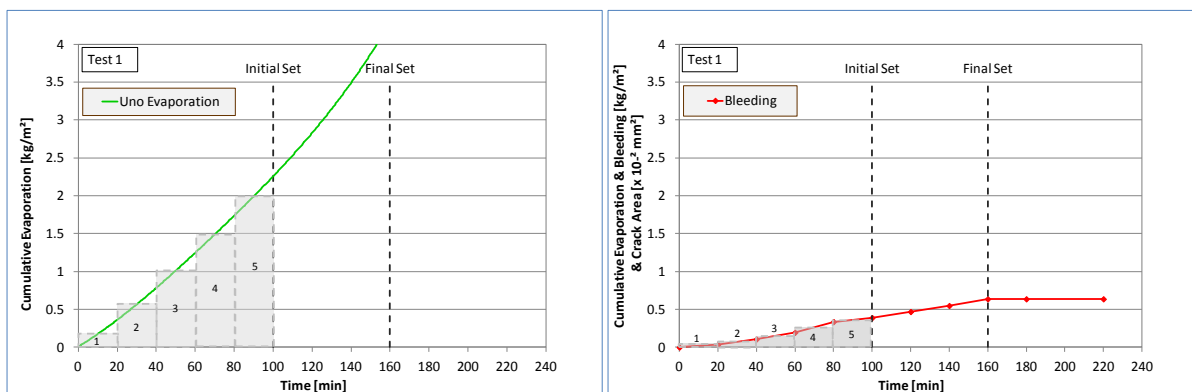


Figure 6-2: Illustration of the determination of the crack prediction value (CPV)

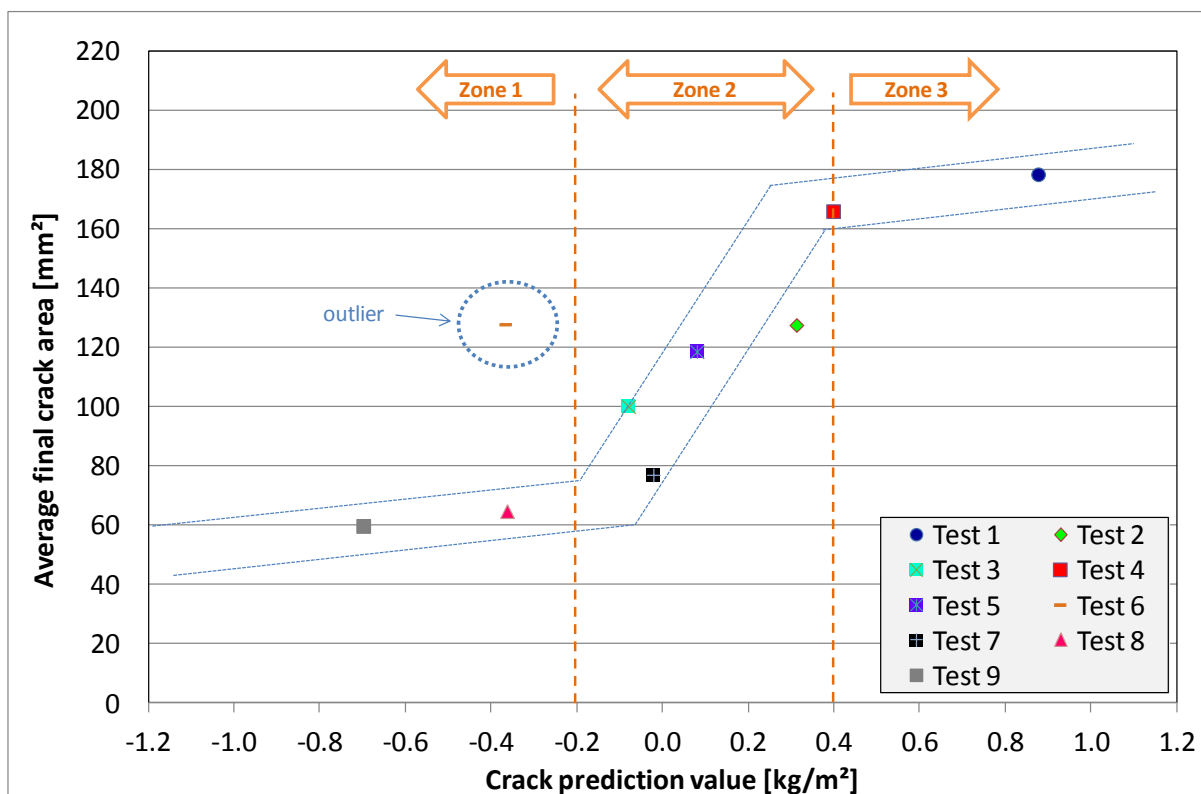


Figure 6-3: Crack prediction model

Zone 1:

This zone shows the crack areas of the tests with a CPV lower than -0.2 kg/m^2 . The zone has a considerably lower final crack area compared to the other zones and can be described as a zone with a low level of PSC severity. It can also be seen that there is very little or no significant decrease in final crack area with a further reduction in CPV. Test 6 is considered as an outlier since the results does not fit into the model. This irregular behaviour of Test 6 can also be seen in Section 6.2.1.

Zone 2:

This zone shows the crack areas of the tests with a CPV between -0.2 and 0.4 kg/m^2 . This is regarded as the transition zone between the lower and higher limits of the plastic shrinkage cracks. The results in this zone tend to show a rapid increase in crack area as the CPV increases. Therefore a slight increase or decrease in CPV within this zone may result in a significant change in the final crack area.

Zone 3:

This zone shows the crack areas of the tests with a CPV higher than 0.4 kg/m^2 . The zone has considerable higher crack areas when compared to the other tests and can therefore be described as

a zone with high PSC severity. However, there seem to be only a slight increase in crack area if the CPV is increased any further.

Summary of all three zones in the crack prediction model:

The crack prediction model indicated an increase in crack area as the CPV increased. The rate of increase, however, depends on the zone in which the CPV falls. The model showed there is an upper and lower limit to the CPV axis, at which a further increase or decrease in CPV will have no significant effect on the plastic shrinkage crack area.

Another possible application of this model is that it can provide a basis for choosing a method of limiting PSC. Depending on the zone in which a concrete specimen occurs, a choice of method for controlling PSC can be made based on the information gained from the crack prediction model. For instance, if the CPV falls in Zone 2, a curing method that influences the evaporation climate conditions (Section 2.1.5) can be chosen since the model indicates that it will have a significant effect on the crack area reduction. On the other hand, if the CPV falls in Zone 3, the addition of a low volume of fibres will be more effective since the model suggests that reducing the CPV through curing will have little effect on the crack area unless it can reduce the CPV to Zone 2.

In addition, the crack prediction model for the LV-FRC tests is also shown in Figure 6-4. This demonstrates how fibres can influence a concrete specimen that originally had a CPV falling in Zone 3 (reference test position on Figure 6-4). This reduction in crack area can be achieved without altering the CPV through for example curing. All the tests (excluding Tests 1 to 9) shown in Figure 6-4 were performed under the same high evaporation conditions but have different fibre properties. It is clear that the addition of the fibres generally decreases the final crack area.

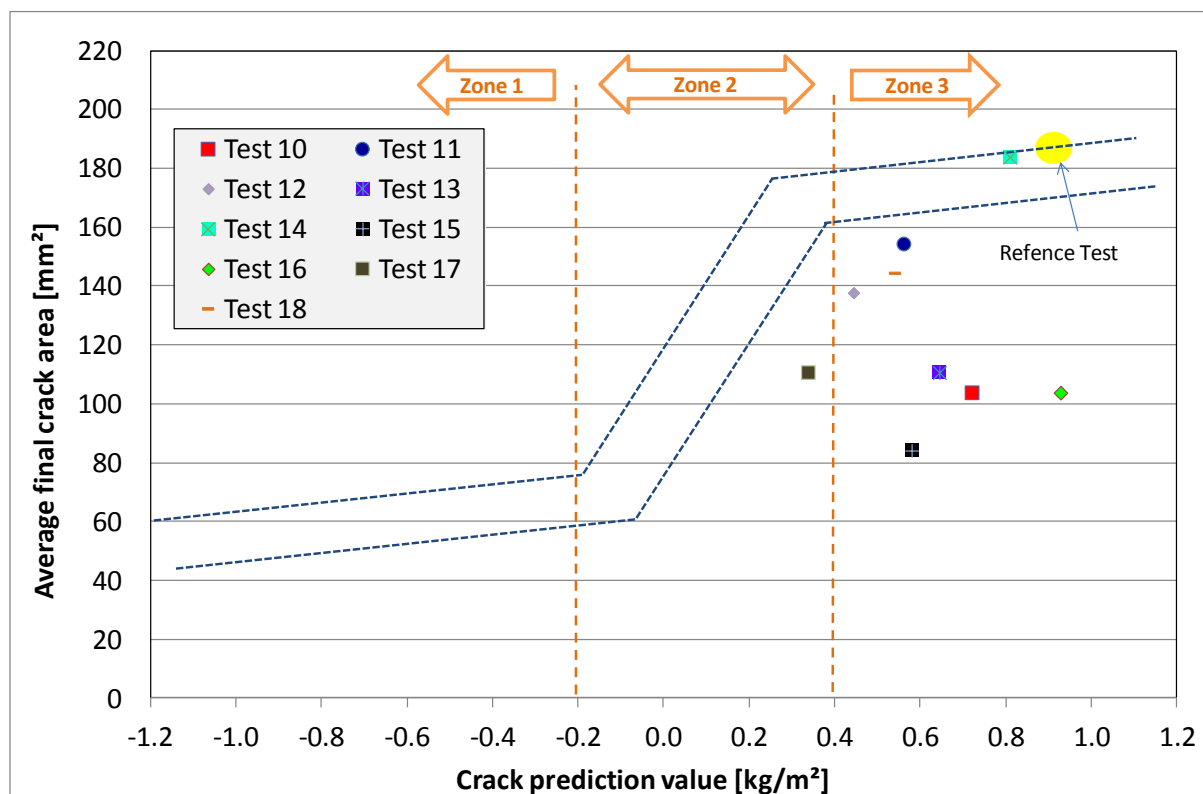


Figure 6-4: Crack prediction model with LV-FRC tests

6.3 Discussion of the test results for Objective 3: Investigation on the effect of fibre properties on PSC and bleeding

This section discusses the results from the tests performed with LV-FRC to investigate the effect of the physical fibre properties on PSC and bleeding. These properties include the fibre volume, length, diameter and type. The section also discusses the effect of fibres for different levels of PSC severity.

6.3.1 Fibre volume

Figures 6-5 and 6-6 show the results for the tests performed with different fibre volumes indicating the effect it has on PSC and bleeding.

Figure 6-5 shows a steady decrease in crack area as the fibre volume increases. This behaviour can be expected since the amount of fibres limiting PSC is increased and therefore agrees with the theoretical discussion in Section 3.4.2. However, the results also indicate that the fibres have no additional effect on PSC for volumes greater than 0.1 %. This suggests that for certain conditions, there exists a certain fibre volume limit for which a further increase in volume will have little effect.

The addition of the fibres also results in a decrease in the bleeding of the concrete as seen in Figure 6-6. As discussed in Section 2.1.1, a decrease in bleeding can result in increased PSC. However, it

Chapter 6: Discussion of experimental results

seems that the effect of the fibres on the control of PSC is more pronounced, since all tests show a decrease in final crack area due to an addition of fibres.

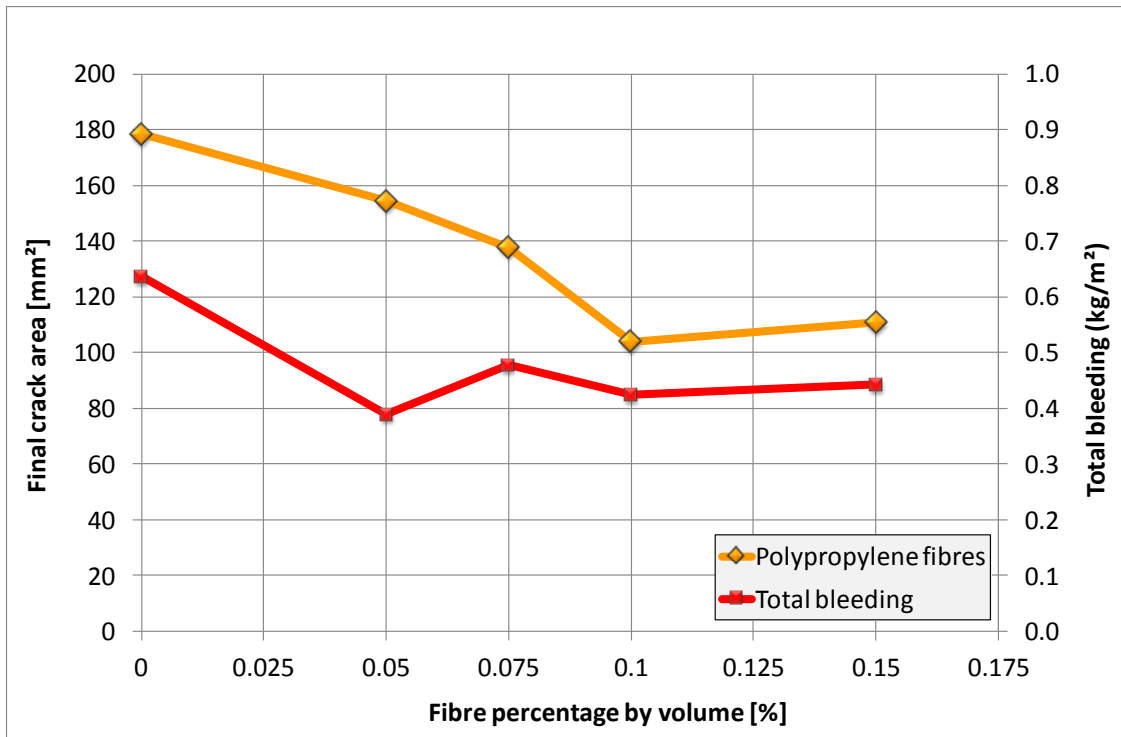


Figure 6-5: Effect of fibre volume on the final crack area and total bleeding

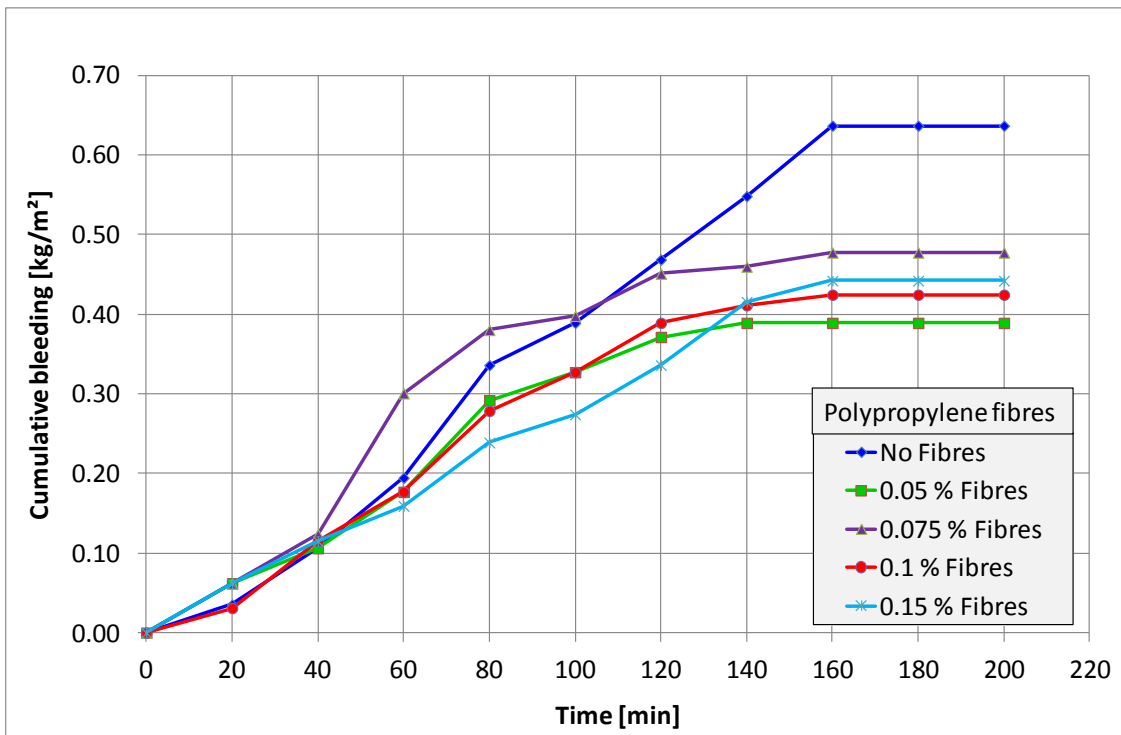


Figure 6-6: Effect of fibre volume on bleeding

6.3.2 Fibre aspect ratio

Figure 6-7 shows the final crack results of two fibre types for different aspect ratios. The results indicate that for the Polyester fibres there was a significant decrease in final crack area when the aspect ratio was increased from 300 to 600. On the other hand, the polypropylene fibres showed a slight increase in final crack area for more or less the same increase in aspect ratio. It is clear that the behaviour of the two fibre types for an increase in aspect ratio is significantly different. Although the difference in fibre type does influence this behaviour, it cannot account for or explain the significant difference between the behaviour of the two fibre types. This indicates that there may be different mechanisms resulting in this behaviour and it is therefore not sufficient to consider the aspect ratio separately, since fibres with the same aspect ratio may differ in fibre length and diameter. For example, a Fibre A has the same aspect ratio as Fibre B, although Fibre B has double the fibre length and diameter as Fibre A. It is therefore necessary to consider the influence of fibre length and diameter on PSC and bleeding separately, as shown in the following sections.

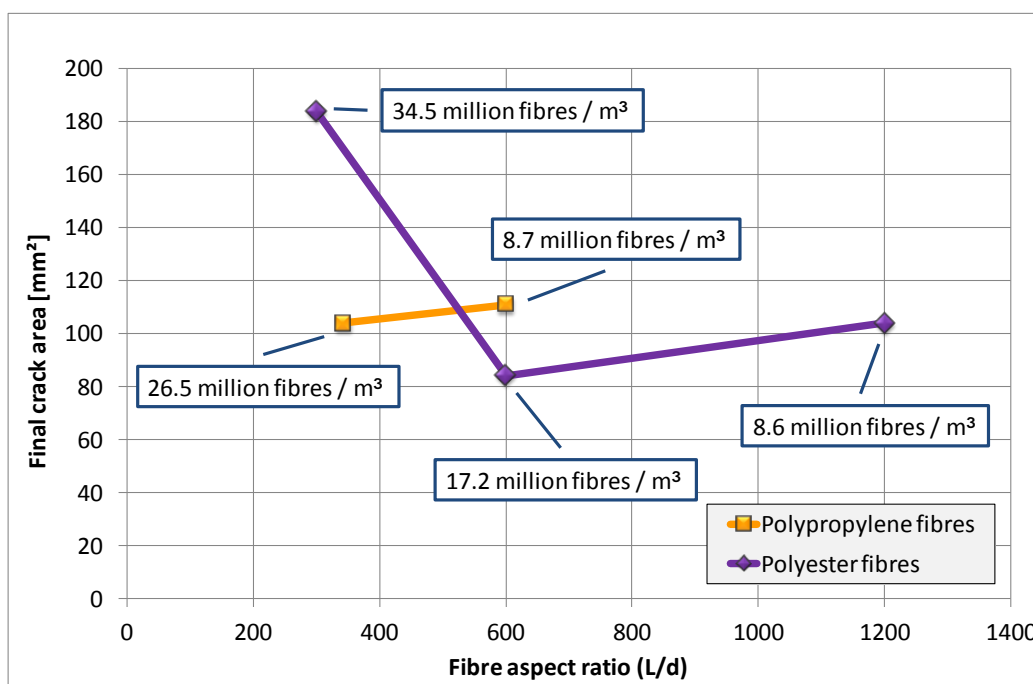


Figure 6-7: Effect of the fibre aspect ratio on the final crack area

6.3.3 Fibre length

These tests were performed with polyester fibres for the reason explained in Section 4.4.3. Figures 6-8 and 6-9 show the effect of different fibre lengths on PSC and bleeding. It also shows the total amount of individual fibres for each test.

Chapter 6: Discussion of experimental results

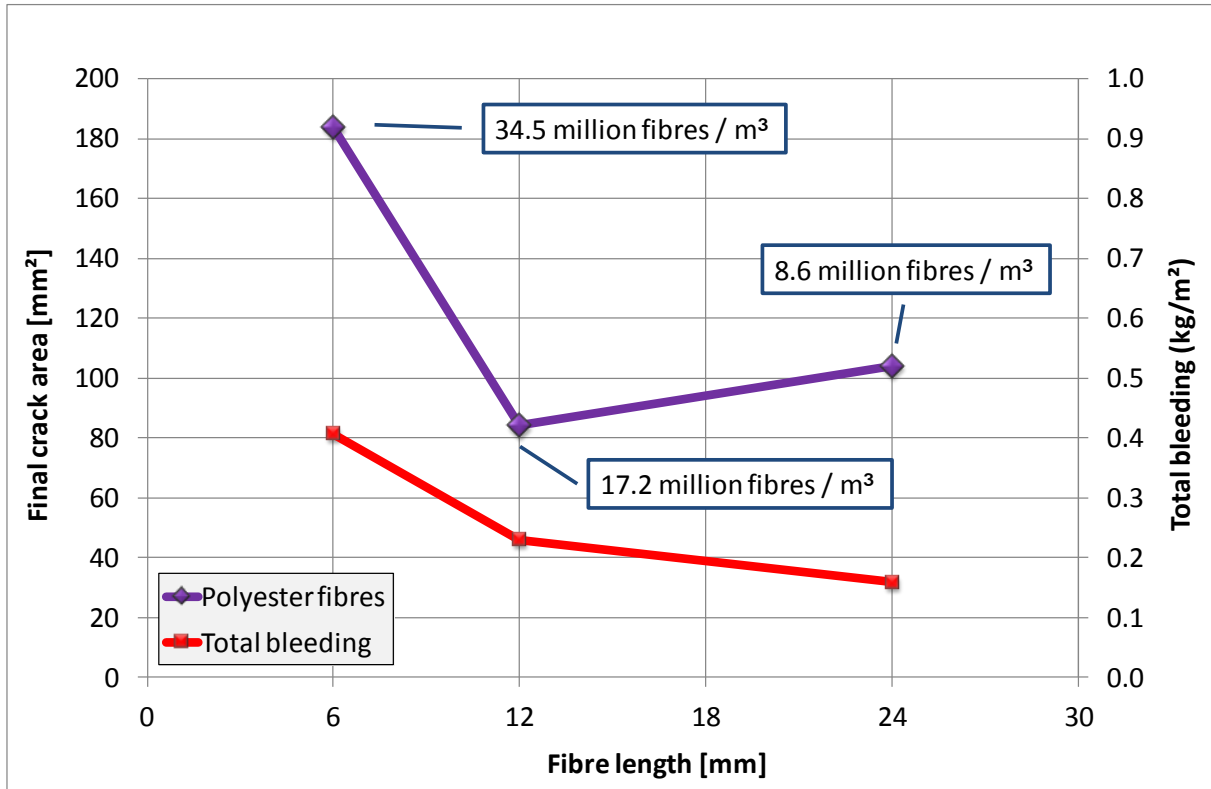


Figure 6-8: Effect of fibre length on the final crack area and total bleeding

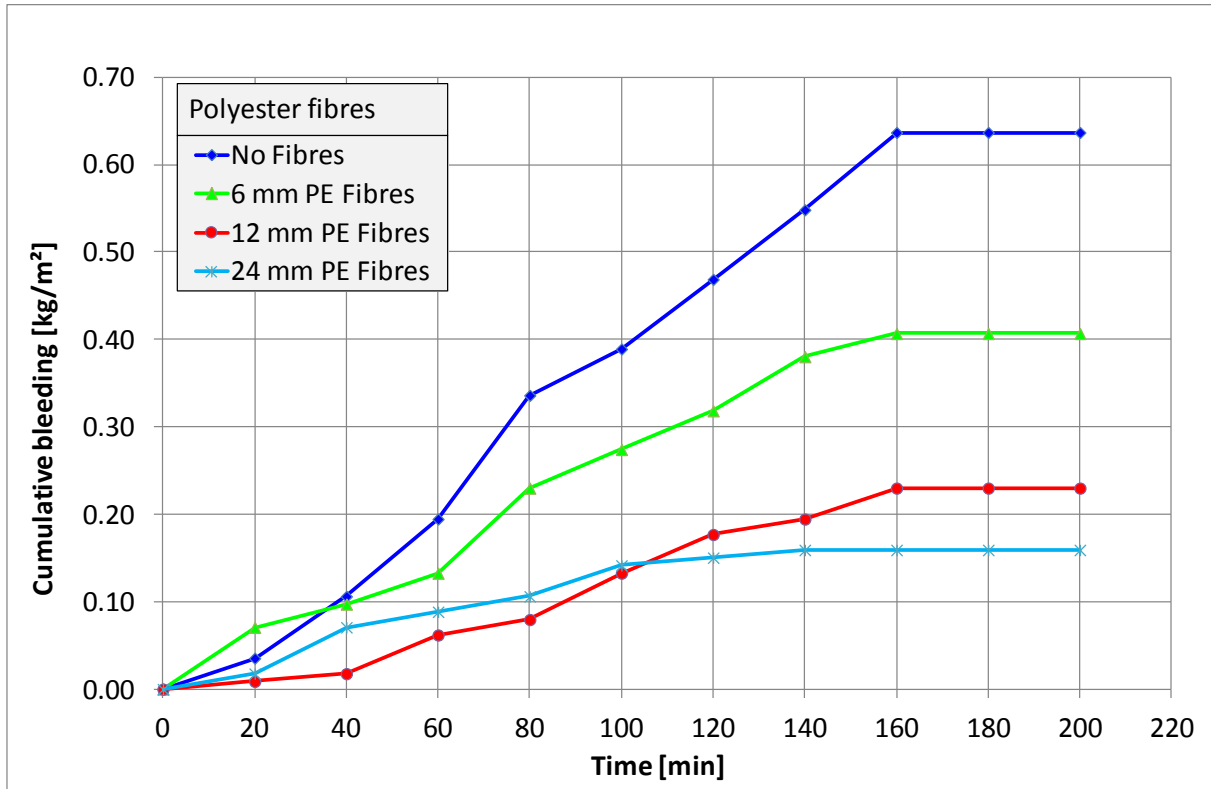


Figure 6-9: Effect of fibre length on bleeding

The results show that the 12 mm fibres are more effective in reducing PSC than the 6 mm fibres even though the tests with the shorter fibres consist of more individual fibres per volume. One explanation for this is that the 6 mm fibres are too short to achieve a sufficient bond on either side of the crack plane and therefore have little effect on reducing PSC.

The results also indicate that a further increase in fibre length to 24 mm has little or no effect on PSC reduction. This means that there exist certain fibre lengths at which full bonding potential is reached (12 mm for this study) and a further increase in length will have little additional effect on reducing PSC. In fact, because of the further decrease in bleeding with increase in fibre length (Figure 6-9), the 24 mm fibre results showed a slight increase in final crack area. This shows the importance of determining the most effective fibre length for each application.

6.3.4 Fibre diameter

Figures 6-10 and 6-11 show the results for the tests performed with different fibre diameters and indicate the effect of fibre diameter on PSC and bleeding respectively.

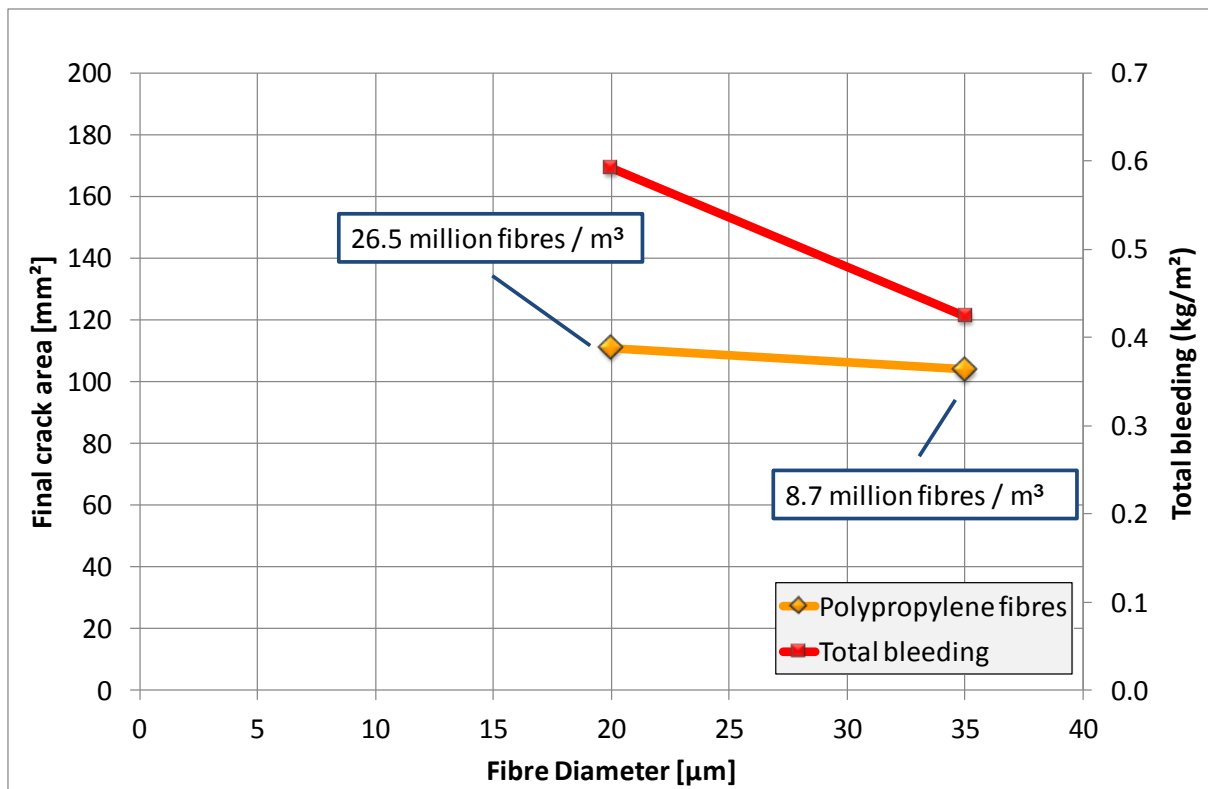


Figure 6-10: Effect of fibre diameter on the final crack area and total bleeding

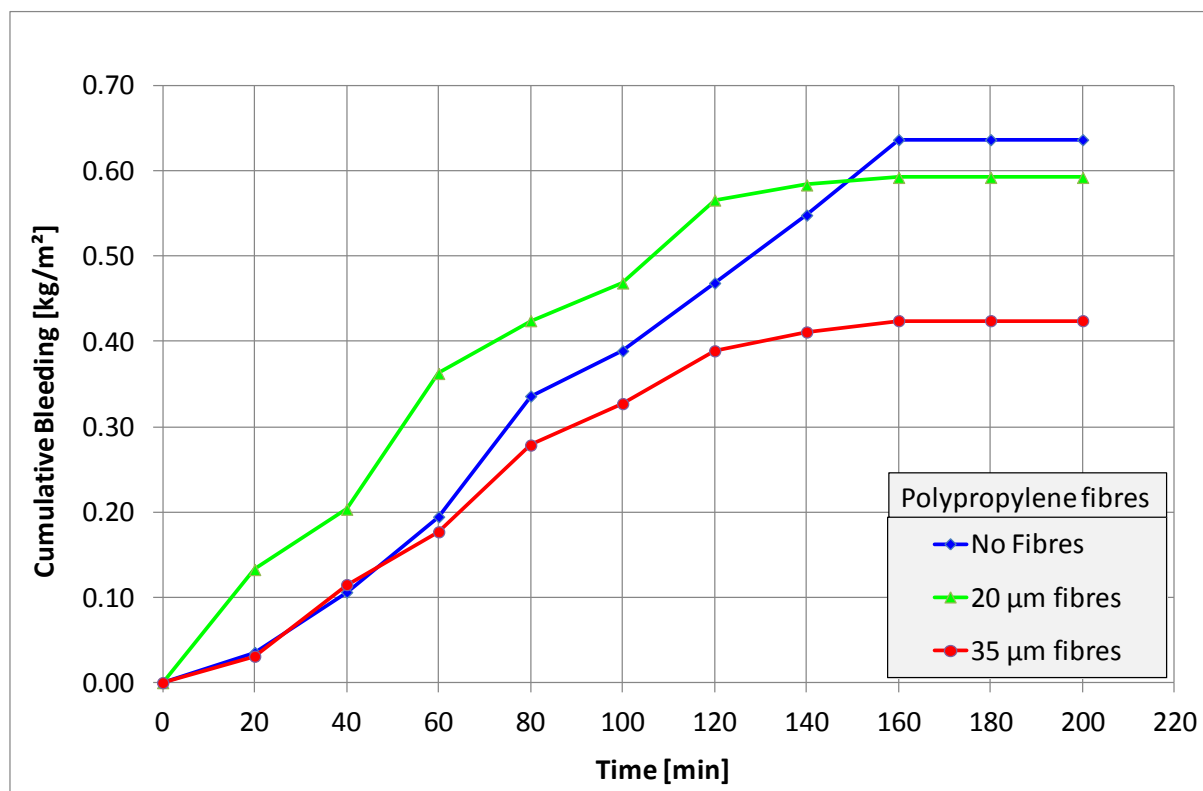


Figure 6-11: Effect of fibre diameter on bleeding

Figure 6-10 shows that there is no significant change in final crack area with a change in fibre diameter from 20 to 35 µm, even though the tests performed with the 20 µm fibres had more than three times the amount of individual fibres than the 35 µm fibre tests. The tests performed with the 35 µm fibres also resulted in less bleeding than with the tests performed with the 20 µm fibres as shown in Figure 6-11. Both these factors would normally be expected to result in a lower final crack area for the tests performed with the 20 µm fibres. However, since this was not the case, there has to be another mechanism playing a role.

A possible explanation could be the significant role of the interfacial shear bond stress in this situation. It is believed that the interfacial shear bond stress of the 35 µm fibres is much higher than that of the 20 µm fibres due to a higher frictional shear resistance between the larger fibres and the surrounding cement and fine aggregates particles. The frictional shear resistance created from the hydrated cement products probably has a similar frictional effect on the 20 and 35 µm fibres. Another important factor to consider is that the frictional shear from the smaller fine aggregate particles is instantaneous while the cement particles only provide significant friction as hydration products are formed. Therefore it is the frictional shear created by the smaller fine aggregate particles that is most likely to have the significant influence on the results obtained in Figure 6-10.

Figure 6-12 illustrates how a fibre with a larger diameter can create a higher frictional shear than a smaller diameter fibre. The smaller diameter fibre may be too small to create efficient contact points for frictional shear to develop. Of course, this mainly depends on the size of the particles surrounding the fibre.

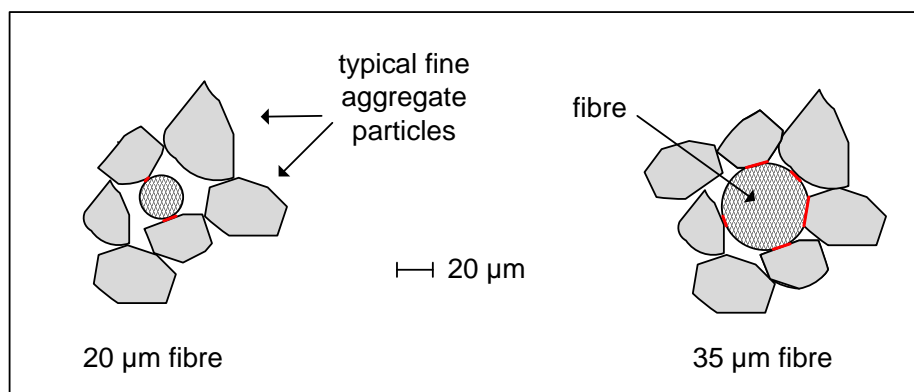


Figure 6-12: Frictional shear on 20 and 35 µm fibre

6.3.5 Fibre type

To ensure that the results that are compared have the same fibre diameter the polyester (fibre diameter of 20 µm) and fluorinated polypropylene (fibre diameter of 35 µm) fibre tests are compared to the 20 and 35 µm polypropylene fibre tests, respectively. Figures 6-13 and 6-14 show the results for the effect of the different fibre types on the PSC and bleeding.

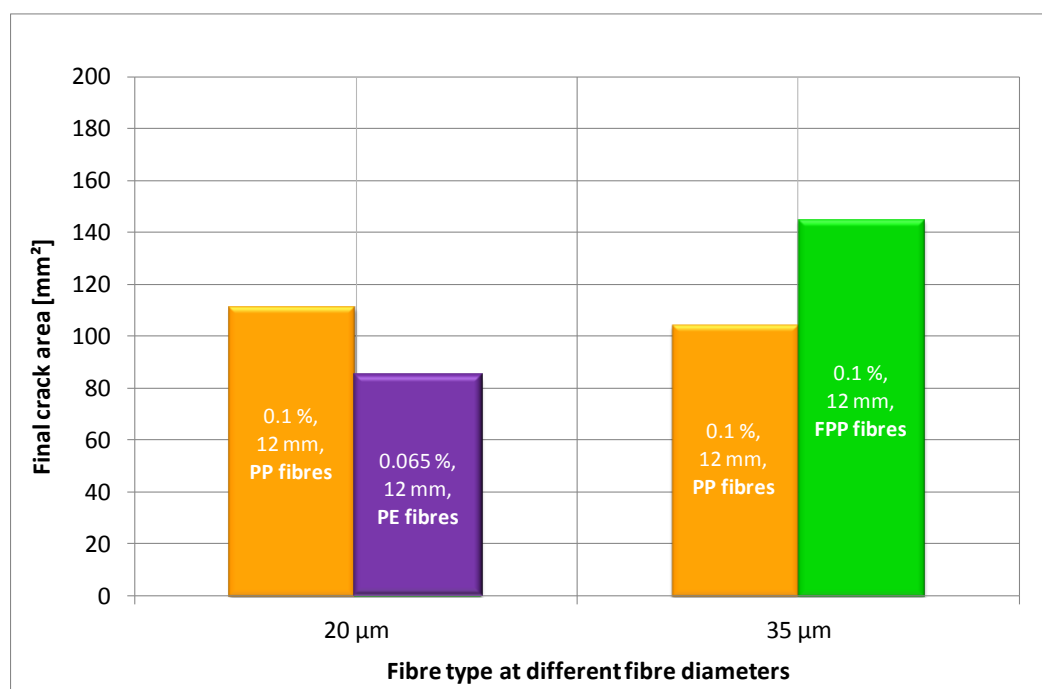


Figure 6-13: Effect of fibre type on the final crack area

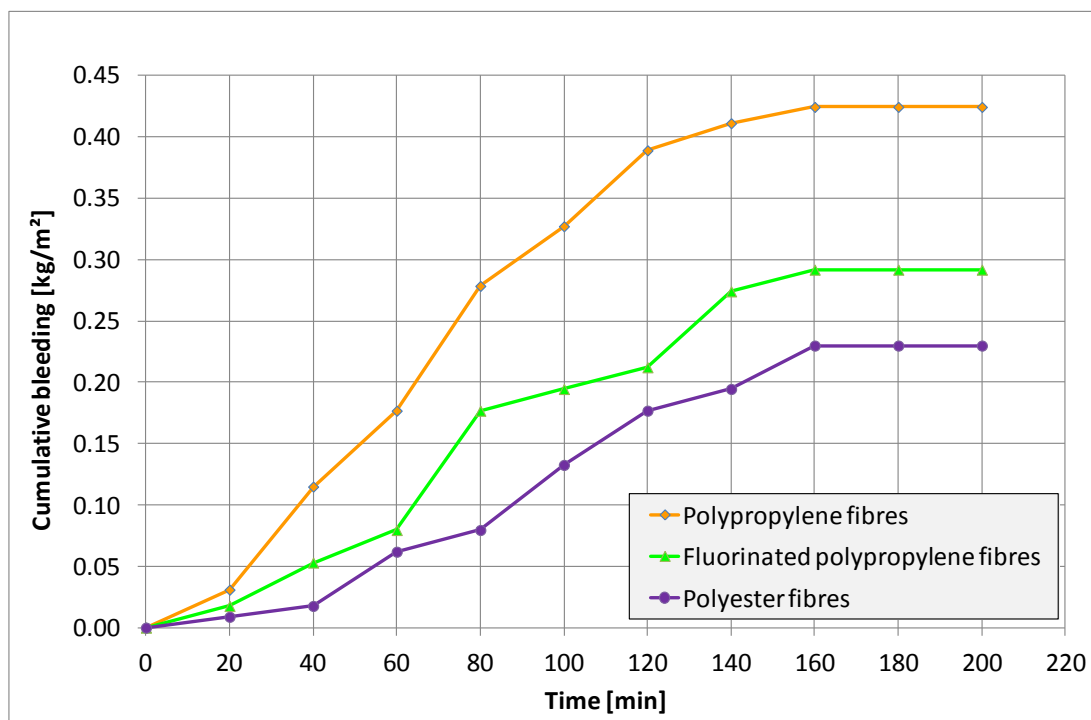


Figure 6-14: Effect of fibre type on bleeding

The results indicate that, although the polyester fibre content was at a lower percentage by volume and also caused less bleeding (Figure 6-14), the final crack area was still less than for that of the polypropylene fibre test. This could be a result of the hydrophilic nature of the polyester. It is possible that the absorbed water could have increased the interfacial shear bond stress and therefore results in a reduced final crack area.

The results from the fluorinated polypropylene fibres indicate that the untreated polypropylene fibres resulted in a lower final crack area. This is unusual since the treatment of the fluorinated polypropylene fibres is done in order to improve the bond stress and therefore result in a lower final crack area. It is also contradictory to Combrinck's results (2011:60) which showed the fluorinated polypropylene fibres to be more effective against PSC. An explanation for this can be that the fluorinated polypropylene fibres resulted in less bleeding (Figure 6-14) and therefore results in a higher final crack area.

However, these results indicate that the effect of fibre type is not yet clearly understood and that there is no conclusive evidence of which fibre type is most effective against PSC.

6.3.6 The effect of fibres on PSC and bleeding for different levels of PSC severity

Tests were performed at a high evaporation climate with low and high bleeding specimens resulting in a low and high level of PSC severity, respectively. Figure 6-15 shows the results for the final crack

area at each PSC level of severity for tests performed with and without fibres. The bleeding results are given in Figure 6-16.

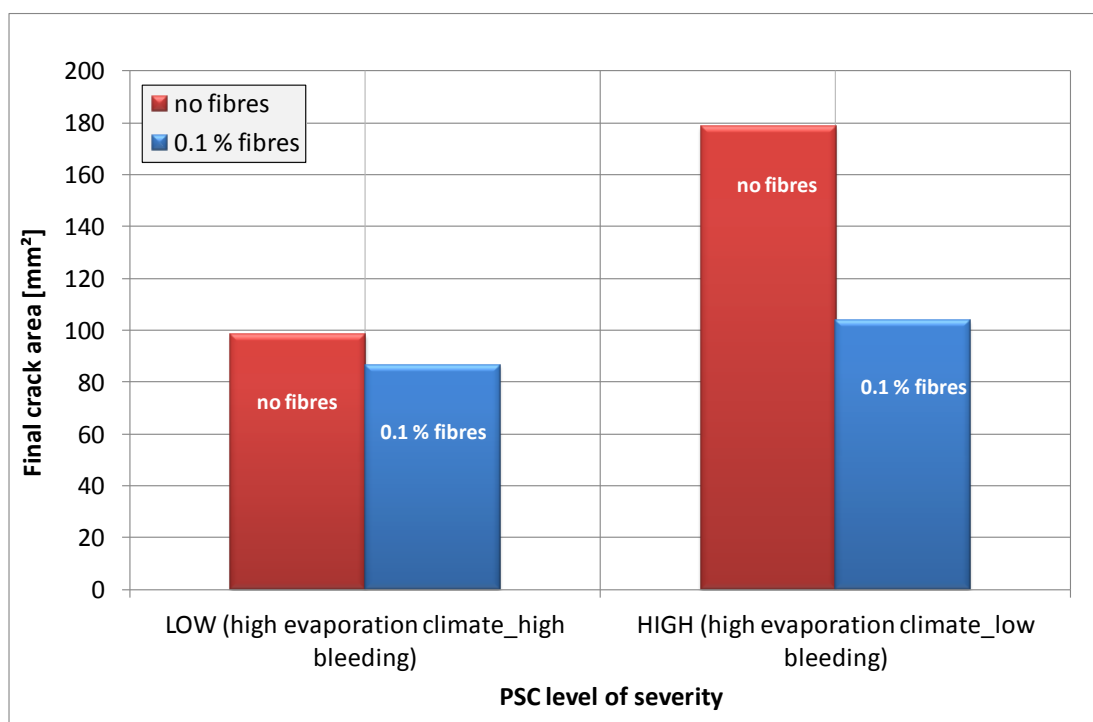


Figure 6-15: Effect of 0.1 % fibre addition on the final crack area for different PSC levels of severity

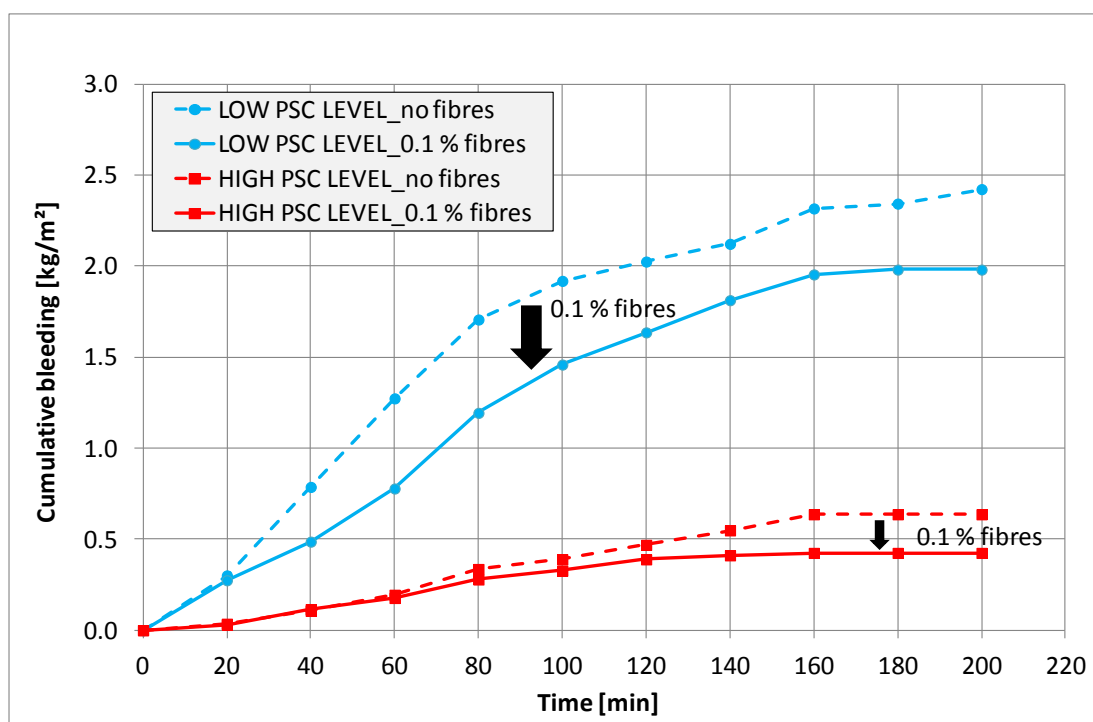


Figure 6-16: Effect of 0.1% fibre addition on bleeding for different levels of PSC severity

Figure 6-15 shows that the addition of fibres resulted in a definite PSC reduction. However, the effect of the fibres at a high level of PSC severity is more pronounced than at a low level of PSC severity. The same can be concluded from the bleeding results. For the addition of the same amount of fibres, the relative reduction in bleeding of the high bleeding mix is more than for the low bleeding mix. This indicates that the effect of the fibres on PSC and bleeding also notably depend on the level of PSC severity.

6.4 Framework for guidelines for the use LV-FRC

The most important factors to consider are when to use LV-FRC and how to apply it. This section includes a description of the situations where LV-FRC would be most effective as well as a description of the factors to consider when deciding on how to apply the LV-FRC. Finally a recommendation is made based on the results of this study.

6.4.1 When to use LV-FRC

LV-FRC is normally applied in situations where other methods of limiting PSC are difficult or impossible to perform. These may include situations with a large surface where effective curing cannot be applied over the entire surface e.g. large roads. Other situations may include inaccessible or remote locations e.g. high buildings with strong winds. In extreme conditions fibres can be combined with other methods to ensure maximum PSC limiting.

Based on the CPV model described in Section 6.2.2 it is important to also consider the margins in which LV-FRC will be most effective. By determining the CPV for the specific application and environmental condition and applying it to a CPV model it could determine whether it will be useful to apply LV-FRC.

6.4.2 How to apply LV-FRC

For the application of LV-FRC it is important to consider the effect of each of the fibre properties on PSC. These include the fibre type, fibre volume, fibre length and fibre diameter of which the last two seems to be critical according to the results from this study. Of course the decision of fibre properties used in the LV-FRC depends on the application thereof. The recommendations for the application and conditions used in this study are provided in Section 6.4.3.

6.4.3 Recommendations for the LV-FRC application based on the results from this study

The following LV-FRC recommendations were made for the conditions used in this study. These conditions include a high evaporation climate (evaporation rate of 1.0 kg/m²/h) and a low bleeding concrete mix as described in Section 4.6.1.

- A fibre volume in the region of 0.1 % should be used since less than this amount is not as effective and a higher volume does not seem to have any further PSC reduction effect.
- A fibre length of close to 12 mm should be used since a shorter fibre (6 mm) does not seem to have any effect on reducing PSC while a longer fibre (24 mm) have no further decrease in PSC.
- A fibre diameter of 35 μm should be used since the smaller diameter fibre (20 μm) does not seem to develop sufficient interfacial shear bond stress to limit PSC.

6.5 Concluding summary

This chapter discussed the results for the PSC tests performed with conventional concrete as well as LV-FRC. It discussed the model for PSC behaviour and proposed a basis for a crack prediction model for conventional concrete. It also discussed the effect of the different fibre properties on PSC and bleeding and reported a framework that can be used as guidelines for the use of LV-FRC. The following chapter provides conclusions drawn from this study as well as some future prospects.

7. CONCLUSIONS AND FUTURE PROSPECTS

The main objectives of this study were to investigate the model for plastic shrinkage cracking (PSC) behaviour for conventional and low volume – fibre reinforced concrete (LV-FRC) as well as investigate the severity of PSC for different evaporation and bleeding conditions. Another objective was to determine the effect of varying physical fibre properties on PSC and bleeding. The following significant conclusions can be drawn from this study:

The model for PSC behaviour describes the events leading to PSC as follows:

- When the cumulative amount of evaporation equals the cumulative amount of bleeding the drying time occurs. At this time capillary pressure starts to build up until the point of air entry at which the capillary pressure instantly drops. From here on cracks can start to initiate, with the majority of crack growth taking place between the initial and final setting times of concrete. Crack stabilisation usually occurs at the final setting time.

This behaviour proved to be accurate for both conventional concrete as well as LV-FRC. However, there seems to be a slight deviation from the model behaviour under low evaporation rate climate conditions ($0.2 \text{ kg/m}^2/\text{h}$).

The results of the effect of bleeding and evaporation conditions on PSC severity showed the following:

- Bleeding has a significant effect on PSC. Generally, an increase in bleeding capacity results in reduced PSC, regardless of the particular evaporation climate conditions.
 - A basis for a crack prediction model was developed using the average differences between the cumulative evaporation and cumulative bleeding to create a crack prediction value (CPV). This preliminary model showed that there exists a certain CPV range (-0.2 to 0.4 kg/m^2 for this study) where a slight decrease in the CPV results in a significant PSC reduction. It also showed that if the CPV falls outside this range, varying the bleeding or evaporation conditions will have very little effect on the PSC.
-

The results of the effect of fibre properties on PSC indicated the following:

- A decrease in PSC with an increase in fibre volume up to 0.1 % of fibres per volume of concrete. Furthermore, any further increase in fibre volume from this point on has little effect on PSC reduction.
- Fibres with the same aspect ratio, however with different combinations of length and diameter result in different PSC behaviour. Therefore the effect of fibre length and diameter should be considered separately.
- There is a certain fibre length (12 mm for this study) which proves most effective in reducing PSC. For a constant fibre volume, a decrease in this fibre length could result in an insufficient interfacial shear bond stress while a increase in fibre length could increase PSC by reducing the bleeding.
- Fibre diameter plays a significant role in the interfacial shear resistance needed to prevent crack widening. If the diameter is too small, there is insufficient frictional shear to reduce PSC.
- The slight hydrophilic nature of polyester fibres may have a significant influence on PSC however the results also indicate that the influence of fibre type on PSC is not yet clearly understood.
- In general, fibre addition reduces PSC but the effect of fibres is more distinct at a high level of PSC severity than at a lower level.

The results of the effect of fibre properties on bleeding indicated the following:

- An increase in fibre length decreases the bleeding.
- An increase in fibre diameter decreases the bleeding.
- The reduction in bleeding due to the addition of fibres is more distinct for a high bleeding mix than for a low bleeding mix.
- There is a definite decrease in bleeding with the addition of fibres; however, there is less reduction as the number of individual fibres is increased.

These results and conclusions were used to develop a preliminary framework of guidelines for the use of LV-FRC based on the findings of this study.

The following are important aspects that require investigation to further this study:

- The crack areas determined in these tests are measured from a single crack caused by restraints in the mould. This does not necessarily represent the actual crack areas that would have occurred in practice under the same conditions. Therefore an investigation of the correlation between these experimental crack areas and the crack areas that occur in typical restrained concrete (reinforced concrete) is recommended.
- The crack prediction model requires further development to a point where a level of PSC severity can be predicted for conventional concrete and then a decision of LV-FRC application can be based on this to reduce the level of PSC severity.
- Based on the knowledge gained from investigating the effect of the physical fibre properties on PSC, further research could quantify the effects of each property and determine the weight of each factor's contribution to PSC.
- This study forms part of a larger research project which will use the knowledge and results gained from this study to develop guidelines for the use of LV-FRC and possibly a more advanced model for PSC behaviour.

8. REFERENCES

Abdulrahman, A. 1995. Effects of low volume fractions of polypropylene fiber on the plastic shrinkage cracking. *The fourth Saudi engineering conference*. 1995.

Addis, B. 1998. *Fundamentals of Concrete*. Midrand: Cement and Concrete Institute.

Alhozaimy, A.M., Soroushian, P. and Mirza, F. 1996. Mechanical Properties of Fiber Reinforced Concrete and the Effect of Pozzolanic Materials. *Cement and Concrete Composites*, 18: 85-92.

ASTM C 1579. 2006. *Standard Test Method for Evaluating Plastic Shrinkage Cracking of Restrained Fiber Reinforced Concrete*. West Conshohocken: ASTM International.

Banthia, N., (ACI 544). 2005. *State of the Art Report on Synthetic Fibre-Reinforced Concrete*. American Concrete Institute.

Banthia, N. and Gupta, R. 2006. Influence of polypropylene fiber geometry on plastic shrinkage cracking in concrete. *Cement and Concrete Research*, 36: 1263-1267.

Bagherzadeh, R., Sadeghi, A. and Latifi, M. 2011. Utilizing polypropylene fibers to improve physical and mechanical properties of concrete. *Textile Research Journal*, 00 (00) 1-9.

Bentur, A. *Early Age Cracking in Cementitious Systems*. RILEM Publications S.A.R.L.

Combrinck, R. 2011. *Plastic shrinkage cracking in conventional and low volume fibre reinforced concrete*. Thesis presented in fulfilment of the requirements for the degree Master of Science in Engineering at Stellenbosch University.

Daniel, J.I., (ACI 544.1R-96). 2001. *Report on Fiber Reinforced Concrete*. American Concrete Institute.

Forrester, R.G. 2004, *"Crypsystem" Treatment Process Enhances Polypropylene Fibre Reinforcement Performance in Shotcrete and Concrete*: Magaliesburg: Omega Consulting Services.

Chapter 8: References

Golding. 1959. *Polymers and Resins*. D. Van Nostrand Co.

Hannant, D.J. 1978. *Fibre Cements and Fibre Concretes*. New York: John Wiley & Sons.

Halse, Y. Koerner, R.M. and Lord, A.E. 1987. Effect of High Levels of Alkalinity on Geotextiles. *Geotextiles and Geomembranes*, 5: 261-282.

Holt, E. And Leivo, M. 2004. Cracking risks associated with early age shrinkage. *Cement and Concrete Composites*, 26: 521-530.

Illston, J.M. and Domone, P.L.J. 2001. *Construction Materials: their nature and behaviour*. New York: Spon Press

Ismail, M., Toumi, A., Francois, R. and Gagne, R. 2004. Effect of crack opening on the local diffusion of chloride in inert materials. *Cement and Concrete Research*, 34: 711 – 716.

Johnston, C.D. 2001. *Fiber-Reinforced Cements and Concretes*. New York: Taylor & Francis.

Josserand, L. and De Larrard, F. 2004. A method for bleeding measurement. *Materials and Structures*, 37:666-670, December.

Kellerman, J. and Crosswell, S. 2009. *Fulton's concrete technology*. Midrand, South Africa: Cement & Concrete Institute.

Ma, Y., Tan, M. and Wu, K. 2002. Effect of different geometric polypropylene fibers on plastic shrinkage cracking of cement mortars. *Materials and Structures*, 35: 165-169, April.

Mehta, P.K. & Monteiro, P.J.M. 2006. *Concrete Microstructure, Properties, and Materials*. New York: McGraw-Hill.

Pelisser, F. 2010. Effect of the addition of synthetic fibers to concrete thin slabs on plastic shrinkage cracking. *Construction and Building Materials*, 24: 2171 – 2176.

Powers, Treval C. 1968. *The properties of Fresh Concrete*. New York: John Wiley & Sons, Inc.

Qi, C., Weiss, J. And Olek, J. 2003. Characterization of plastic shrinkage cracking in fibre reinforced concrete using image analysis and a modified Weibull function. *Materials and Structures*, 36:386-395, July.

SANS 50196-3. 2006. Methods for testing cement Part 3: *Determination of setting times and soundness*. 2nd ed. Pretoria: Standards South Africa.

Chapter 8: References

SANS 1083. 2002. *Aggregates from natural sources – Aggregates for concrete*. Edition 2.1. Pretoria: Standards South Africa.

Slowik, V., Schmidt, M. & Fritzsche, R. 2008. Capillary Pressure in fresh cement-based materials and identification of the air entry value. *Cement & Concrete Composites*, 30: 557-565.

Slowik, V., Schmidt, M., Hubner, T. & Villmann, B. 2009. Simulation of capillary shrinkage cracking in cement-like materials. *Cement & Concrete Composites*, 31:461-469.

Uno, P.J. 1998. Plastic Shrinkage Cracking and Evaporation Formulas. *ACI Materials Journal*, 95(4):365-375, July-August.

List of appendices

Appendix A: Scale measured evaporation and Uno evaporation	83
Appendix B: Climate chamber test results	84
Appendix C: Capillary pressure measurements	98
Appendix D: Crack area results	99

Appendix A: Scale measured evaporation and Uno evaporation

The initial proposal of this study suggested that the evaporation from the concrete specimens should be determined using electronic scales. However, most of the data obtained from the electronic scales was inconclusive because of a complication with the scale measurement. This is due to the temperature of the climate chamber influencing the resistance in the electrical wiring resulting in an incorrect voltage output in mV. The voltage output is then converted to incorrect data in kilograms.

The majority of test results had this problem since the climate chamber was only turned on about 2 hours before testing time. This was enough time for the air temperature, relative humidity and wind speed within the climate chamber to stabilise at the required values, but not long enough for the temperature of the electrical wiring within the scales to reach stabilization. Once this was realised, the climate chamber was switched on 12 hours before testing time to ensure overall temperature stabilisation. However, most of the tests already contained inconclusive scale evaporation results and therefore the Uno evaporation was used to ensure that the evaporation results was comparable for all experimental tests.

Figure A-1 compares the results for the scale measured evaporation and the Uno evaporation for a test performed after the climate chamber has been operating for 12 hours and the temperature has fully stabilised. It indicates that although the Uno evaporation has a slightly higher evaporation rate, the results up until the initial setting time show more or less similar behaviour. Since the Uno evaporation provides consistent results and tend to agree to the scale results up until the point of interest (initial setting time) it is regarded as acceptable for this study.

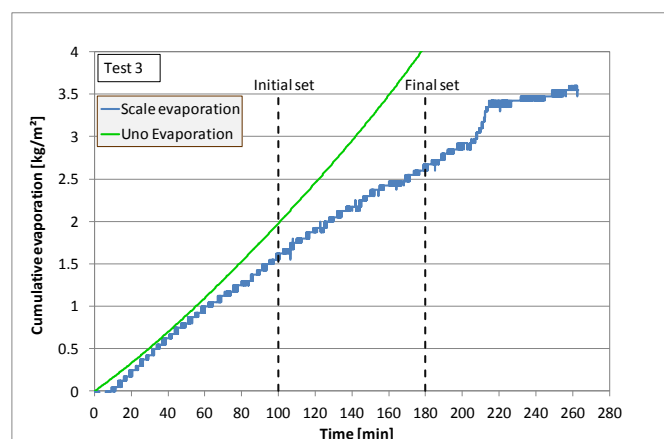


Figure A-1: Comparison of scale measured evaporation and Uno evaporation

Appendix B: Climate chamber test results

B.1. Plastic shrinkage cracking test results:

Appendix B.1 provides the results obtained for all the experimental tests with conventional and LV-FRC each consisting of two concrete specimens. The results of each specimen are shown on a separate graph and include the Uno evaporation, bleeding measurements, capillary pressure, crack area measurements and setting times. It should be noted that some capillary pressure results were not available due to errors with the pressure sensors. These errors are explained in Appendix C.

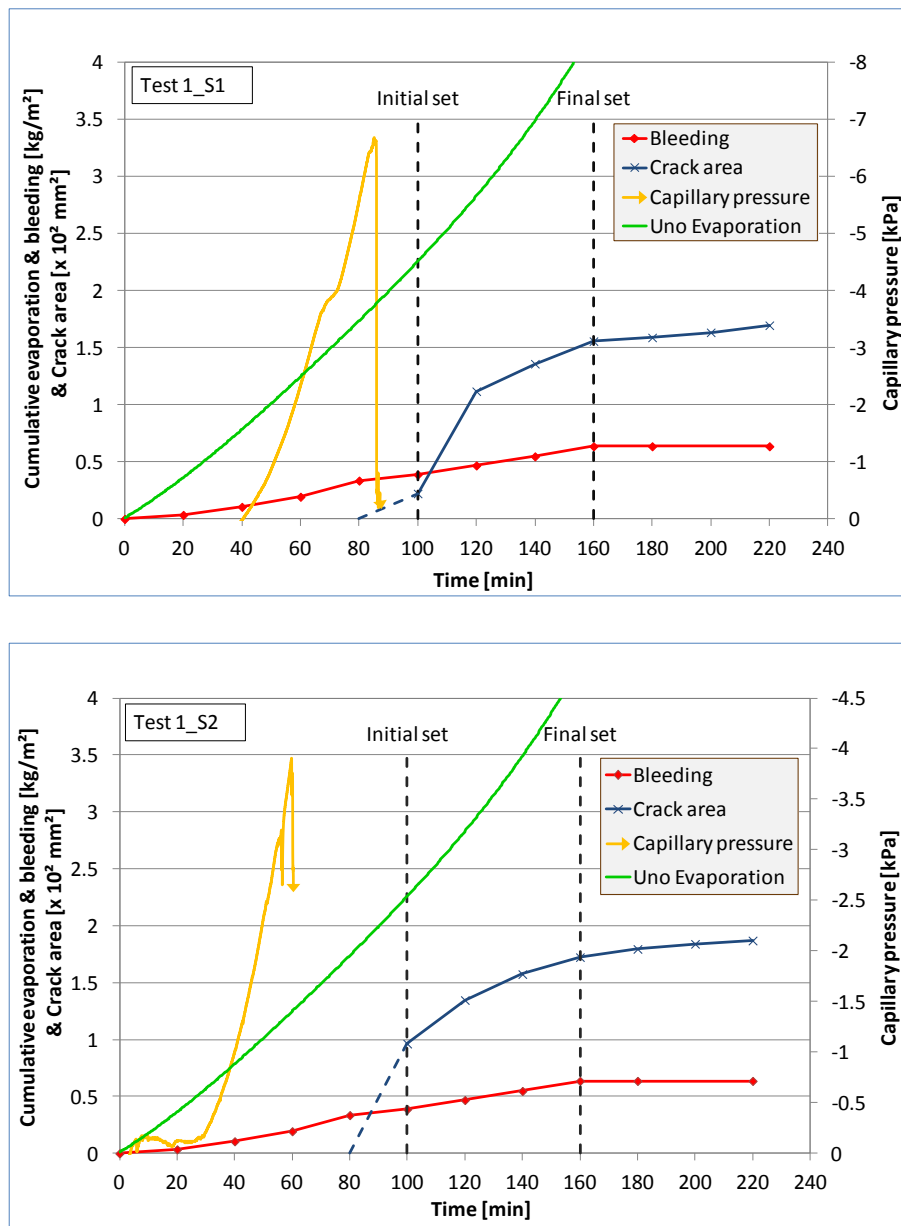


Figure B-1: Results for Specimen 1 and 2 of T1_HE_LB

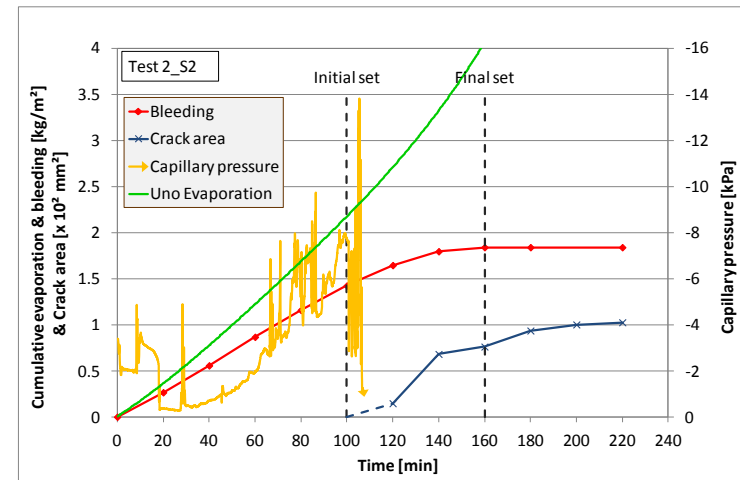
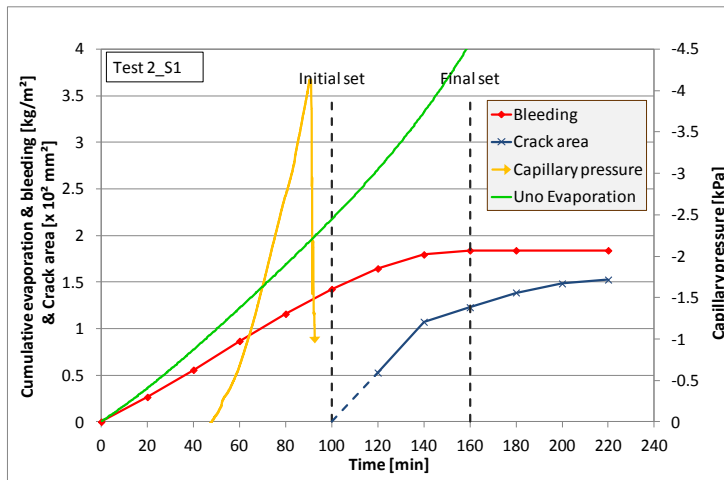


Figure B-2: Results for Specimen 1 and 2 of T2_HE_MB

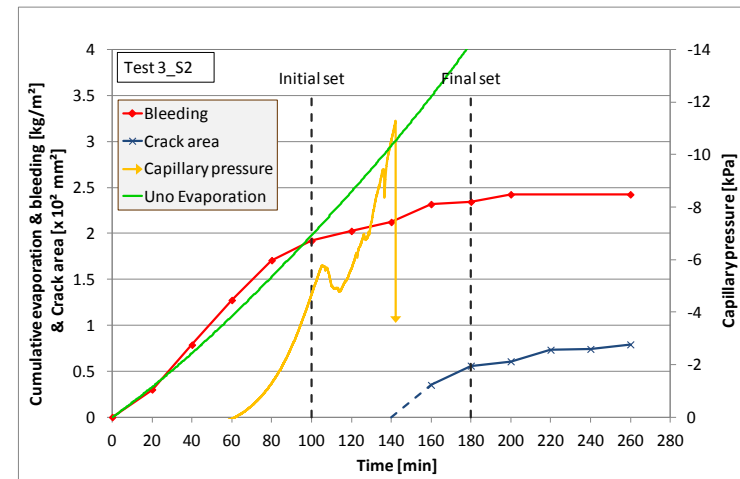
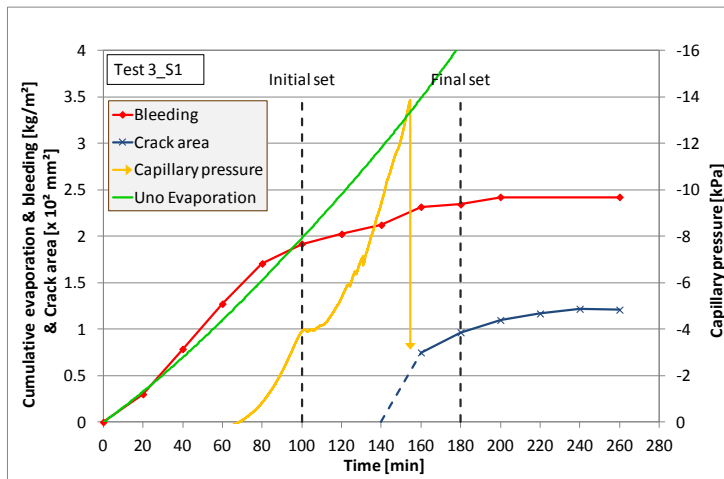


Figure B-3: Results for Specimen 1 and 2 of T3_HE_HB

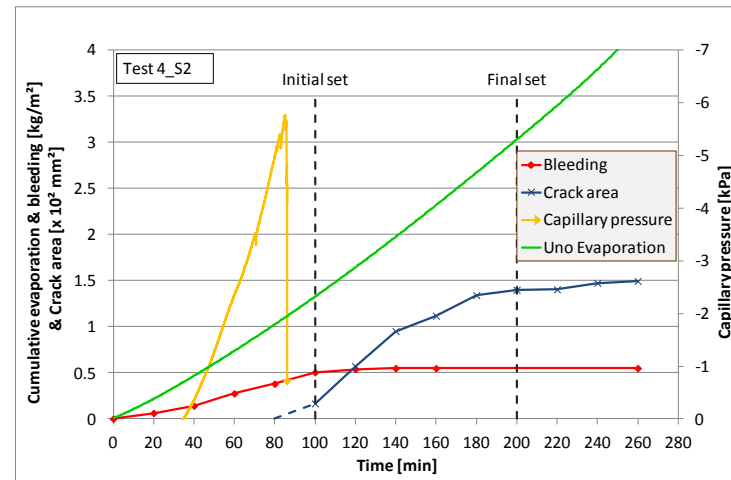
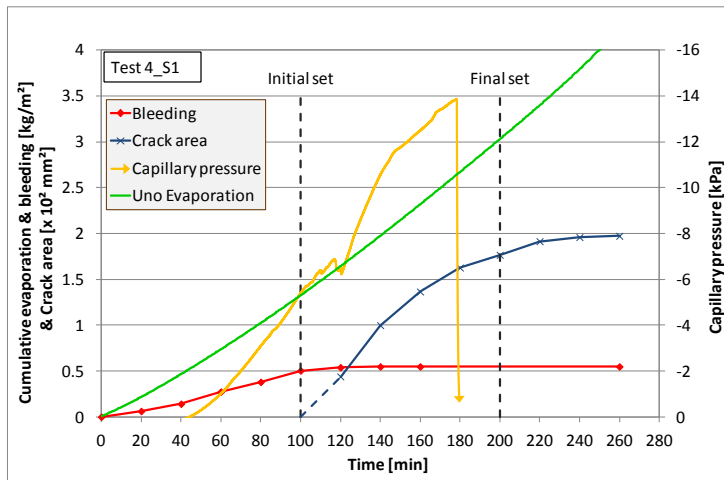


Figure B-4: Results for Specimen 1 and 2 of T4_ME_LB

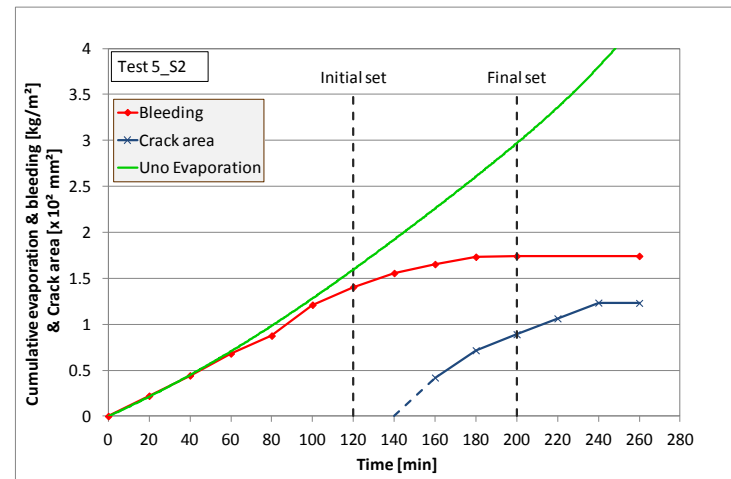
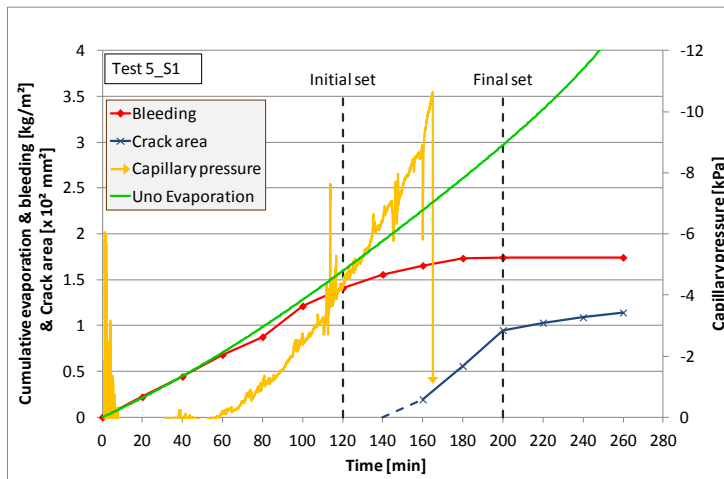


Figure B-5: Results for Specimen 1 and 2 of T5_ME_MB

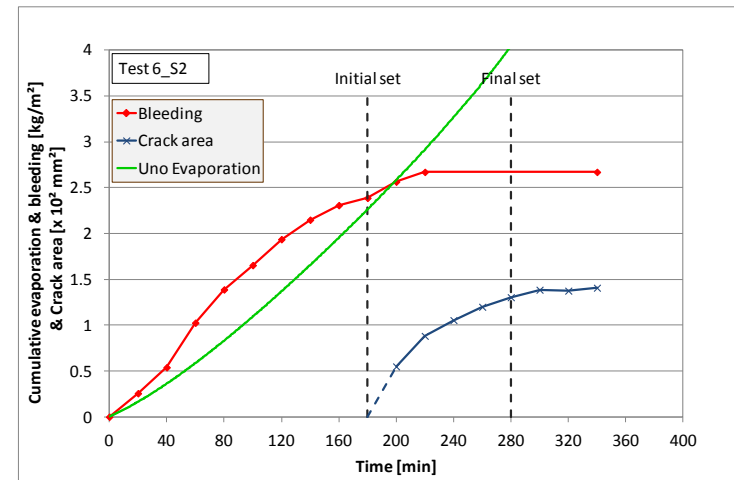
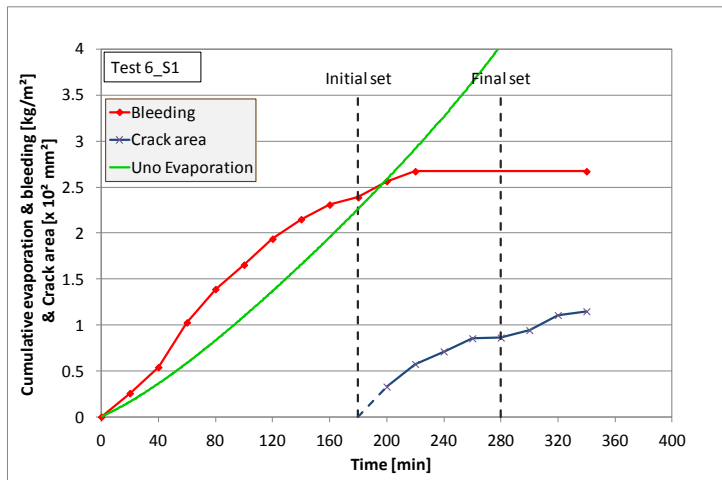


Figure B-6: Results for Specimen 1 and 2 of T6_ME_HB

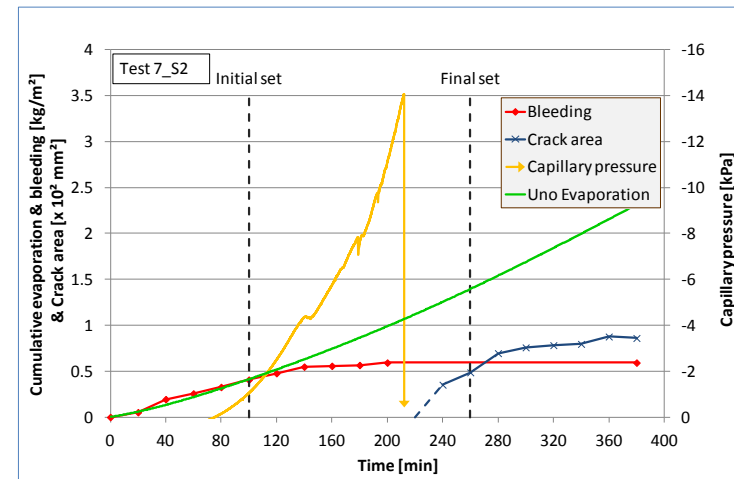
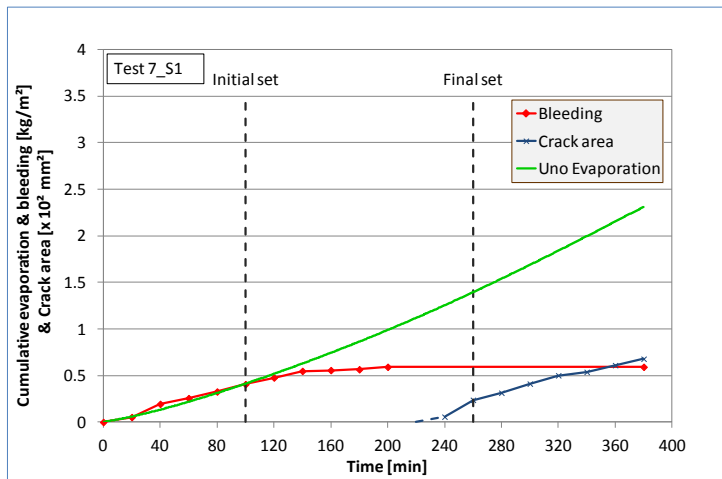


Figure B-7: Results for Specimen 1 and 2 of T7_LE_LB

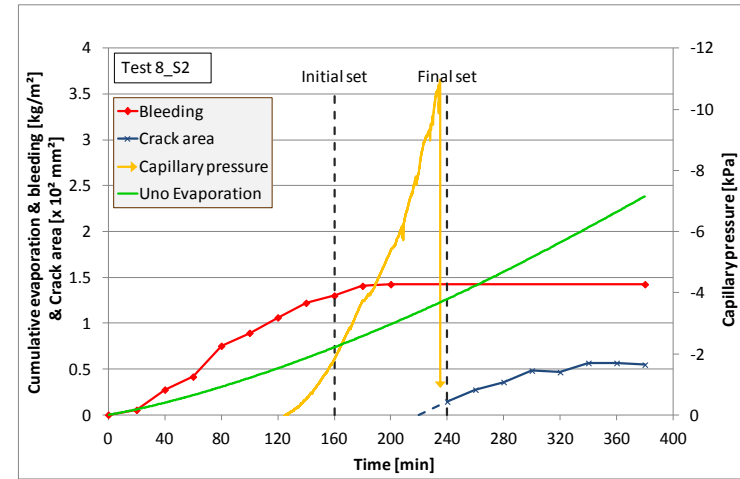
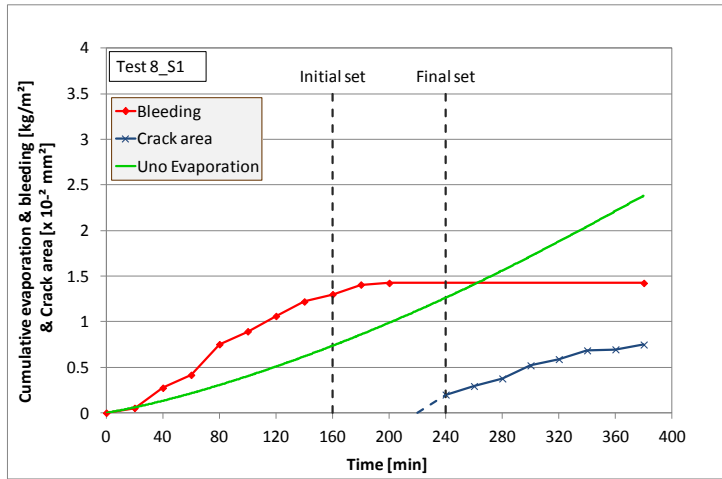


Figure B-8: Results for Specimen 1 and 2 of T8_LE_MB

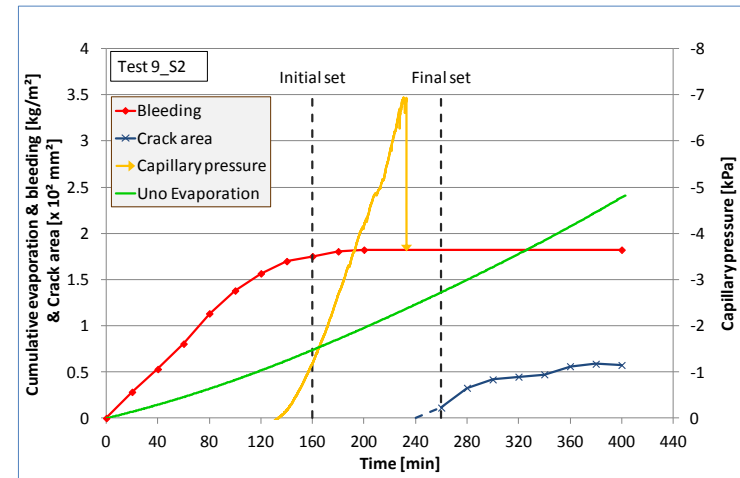
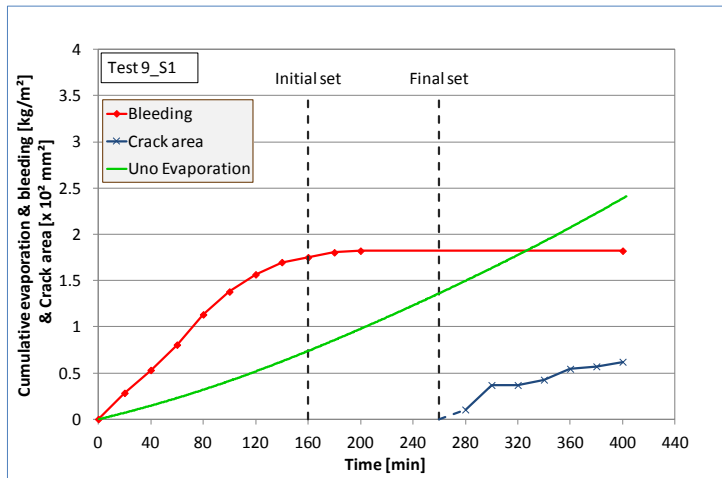


Figure B-9: Results for Specimen 1 and 2 of T9_LE_HB

Appendix B

The following tests were performed with LV-FRC and are used to investigate both Objective 1 and Objective 3. Test 10 is the standard (control) test and therefore was performed twice (Test 10a and Test 10b, with two specimens each) to ensure reliable results. It should be noted that the first crack area measurements for Tests 14 and 16 was performed at 90 minutes instead of 80 minutes due to complications with the camera. However this had no effect on the results.

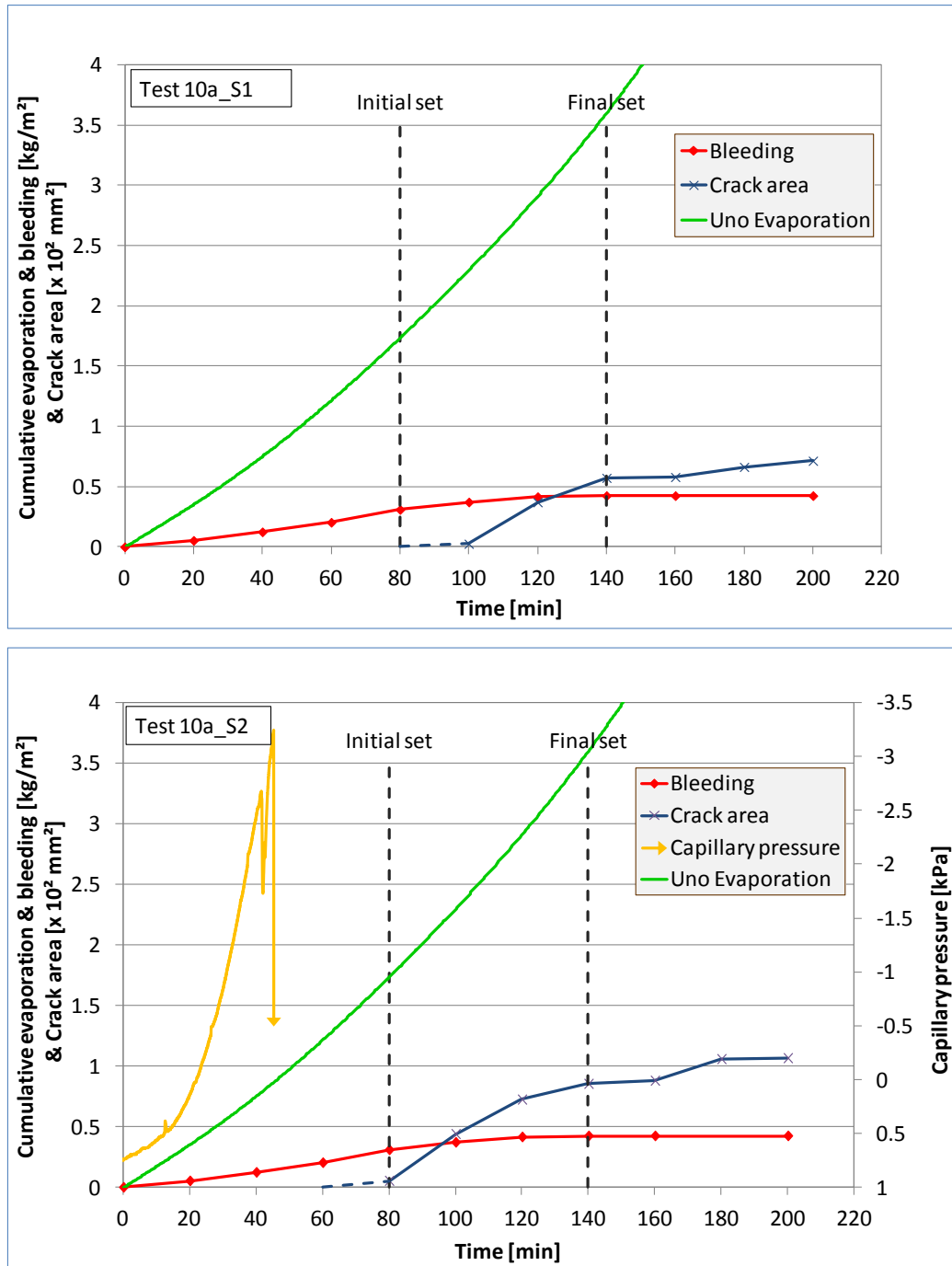


Figure B-10: Results for Specimen 1 and 2 of T10a_HE_LB_PP_0.1%_12mm_35µm

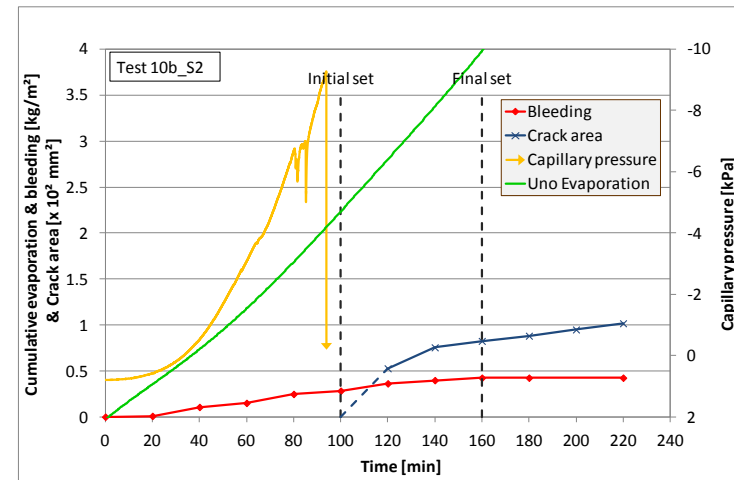
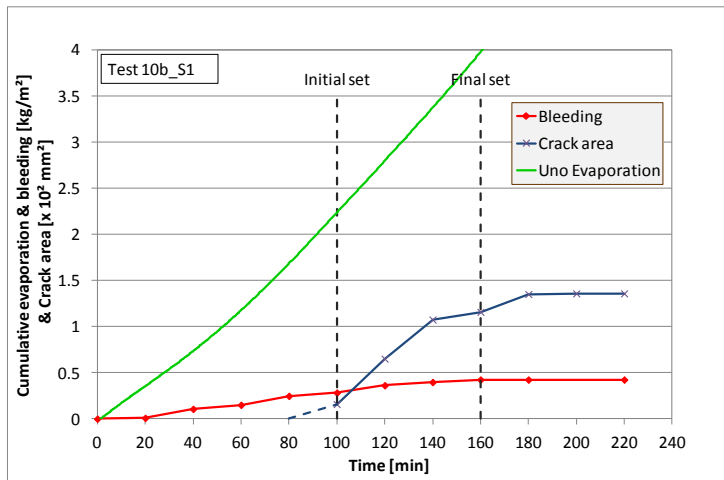


Figure B-11: Results for Specimen 1 and 2 of T10b_HE_LB_PP_0.1%_12mm_35 μm

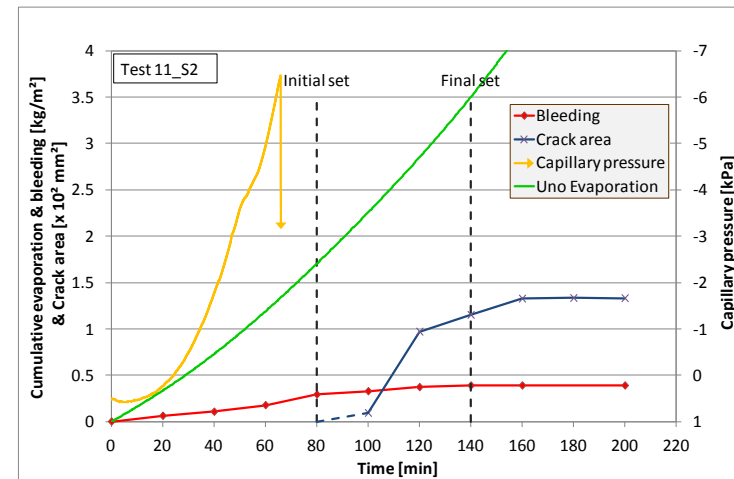
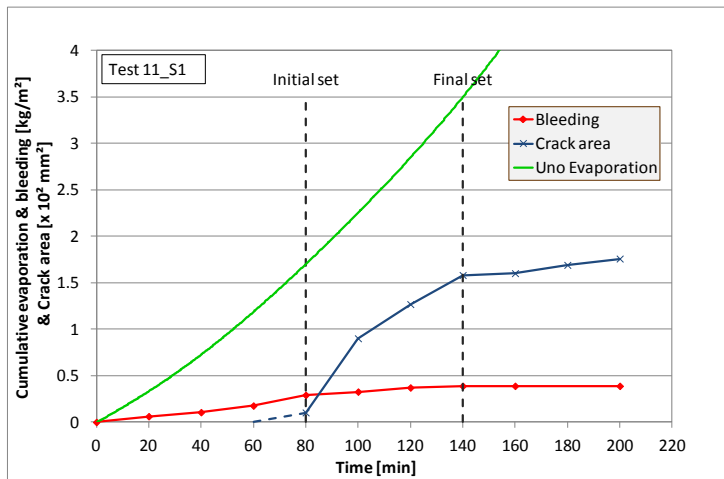


Figure B-12: Results for Specimen 1 and 2 of T11_HE_LB_PP_0.05%_12mm_35 μm

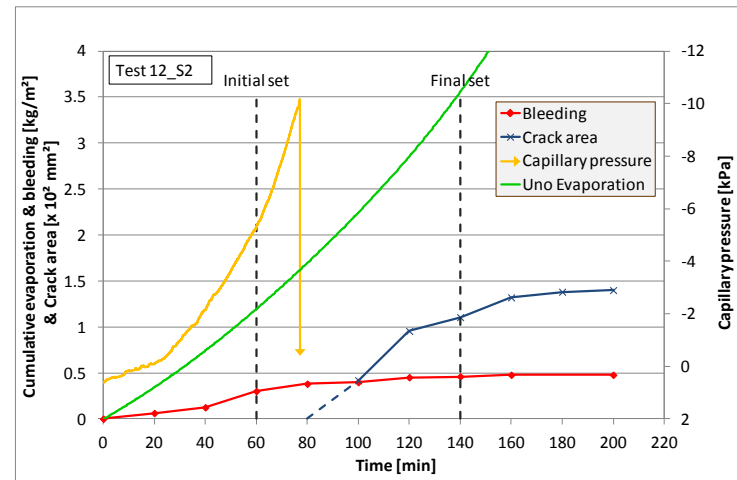
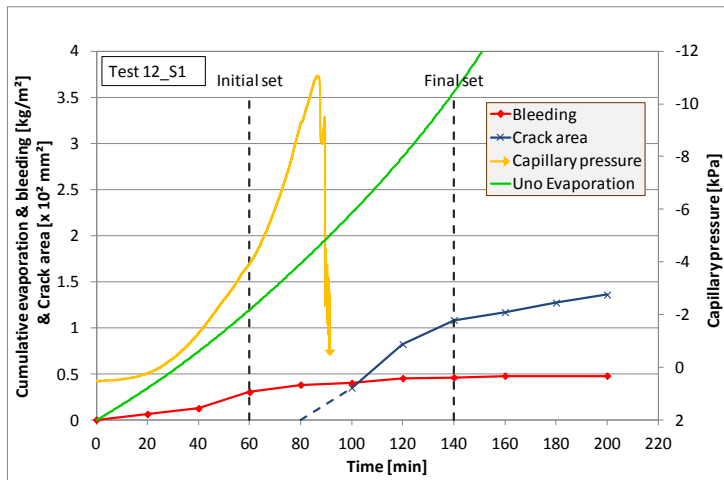


Figure B-13: Results for Specimen 1 and 2 of T12_HE_LB_PP_0.075%_12mm_35μm

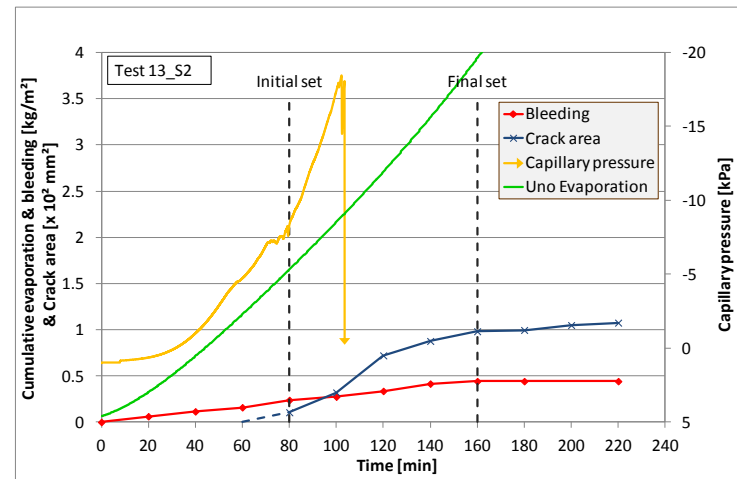
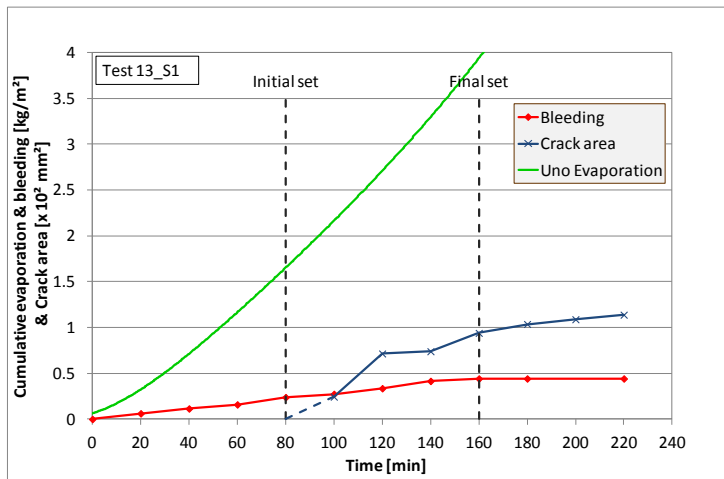


Figure B-14: Results for Specimen 1 and 2 of T13_HE_LB_PP_0.15%_12mm_35μm

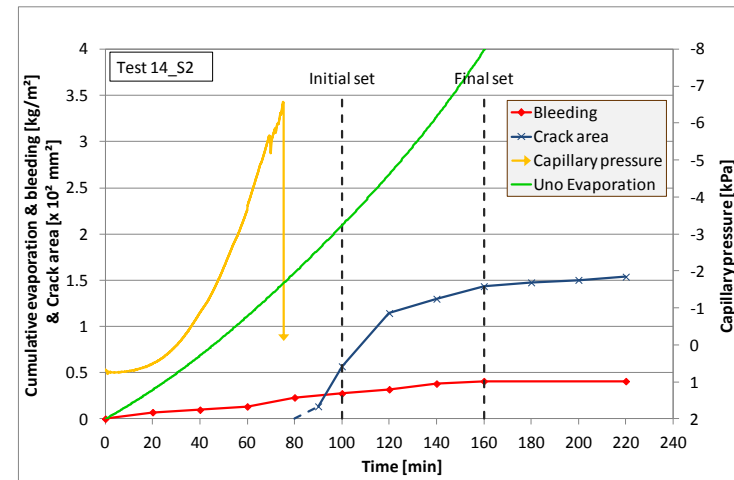
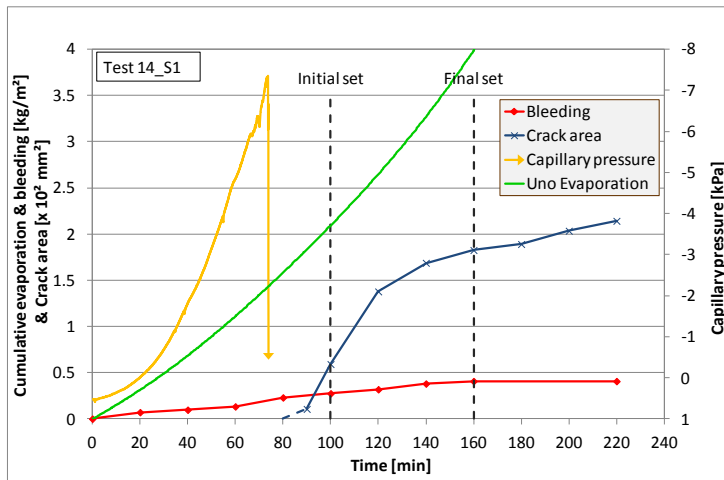


Figure B-15: Results for Specimen 1 and 2 of T14_HE_LB_PE_0.065%_6mm_20 μm

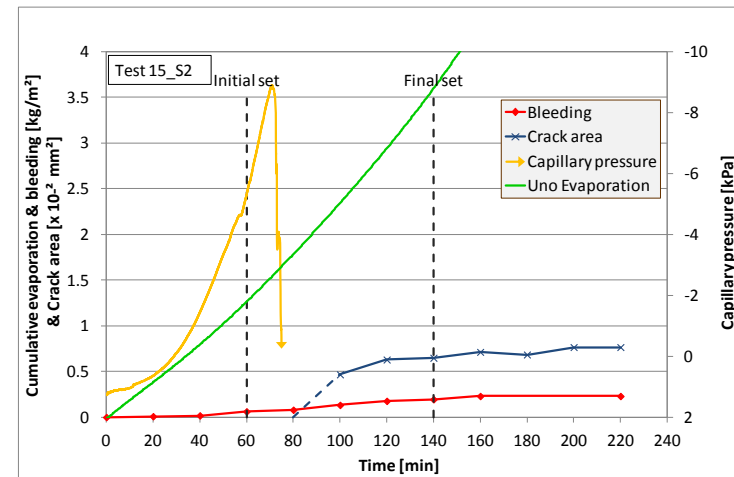
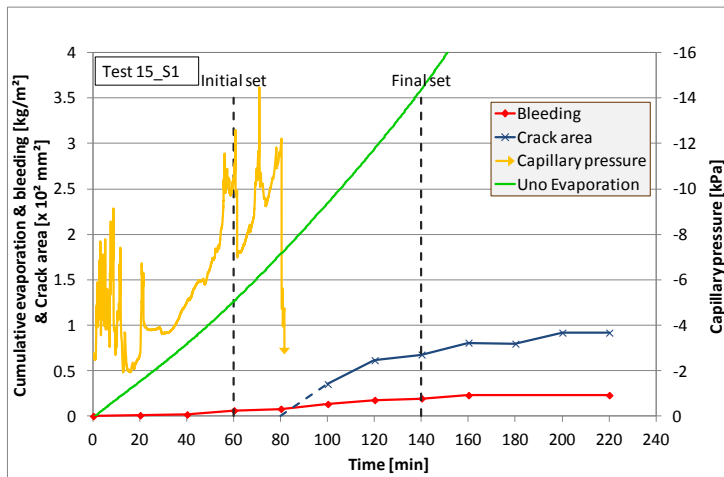


Figure B-16: Results for Specimen 1 and 2 of T15_HE_LB_PE_0.065%_12mm_20 μm

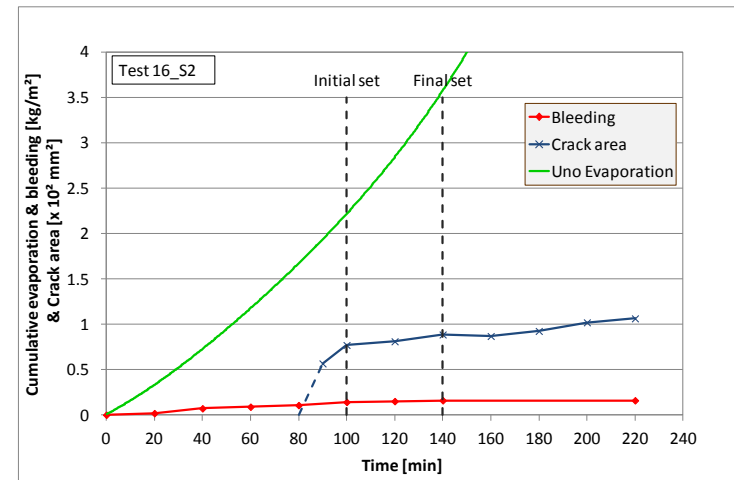
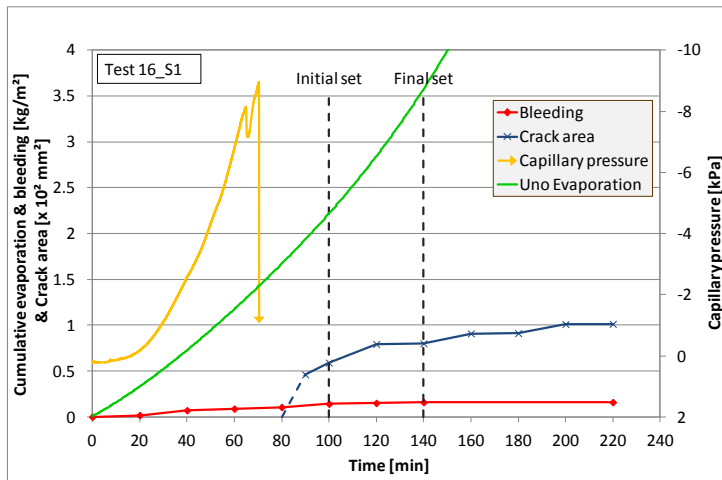


Figure B-17: Results for Specimen 1 and 2 of T16_HE_LB_PE_0.065%_24mm_20µm

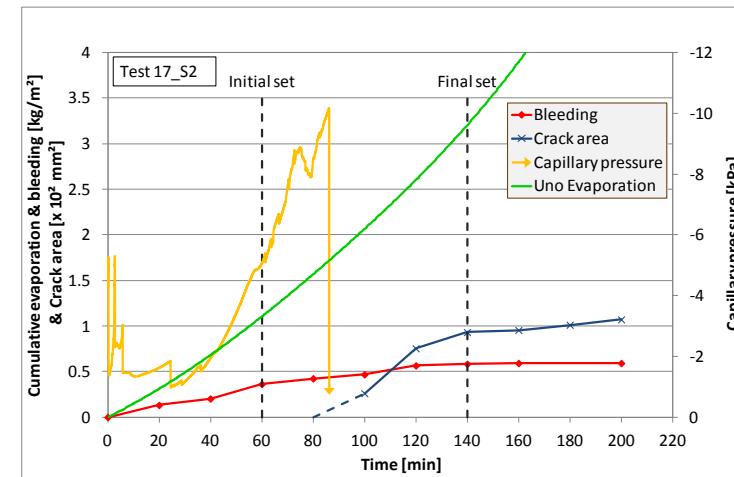
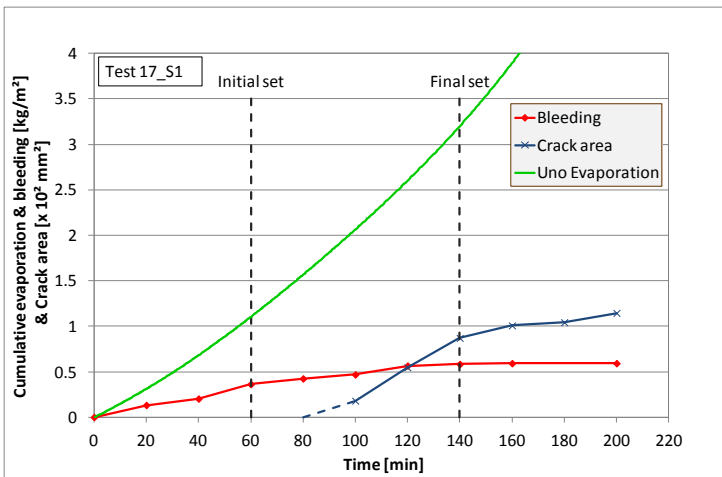


Figure B-18: Results for Specimen 1 and 2 of T17_HE_LB_PP_0.1%_12mm_20µm

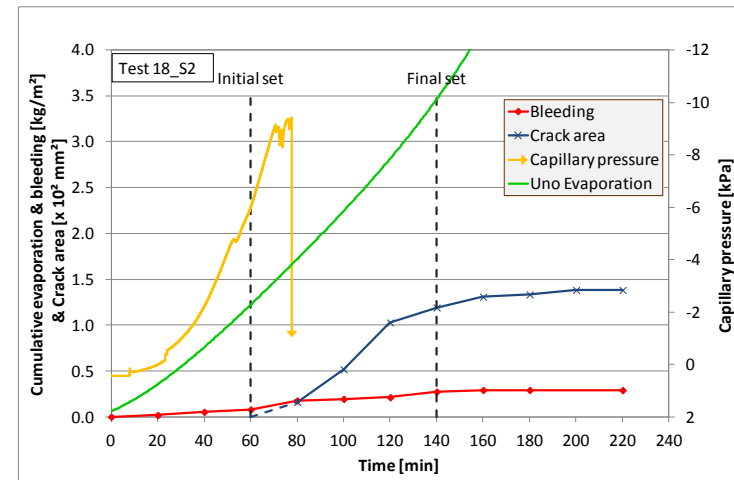
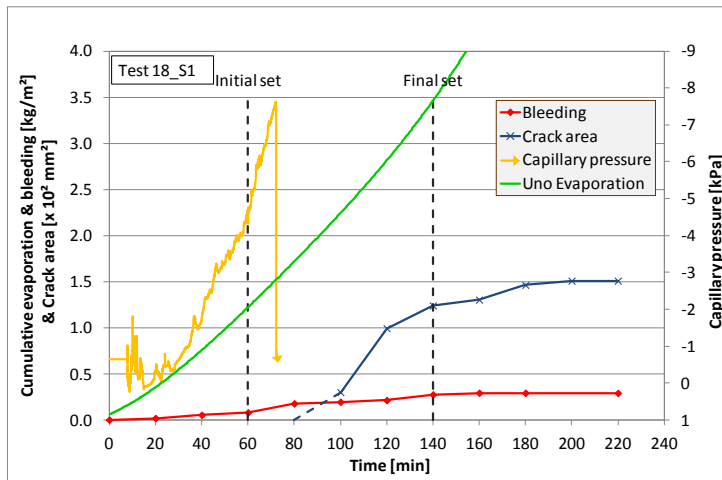


Figure B-19: Results for Specimen 1 and 2 of T18_HE_LB_FPP_0.1%_12mm_35 μm

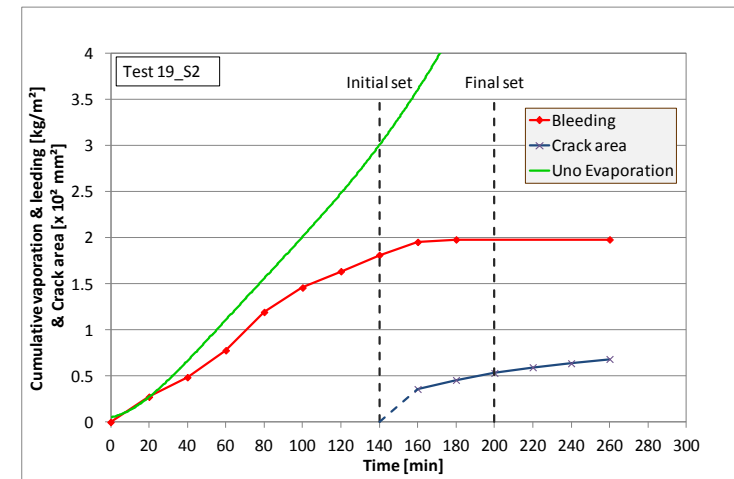
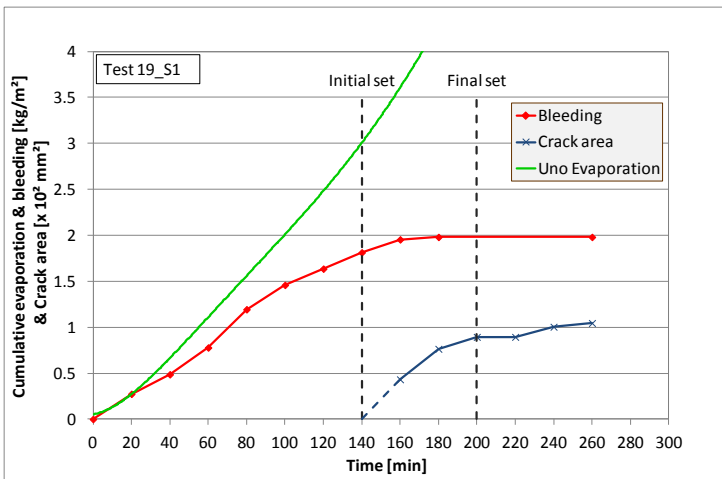
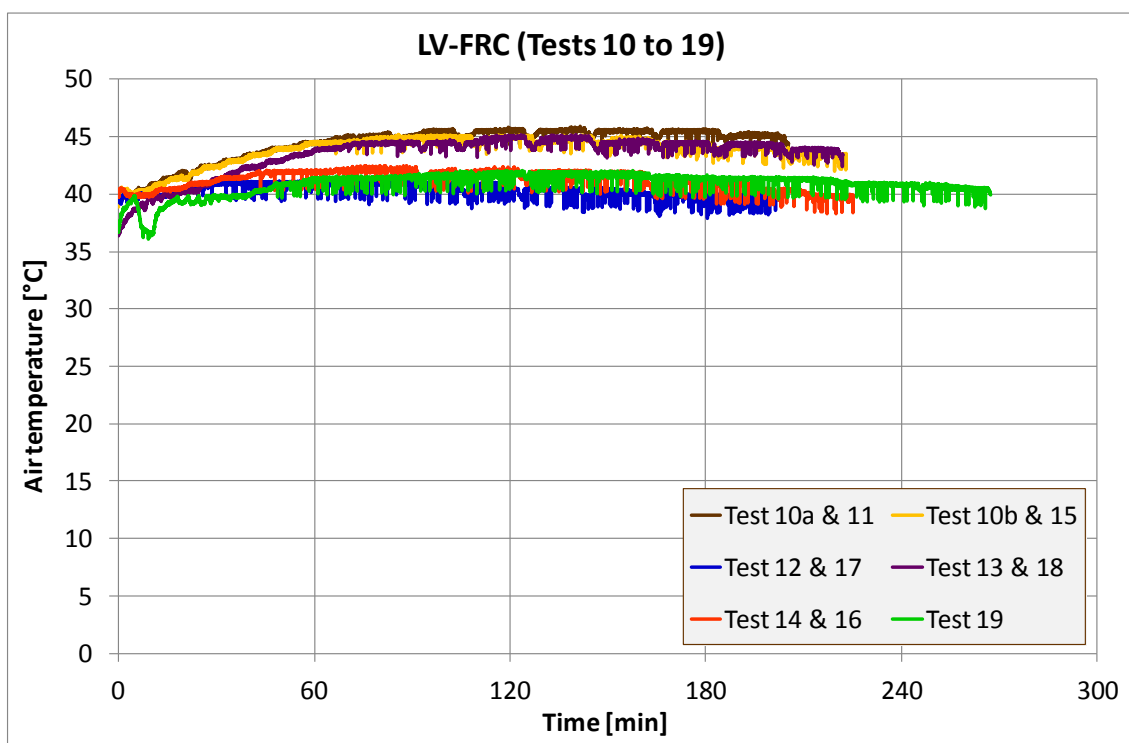
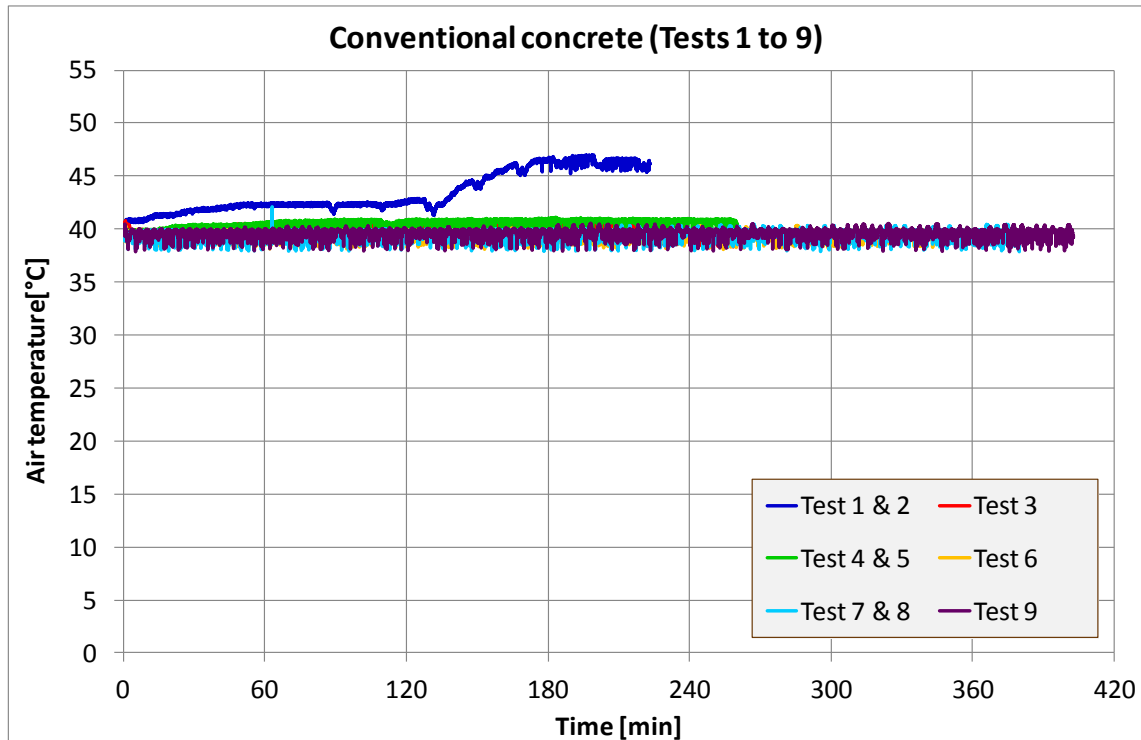


Figure B-20: Results for Specimen 1 and 2 of T19_HE_HB_PP_0.10%_12mm_35 μm

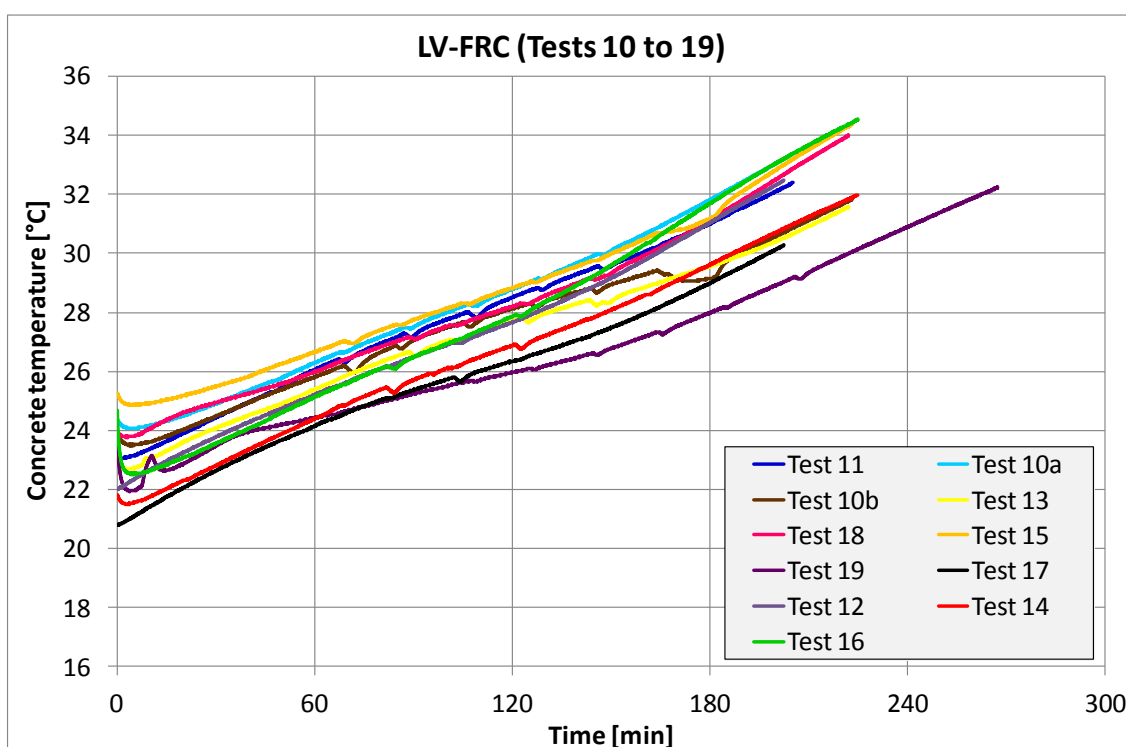
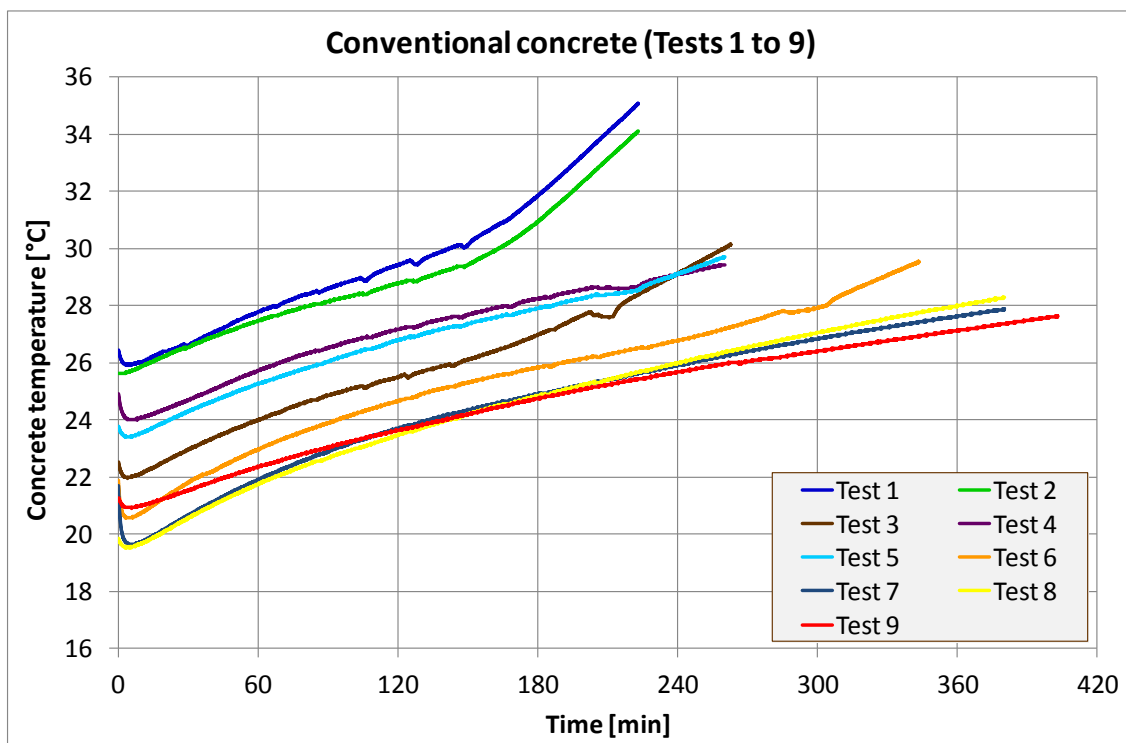
B.2. Summary of climate chamber air temperature results:

The results indicate that the required air temperature of 40°C was achieved and that most of the tests show temperature stabilization at this point. In some cases the temperature has increased past this mark. These results are still acceptable since it is still taken into account in Uno's equation.



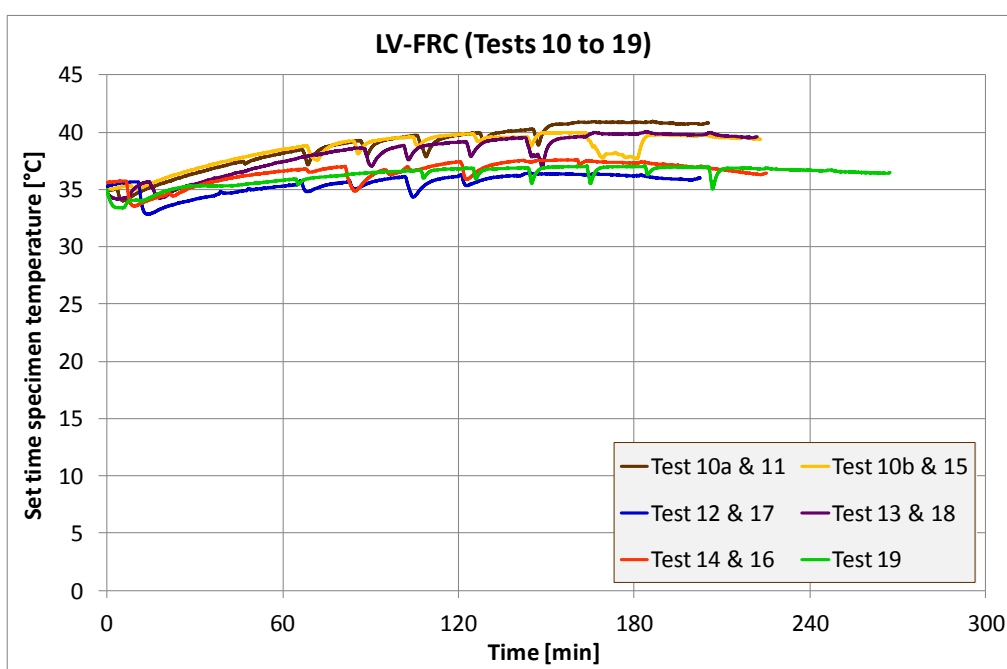
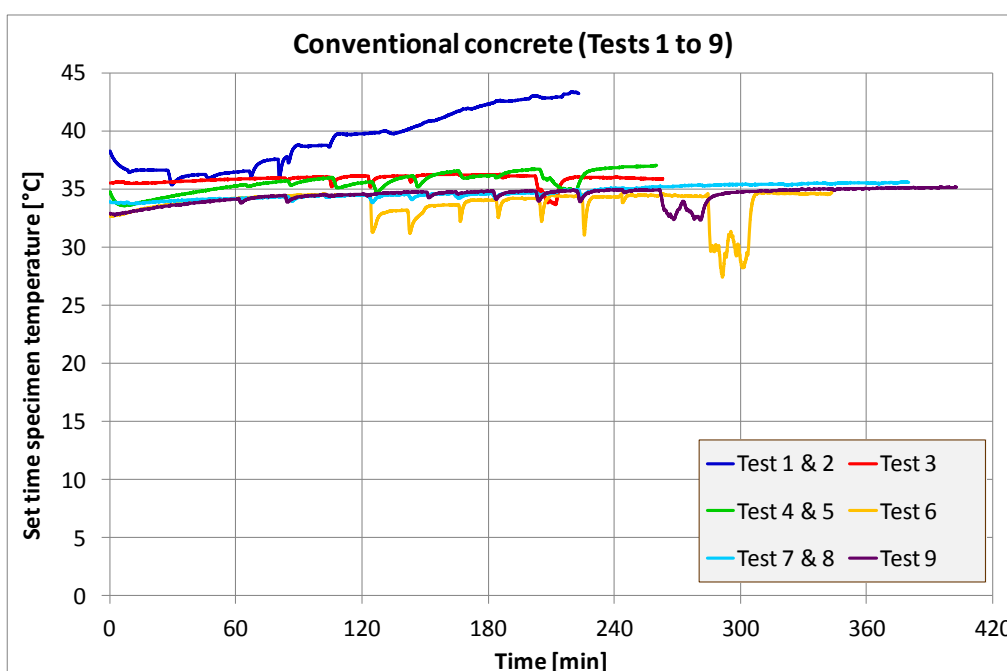
B.3. Summary of concrete specimen temperature results:

The results indicate an initial concrete temperature of more or less 23°C as required. The increase in concrete temperature is a result of heat of hydration. The identical rate in heat increase for all the tests indicate that hydration products form more or less at the same rate.



B.4. Summary of set time specimen temperature results:

The results indicate that the air temperature around the setting time specimens has an average temperature of 5°C less than the overall climate chamber temperature. This indicates that the temperature distribution is not consistent throughout the climate chamber. A lower air temperature around the setting time specimen could influence the measured initial and final setting time. However, this study regards this small temperature variance and the effect on the setting times as acceptable.



Appendix C: Capillary pressure measurements

The capillary pressure sensors are very sensitive and often provide irregular results. These irregularities can be a result of one of the following:

- If the metal tube and sensor is not completely filled with distilled water it will result in air voids that can influence the readings of the pressure sensor and result in irregularities (spikes) in the data. Air voids can also occur if the connection between the metal tube and the sensor is not sound.
- The electrical wiring of the sensors is very delicate and a complication with the wiring connection, especially during the casting and placement process. This complication results in irregularities in the data or in some cases produce no data at all. This problem can be overcome by regularly inspecting the performance of the sensors and replace the electrical wiring if necessary.

Figure C-1 provides typical results for capillary pressure with and without these irregularities.

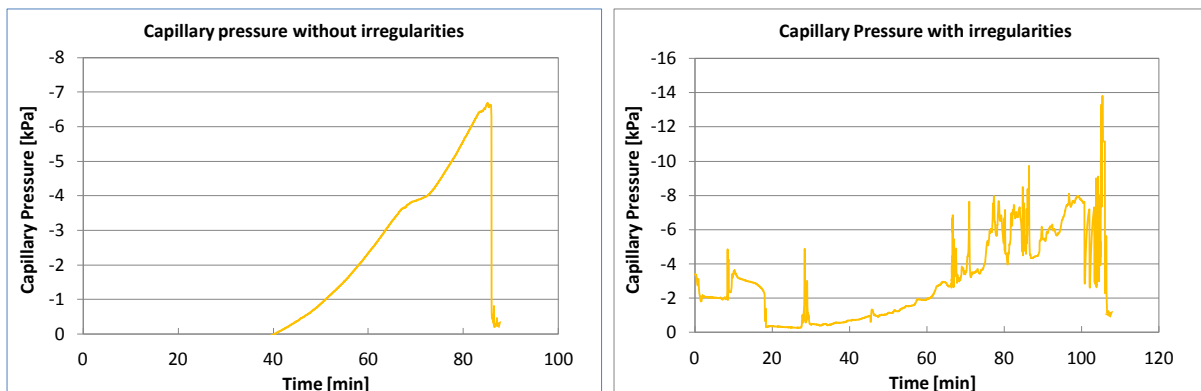


Figure C-1: Typical capillary pressure results with and without irregularities

Appendix D: Crack area results

D.1 Commencement of crack area results

The first 20 minutes of all crack growth results are indicated with a dashed line because it is not sure at exactly what time the crack has started since measurements were only taken once every 20 minutes. If the results are shown as in Figure D-1 (without the dashed lines) it can create the false illusion that the crack has started after 80 minutes when in fact it could have started at any time within the 80 to 100 minute time segment.

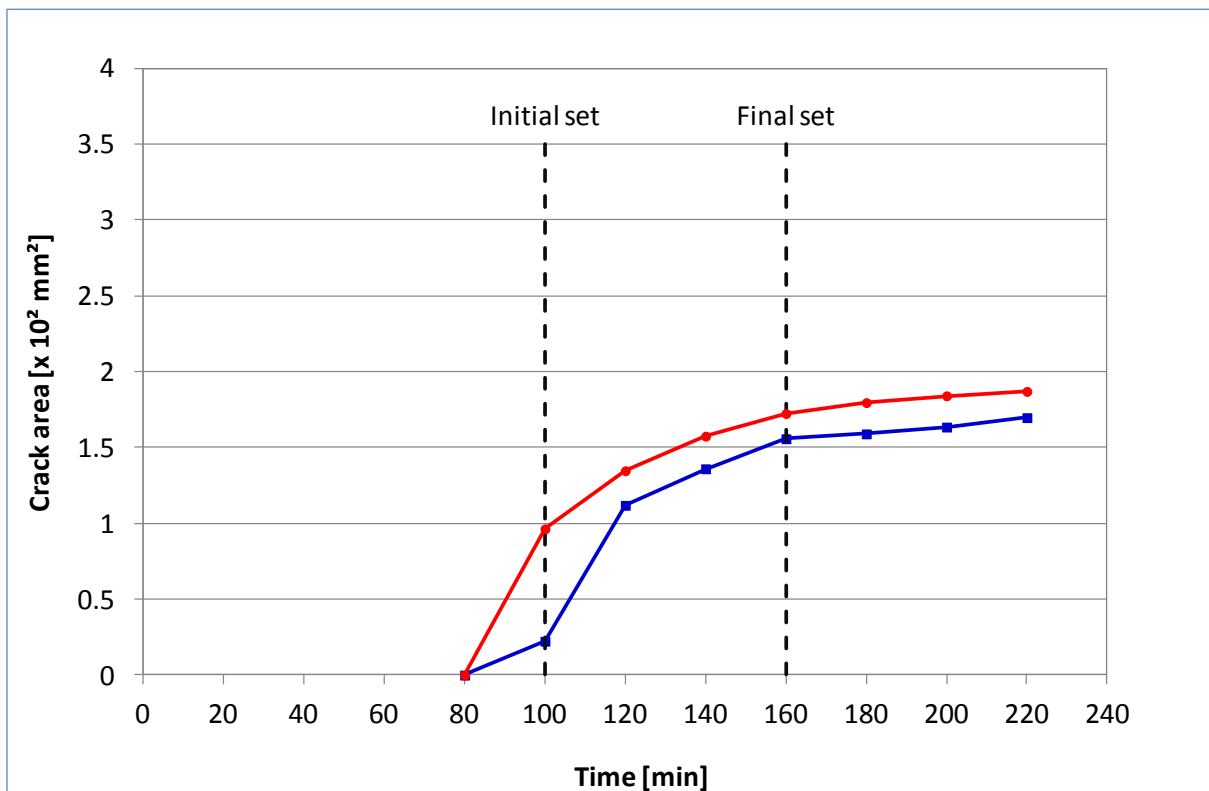


Figure D-1: Indication of crack results from the zero measurements

Appendix D

D.2 Percentage of crack area at final setting time to final crack area

The final crack area was measured at 60 minutes after the final setting time for all tests except Tests 7 to 9. The percentage value in Table D-1 indicates the percentage of crack growth that has occurred before final set (or one hour before final crack area was measured for Tests 7 to 9). This gives an indication of the crack stabilization at final set.

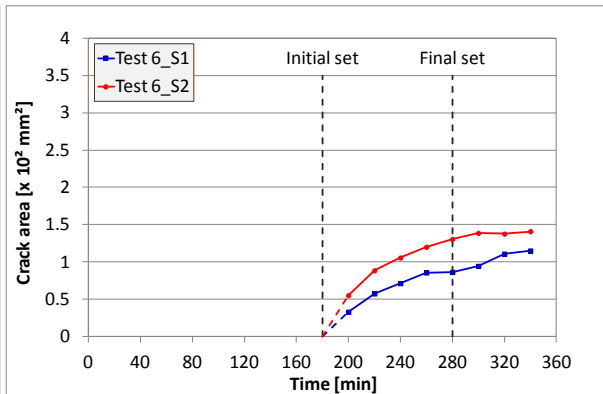
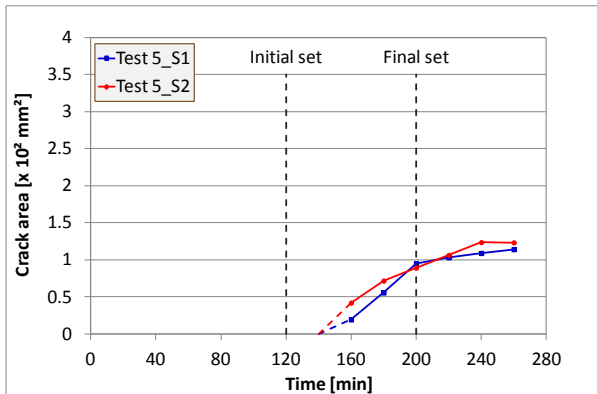
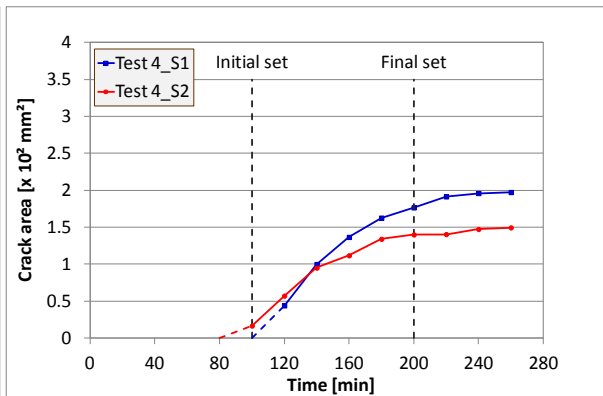
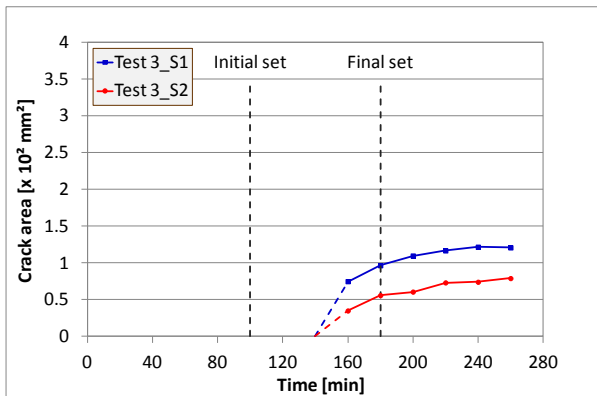
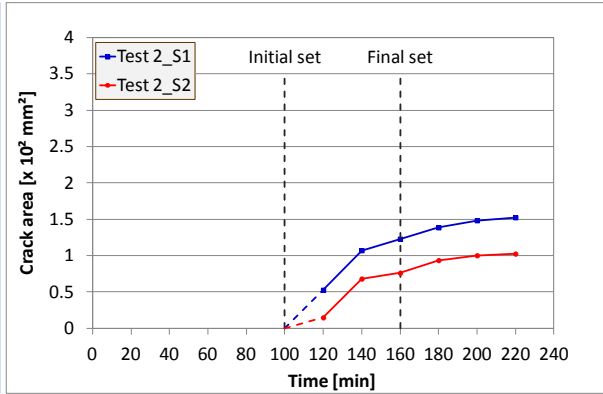
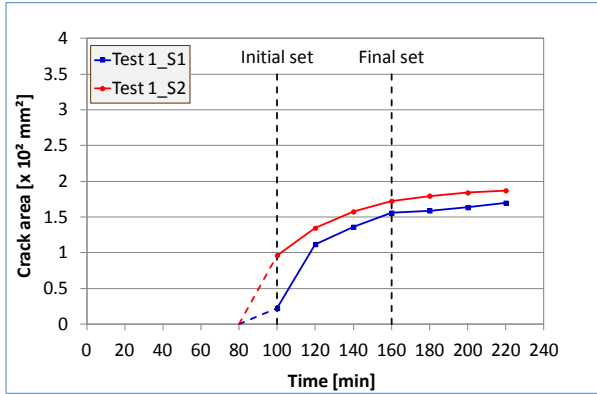
Table D-1: Percentage of crack area at final set to final crack area

TEST #	Crack area at final set [mm ²]	Final crack area [mm ²]	Percentage of crack area at final set to final crack area [%]
1	164.1	178.36	92.0
2	99.5	127.5	78.0
3	76.25	97.95	77.8
4	158.25	173.38	91.3
5	91.15	118.55	76.9
6	108.25	127.75	84.7
7	*64.15	**76.95	83.4
8	*52.65	**64.7	81.4
9	*44.95	**59.7	75.3
10a	71.3	89	80.1
10b	99.2	118.85	83.5
10 (average)	85.25	103.925	82.0
11	136.65	154.5	88.4
12	109.35	137.8	79.4
13	96.1	110.65	86.9
14	162.95	183.9	88.6
15	66.24	84.11	78.8
16	88.85	103.8	85.6
17	90.1	110.8	81.3
18	130.5	144.54	90.3
19	71.3	86.45	82.5
Average			83.2
* Crack area measured at 60 minutes after final set			
**Final crack area measured at 120 minutes after final set			

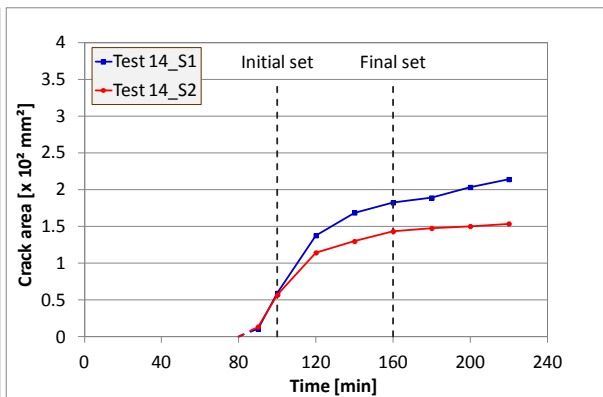
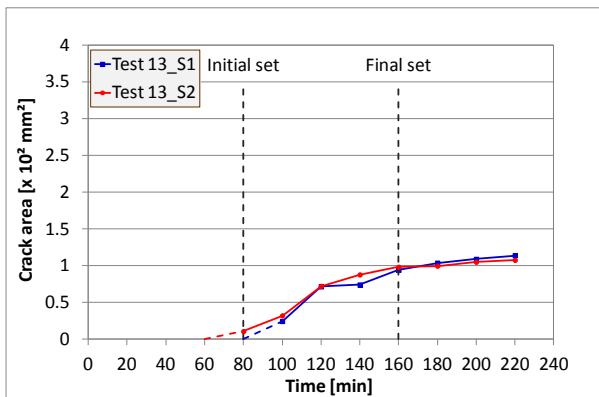
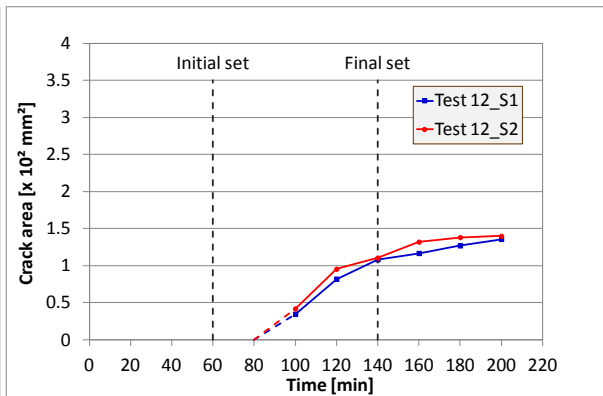
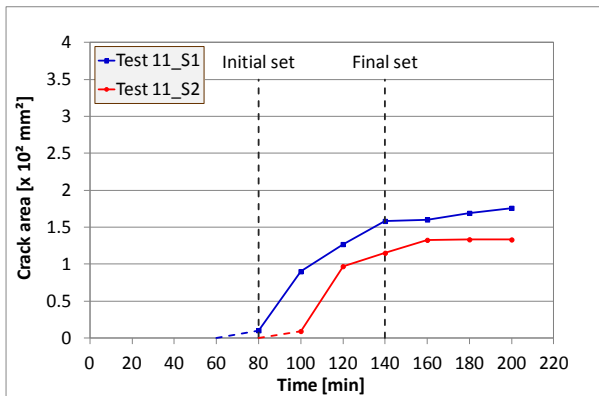
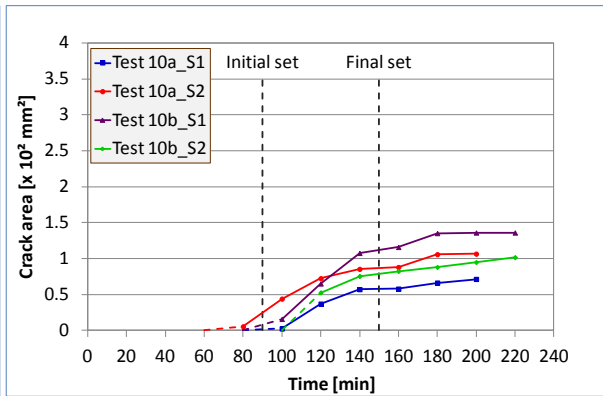
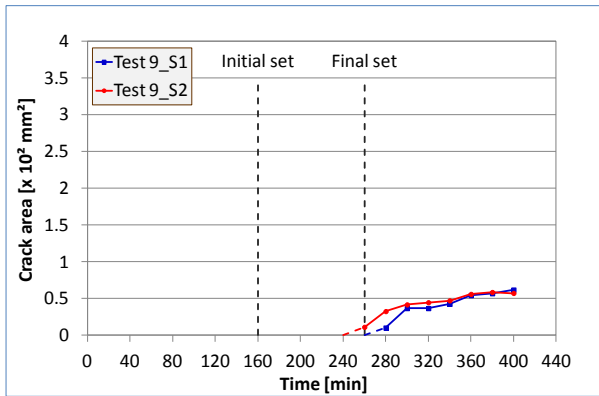
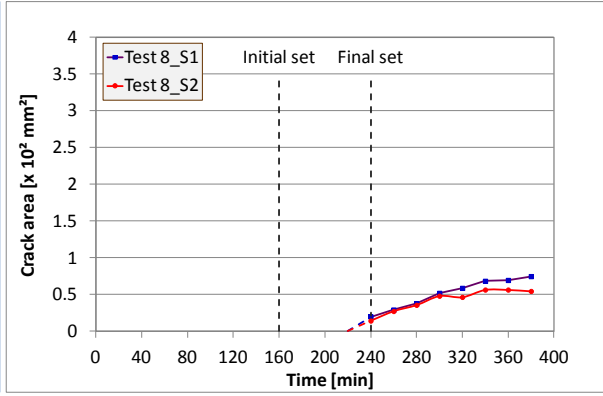
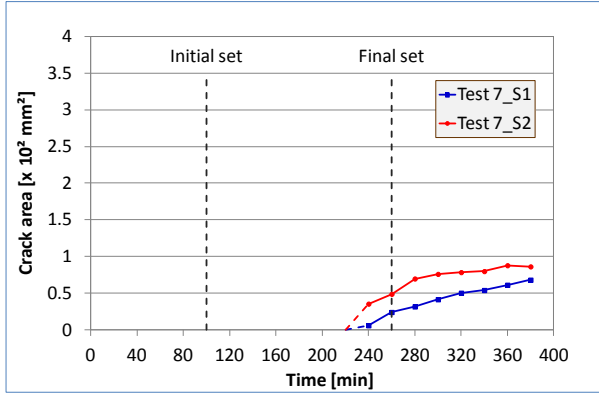
Appendix D

D.3 Complete crack area results

This section compares the crack growth results for both specimens of each test.



Appendix D



Appendix D

